PHP APPLICATIONS, K-WAVE SIMULATIONS AND EXPERIMENTAL STUDIES FOR MEDICAL ULTRASOUND

A THESIS SUBMITTED TO
THE GRADUATE SCHOOL OF NATURAL AND APPLIED SCIENCES
OF
MIDDLE EAST TECHNICAL UNIVERSITY

BY

UTKU BARAN KULGA

IN PARTIAL FULFILLMENT OF THE REQUIREMENTS
FOR
THE DEGREE OF MASTER OF SCIENCE
IN
ELECTRICAL AND ELECTRONICS ENGINEERING

FEBRUARY 2017

Approval of the thesis:

PHP APPLICATIONS, K-WAVE SIMULATIONS AND EXPERIMENTAL STUDIES FOR MEDICAL ULTRASOUND

submitted by **UTKU BARAN KULGA** in partial fulfillment of the requirements for the degree of **Master of Science in Electrical and Electronics Engineering Department, Middle East Technical University** by,

Prof. Dr. Gülbin Dural Ünver
Dean, Graduate School of **Natural and Applied Sciences** _____

Prof. Dr. Tolga Çiloğlu
Head of Department, **Electrical and Electronics Engineering** _____

Prof. Dr. Nevzat Güneri Gençer
Supervisor, **Electrical and Electronics Eng. Dept., METU** _____

Examining Committee Members:

Prof. Dr. Behçet Murat Eyüboğlu
Electrical and Electronics Engineering Dept., METU _____

Prof. Dr. Nevzat Güneri Gençer
Electrical and Electronics Engineering Dept., METU _____

Assoc. Prof. Dr. Yeşim Serinağaoğlu Doğrusöz
Electrical and Electronics Engineering Dept., METU _____

Assoc. Prof. Dr. Barış Bayram
Electrical and Electronics Engineering Dept., METU _____

Asst. Prof. Dr. Özlem Birgül
Biomedical Engineering Dept., Ankara University _____

Date: 07.02.2017

I hereby declare that all information in this document has been obtained and presented in accordance with academic rules and ethical conduct. I also declare that, as required by these rules and conduct, I have fully cited and referenced all material and results that are not original to this work.

Name, Last Name : UTKU BARAN KULGA

Signature :

ABSTRACT

PHP APPLICATIONS, K-WAVE SIMULATIONS AND EXPERIMENTAL STUDIES FOR MEDICAL ULTRASOUND

Kulga, Utku Baran
M.S. Department of Electrical and Electronics Engineering
Supervisor: Prof. Dr. Nevzat Güneri Gençer

February 2017, 124 pages

This study has three parts related to theoretical calculations, numerical simulations and experimental studies in the field of medical ultrasound. The goal of the first part is to prepare computer codes for the education of biomedical engineering students. For this purpose, a series of computer applications is prepared using the hypertext preprocessor (PHP) programming language. Accessing the associated internet address, the students will be able to learn the basics of ultrasound using the interactive, visual, cost-effective infrastructure of the developed computer applications. Snell's Law, Reflection and Transmission Characteristics of Ultrasound, Attenuation Phenomenon, Pressure Wave, Power Intensity Concepts, Doppler Effect, Piezoelectric Materials, Near and Far Field Calculations, Transducer Design, A-Mode and B-Mode Ultrasound, Effects of Frequency and Tissue Types can be studied by means of these applications.

The second part includes simulation studies made for the calculation of ultrasound waves in biological tissues. In these simulations, an open source acoustic toolbox for

MATLAB (k-Wave) is used. The accuracy and speed in solutions are assessed using simple sources and body geometries.

The third part is on the experimental studies. Experiments are conducted using an ultrasound system that employs a 16-channel phased array ultrasound transducer. Ultrasound phantoms are developed and used to acquire pulse-echo signals. The same geometry and acoustic properties of the phantom are used to acquire one-dimensional pulse echo signals in the PHP application and in the K-Wave simulations. The similarities and differences in the signals obtained from the PHP application, K-Wave simulation, and experimental studies are discussed.

Keywords: Medical Ultrasound Systems, Transducer Design, Ultrasound Applications, PHP Based Applications.

ÖZ

TIBBİ ULTRASON İÇİN PHP TEMELLİ BİLGİSAYAR UYGULAMALARI, K-WAVE BENZETİMLERİ VE DENEYSEL ÇALIŞMALAR

Kulga, Utku Baran
Yüksek Lisans, Elektrik ve Elektronik Mühendisliği Bölümü
Tez Yöneticisi: Prof. Dr. Nevzat Güneri Gençer

Şubat 2017, 124 pages

Tıbbi ultrason alanında hazırlanmış bu çalışma; teorik hesaplamalar, sayısal simülasyonlar ve deneysel çalışmalar olmak üzere üç bölümden oluşmaktadır. Birinci bölümün amacı biyomedikal mühendislik öğrencilerinin etkileşimli eğitimlerine katkıda bulunmak için bilgisayar kodları hazırlamaktır. Bu amaçla PHP hypertext preprocessor programlama dili kullanılarak bilgisayar temelli Tıbbi Ultrason uygulamaları hazırlanmıştır. Bilgisayar uygulamalarının yayınlandığı internet adresinin sağladığı etkileşimli, görsel ve görece ucuz altyapı sayesinde öğrenciler ultrason temellerini kavrama imkanı bulacaktır. Bu uygulamalar sayesinde Snell Kanunları, Ultrason Yansıma ve İletim Karakteristiği, Sönümlenme Kavramı, Basınç Dalgası, Güç ve Enerji Konseptleri, Doppler Etkisi, Basınç-Elektrik Üretimli Maddeler, Yakın Alan, Uzak Alan Hesaplamaları, Dönüştürücü Tasarım, A-Mod ve B-Mod Ultrason Sistemleri, Frekans ve Doku Tipi Değişimlerinin Etkisi gibi konular çalışılabilecektir.

İkinci bölüm; biyolojik dokulardaki ultrason dalga hesaplamalarını için hazırlanmış benzetim çalışmalarını içermektedir. Bu benzetimlerde MATLAB için hazırlanmış açık kaynak kodlu bir akustik araç kutusu olan k-Wave kullanılmıştır. Çözümlerdeki doğruluk ve hız, basit kaynak ve geometriler kullanılarak değerlendirilmiştir.

Üçüncü bölüm deneysel çalışmalara ayrılmıştır. İlgili ölçümler gerçek bir ultrason görüntüleme sistemi ile yapılmış ve 16 kanallı doğrusal faz dizi dönüştürücü kullanılmıştır. Ölçüm ve deneyler için akustik fantomlar hazırlanmıştır. Fantom deneylerinin yapıldığı aynı geometri ve akustik özellikler, PHP temelli tek boyutlu pulse eko uygulaması ve k-Wave benzetimleri için de hazırlanmış ve uygulanmıştır. PHP uygulaması, k-Wave benzetimi ve deneysel çalışmalarda elde edilen sinyallerin benzerlik ve farklılıkları tartışılmıştır.

Anahtar Kelimeler: Tıbbi Ultrason Sistemleri, Dönüştürücü tasarımı, Ultrason Sistem Uygulamaları, PHP Temelli Uygulamalar.

To my family

ACKNOWLEDGMENTS

This project would not have been possible without the support of many people. First, I would like to express my sincere gratitude to my supervisor Prof. Dr. Nevzat Güneri Gençer for his guidance, advice and continuous support throughout my master program. His suggestions and comments has drawn a path and put all the work in a scientific form. It has always been a great opportunity to work under his guidance and to profit from his immense knowledge and technical experiences.

I would also like to thank all of my family and special ones for their trust, patience and encouragement at every stage of my personal and academic life.

In addition, I gratefully acknowledge Erhan Şahin and Alişan Çetinkaya for their auxiliary support and friendship. I also appreciate Ahmet Önder Tetik for his time and support for phantom preparation, measurements phase and experimental studies.

TABLE OF CONTENTS

LIST OF TABLES

TABLES

LIST OF FIGURES

FIGURES

CHAPTER 1

INTRODUCTION

Ultrasound Imaging is one of the popular medical imaging methods, which is commonly used in clinical applications for diagnostic purposes. It is common and popular because it is an inexpensive, quick and non-invasive imaging technique. The theory of its operation is based on the propagation and reflection of the high frequency sound waves inside the body tissues. By means of piezoelectric effect and piezoelectric materials, ultrasound waves are produced and waves reflected from tissue interfaces are detected. Using the detected waves and mathematical calculations, cross-sectional images of soft body tissues can be displayed.

The focus of this thesis study is on three topics related to medical ultrasound: 1) preparation of assistive computer tools for the education of ultrasound based on theoretical calculations, 2) simulating ultrasound waves in biological tissues based on k-Wave which is an open source acoustic toolbox for MATLAB, 3) preparation of ultrasound phantoms and conducting experimental studies related to medical ultrasound. The latter two studies complement the efforts on the development of education tools and form the basis of future works on the realization of more realistic software tools for education.

Computers Tools for Education

The goal of the first part is to prepare a series of computer applications for interactive education on medical ultrasound. Mathematical formulations and physical phenomenon of ultrasound, such as reflection and transmission characteristics, Snell's rule, piezoelectric effect and piezoelectric materials, attenuation

characteristics, Doppler Effect, different wavelength and tissue (fat, muscle, blood, etc.) conditions are included and related applications are prepared.

To achieve the first goal of this thesis study, the most efficient and widespread tools must be chosen in order to make the codes easily accessible and usable worldwide. For this purpose, following topics are investigated:

- e-devices ownership trends such as desktops, tablets, and mobile handhelds,
- worldwide operating system usage trends such as Windows, Android, IOS, and Symbian,
- Programming languages such as Java, PHP, Python, Ruby, .Net, etc… Their widespread availability, platform and operating system free access advantages are also assessed.

Next, the theory behind the ultrasound imaging is reviewed. Propagation of the sound waves, the effects of body properties (compressibility and density) over sound propagation, reflection characteristics of the sound at the boundary of two different mediums, echo and refraction conditions of the sound waves, piezoelectric materials and piezoelectric effect, transducer design and transducer characteristics are examined. Theory, formulations and technical information is put together and finally a series of applications are prepared by means of the chosen computer based programming language.

In the software design and code implementation phase, basic ultrasound applications and ultrasound system applications are developed and coded. Different cases, shapes, wavelength types, tissue types and media conditions are examined.

The output of this thesis work provides a computer tool that may contribute to interactive education in the field of biomedical engineering. By means of its worldwide accessibility, operating system, device/platform independent structure, students can use the prepared applications and understand the principles of ultrasound.

Electronic Learning

Electronic learning or e-learning can be defined as the study of taking courses or developing educational skills by using computer based software and on-line resources. The term e-learning is normally used for flexible learning and long distance learning, however can likewise be utilized as a part of conjunction with up close and personal instructing, in which case the term blended education is usually utilized [1].

When you compare with the traditional learning techniques, electronic learning procedures, items and lectures has a lot of plus points in terms of accessibility, content delivery and affirming understandability. In addition, it gives simple access to an incredible measure of worldwide data. Participants can investigate, seek and access any kind of document and information rapidly and the resources are continuously reachable whenever you need. According to the online servers' capabilities, e-learning documents and information are available for a large group of people worldwide on one time contrary to the standard common person-to-person classroom lectures.

Another favorable property of e-learning is its adaptability which provides easy access and enhanced efficiency. Subsequently, one can access the needed information whenever he/she wants or wherever he/she is. In addition, the nature of e-learning has a positive effect on the learning mechanism.

E-learning materials can be available both in stationary passive forms such as e-books, lecture notes, stable world wide web internet pages and in the form of active materials. Active e-learning materials such as programmed software and HTML, Java, PHP or similar language based coded applications offer interactive interface to set up experiments and repeated on-line actions.

E-Devices Ownership and Operating System Trends

More individuals around the world are getting to the Internet through cell phones and mobile handhelds than stable desktop gadgets with respect to the report from comScore [2]. Total amount of stable desktop devices used to get internet access were drag behind the mobile handheld amounts by 2014 and the scissors is opening as the time pass by (Figure 1).

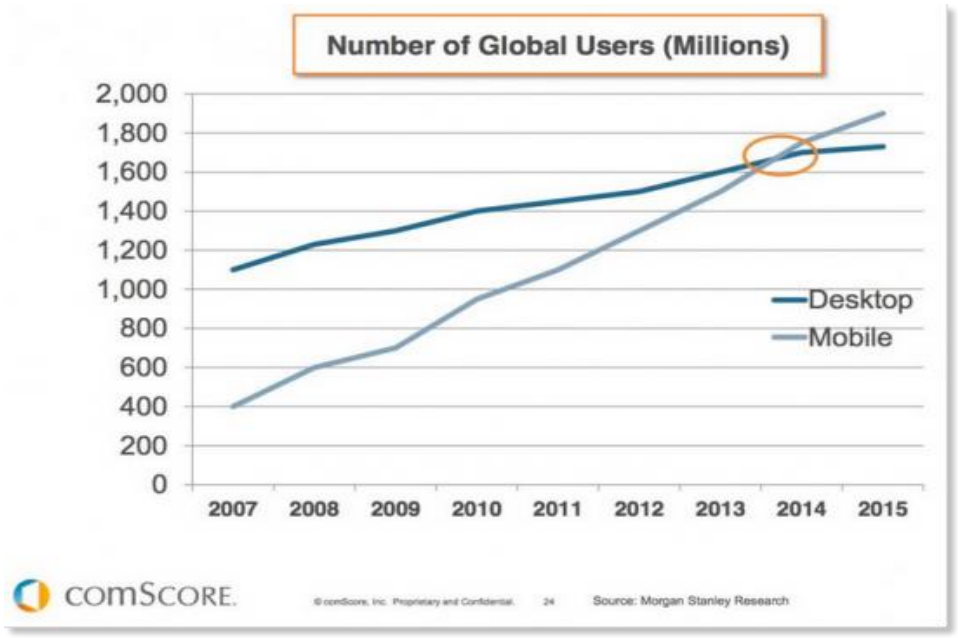

Figure 1: Global number of mobile and desktop device change.
Graph from Morgan Stanley, 2015 [2].

Another site survey (Figure 2) additionally expresses that the mostly used technical devices for getting to the Internet are mobile handhelds (Ofcom's Eighth Market Report for International Communications, 2014).

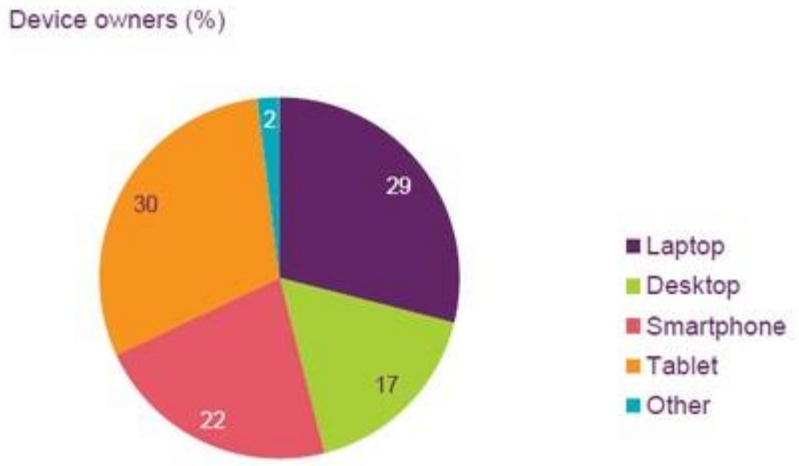

Figure 2: Mostly used device type ownership for internet access from Ofcom research, 2014 [3].

Figure 3 shows the estimate of the operating system share. It is observed that the electronic device share is commanded by Android operating system. If you compare with the most popular competitor, Gartner indicates that there will be more than 6 non-windows operating system powered device for every single windows operating system powered device in 2016.

Worldwide Device Shipments by Operating System (Thousands of Units)

Operating System	2013	2014	2015
Android	898,944	1,168,282	1,370,893
Windows	326,060	333,419	373,694
iOS/Mac OS	236,200	271,115	301,349
Others	873,195	660,112	545,817
Total	**2,334,400**	**2,432,927**	**2,591,753**

Shipments include mobile phones, ultramobiles (including tablets) and PCs

Figure 3: Shipped device types in accordance with operating systems [4].

Programming Language for e-Learning

There are plenty of programming language alternatives in programming and one of them is hypertext Preprocessor (PHP) which is a platform independent structure and can run on any platform such as; Linux, Unix, Mac OS X, Windows, etc.

Freelancer.com is one of the most advanced platforms and market leaders for computer based software development and distribution [5]. The web page aims to bring together more than fourteen millions of freelance software developers all over the world. Freelancer.com states that PHP has major importance and magnitude for software development steps, application writing, data processing and engineering designs. It was reported that, more than 2 million projects were created related to PHP only since 2001 (almost 67% of the completed projects). The second large programming language is the JavaScript followed by .NET and C/C#/C++. The number of projects using Perl, Python, and Ruby on rails is relatively small compared to all other programming languages as shown in the Figure 4.

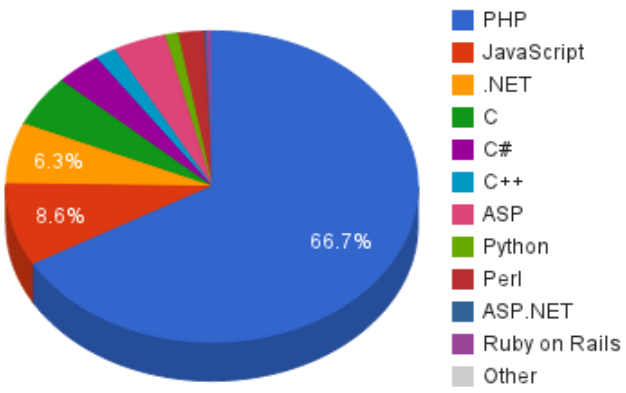

Figure 4: Programming languages global distribution in freelancer.com [6].

PHP is a rapid application development language specifically designed for websites and web applications. It is a server side scripting language that is extensively used to create dynamic web pages by embedding the PHP code into the HTML source

document. It is also a general-purpose programming language. The structure of PHP supports client-server based Cloud Language. It is a dynamic interpreted language, which reduces programmer's time to compile and deploy the project as being part of a rapid application development system. PHP itself is an open source code language. The complete code of PHP is open and the developers, who wish to benefit from the open source codes, can use it free.

It provides different platforms, which is truly platform independent where developers can develop their programs on a windows operating system and run it on a Linux system. The power of platform independence also does not result any loss of performance. PHP, besides, is Platform Independent and compatible with a whole series of Web Servers; not strictly limited to any company's monopolistic strategies.

Because of its widespread usage, worldwide accessibility, web page specific infrastructure, open source codes, free development tools, operating system, e-device and platform independent structure, PHP programming language is chosen in this thesis study to prepare, implement and develop a series of software applications.

Available Computer tools for Ultrasound education

There are plenty of commercial products and many highly developed professional ultrasound simulators for the medical centers, hospitals and for the education of medicine students. These kind of applications provide an infrastructure to implement variety of scenarios and to setup unlimited realistic practices before the usage on the patients. They have their own computer, hardware, software and other equipments like probes or mannequins like Medsim's UltraSim [7] or Sonosim [8].

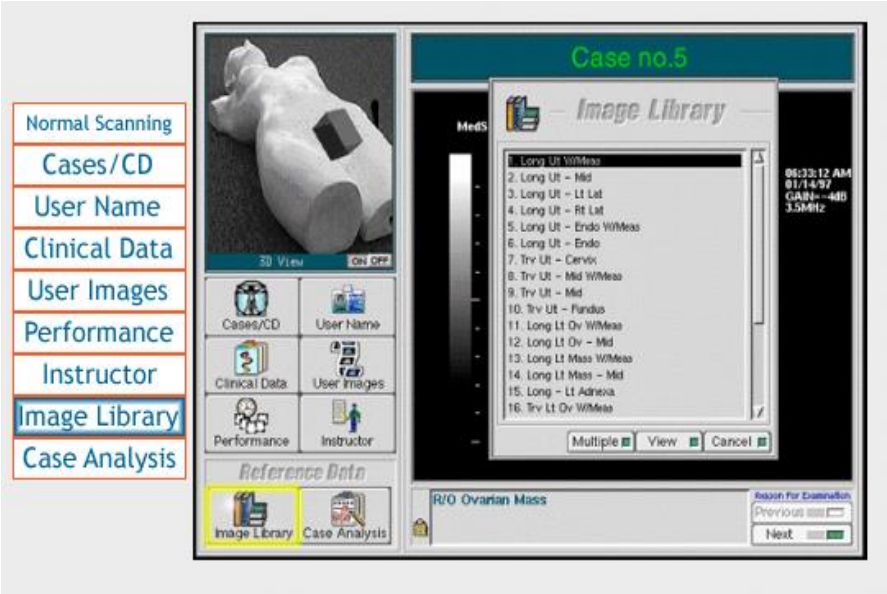

Figure 5: Some screens and menus of an ultrasound simulator Ultrasim [7].

UltraSim has professional expansions and educational modules for the purpose of usage such as Abdomen, Obstetrics, Gynecology, Breast, Vascular and Pelvic modules. The aim of this kind of professional simulations are mostly measure, monitor, improve student skills and progress, identify weaknesses and provide focused critique during practice sessions and educate ultrasound professionals [7].

If the aim of the simulator is not to educate an ultrasound technician with professional tools, but to provide the engineering background of ultrasound theory then there are very rare online applications or simulations available. Non Destructive Testing (NDT) [9] is an organization, which mainly consists of Iowa State University, and four Midwest colleges who work in the Nondestructive Testing domain. NDT allows parts and material to be inspected and measured noninvasively. NDT technicians and engineers define and implement tests that locate and characterize material conditions and flaws that might otherwise cause planes to crash, reactors to fail, trains to derail, pipelines to burst, and a variety of less visible, but equally troubling events. Although NDT do not focus on the field of biomedical imaging, they also have some Ultrasonic Testing (UT) applications and simulations in material science to detect imperfections or to locate changes in material properties.

Some Java based Ultrasound Simulations prepared by NDT Group can be shown in Figures 6, 7 and 8, which are publicly available at https://www.nde-ed.org.

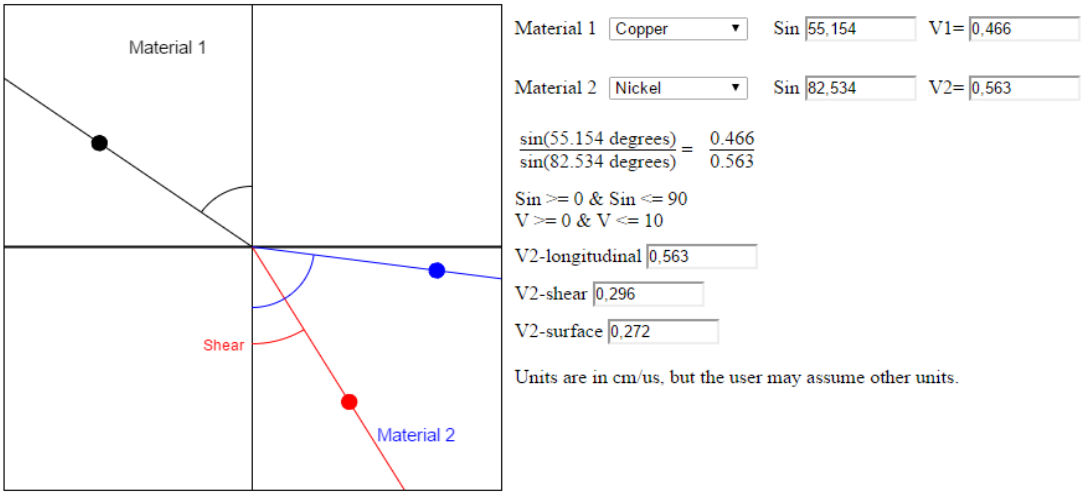

Figure 6: Java based Snell's law application of NDT organization [9].

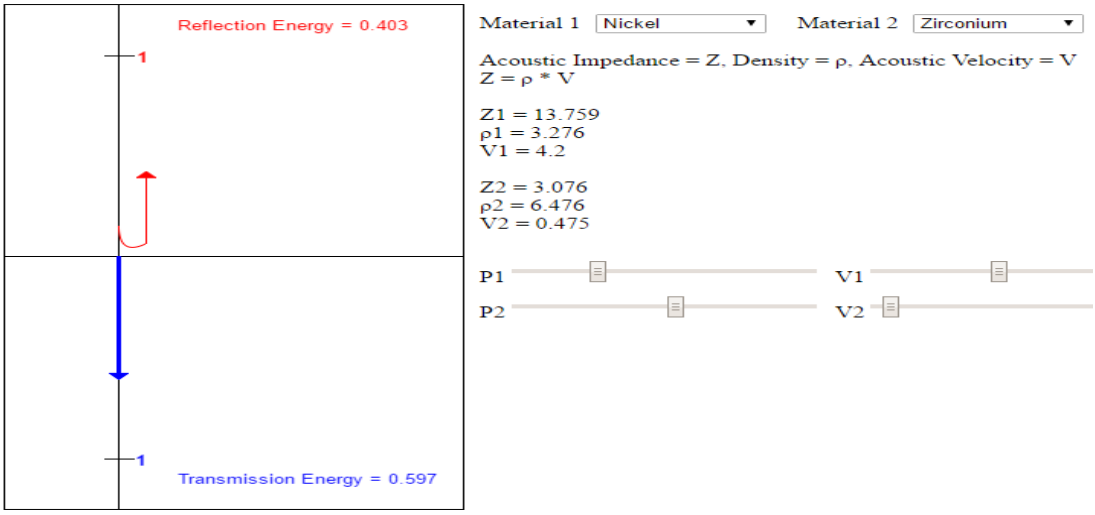

Figure 7: Java based acoustic impedance application of NDT organization [9].

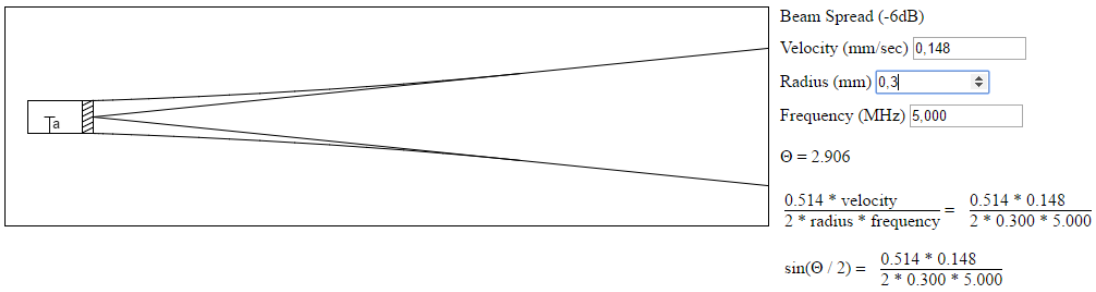

Figure 8: Java based transducer beam spread application [9].

Other ultrasound applications, which were coded using MATLAB, are also available. Abersim team from the Norwegian University of Science and Technology (NTNU) prepared a code named as Abersim toolkit. It simulates 3D nonlinear acoustic forward wave propagation through an attenuating medium. It was designed to be used in the field of medical ultrasound imaging. Although it was coded with "C" language for efficiency and quickness, it also has a MATLAB interface for visualization, pre and post processing [10].

FOCUS is an ultrasound simulator designed to simulate ultrasound waves in a variety of media, which calculates the pressure fields generated by single transducer and phased arrays. The Fast Nearfield Method (FNM) of FOCUS is used for calculating pressure fields near the transducer face (Figure 9), and the Angular Spectrum Approach (ASA) is used to quickly calculate the far field pressure [11].

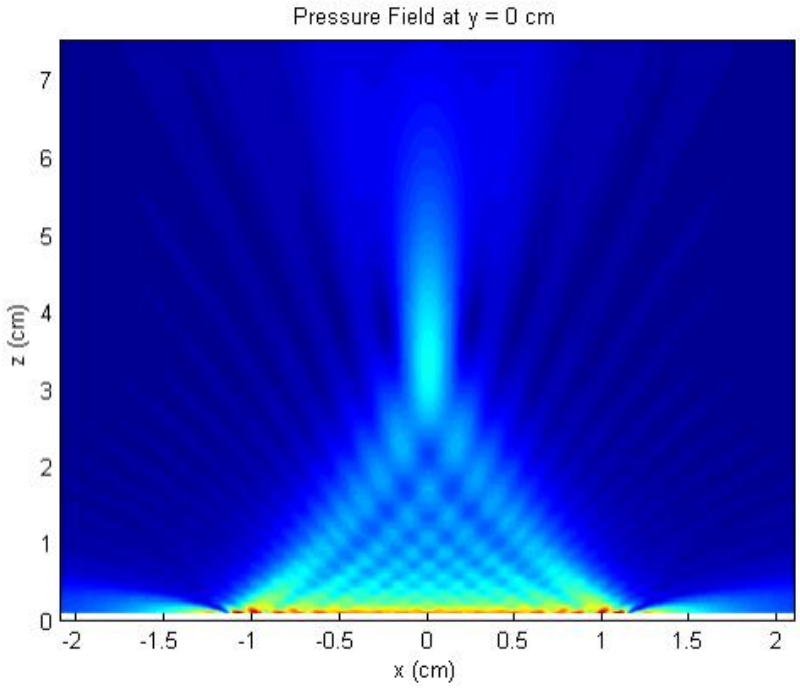

Figure 9: Pressure field distribution diagram from FOCUS simulation [11].

Another ultrasound simulator is named as Simsonic. It is based on the finite-difference time-domain (FDTD) computations of the electrodynamic equations. The SimSonic suite consists of several compiled programs and C source codes and capable to solve two-dimensional (2D) and three-dimensional (3D) electrodynamic equations [12].

k-Wave is another means (an open source MATLAB toolbox) that can be used for education. It was designed for the time-domain simulation of acoustic waves in one-dimensional, 2D, or 3D bodies. It is an advanced numerical model that can be used for the analysis of linear or nonlinear wave propagation. An arbitrary distribution of material properties can be assigned while employing power law acoustic absorption [13]. The model was optimized for speed and accuracy in solutions.

A brief comparison of some of the ultrasound simulators is given in Table 1.

Table 1: Ultrasound simulators comparison table

Tool Name	Main Developer	Some Usage	Field	Rendering Method	Programming Language	Device / OS Dependence
Ultasim	Medsim Inc.	Complate ultrasound system simulator.	Biomedical	On device	Own OS	Yes
NDT	NDT- Group Iowa State University	Magnetic Particle Testing (MT), Penetrant Testing (PT) Visual and Optical Testing (VT), Acoustic Emission Testing (AE).	Biomedical Industrial	Client Side	Java	Yes
Simsonic	Emmanuel Bossy	Simulation of ultrasound propagation, based on finite-difference time-domain (FDTD) computations of the elastodynamic equations.	Biomedical	Client Side	C MATLAB	Yes
Abersim	Aberteam NTNU	3D nonlinear acoustic forwar wave propagation through ar attenuating medium.	Biomedical Industrial	Client Side	C MATLAB	Yes
FOCUS	Michigan State University	Continuous and transient wave ultrasound simulator designed to simulate ultrasound. waves in a variety of media.	Biomedical	Client Side	C MATLAB	Yes
k-Wave	k-Wave.org	Complate ultrasound system simulator.	Biomedical Industrial	Client Side	C MATLAB	Yes

In this thesis study, the open source k-Wave simulation toolbox is selected for simulation studies. The rationale in the selection process is itemized as follows: 1) it is user friendly, 2) several functions of this toolbox can be called using MATLAB scripts, 3) an arbitrary body geometry (1D, 2D or 3D) and heterogeneity can be assigned, 4) it is fast and accurate, 5) it is well documented with a number of examples, and 6) it is still under development,

1.1 Scope Of This Thesis Study

In this thesis study, a series of interactive computer applications are prepared to assist education in the field of medical ultrasound. To improve these applications, a simulation toolbox is employed to simulate ultrasound propagation for various source and body geometries. In addition, ultrasound phantoms are prepared and experimental studies are conducted using a commercial ultrasound system. The scope of this thesis study can then be itemized as given below:

- To prepare computer applications for the education of ultrasound, based on theoretical calculations,
- To simulate ultrasound waves in biological tissues based on k-Wave toolbox,
- To prepare phantoms mimicking acoustic properties of biological tissues,
- To conduct experimental studies using the developed phantoms.

1.2 Thesis Organization

Chapter 2 is on the principles of ultrasound. Ultrasound wave equation, transmission, reflection, refraction, scattering of ultrasonic waves, and attenuation properties of body tissues are presented in this chapter.

Chapter 3 introduces nine computer applications prepared using PHP language. Applications include the following basic topics: transmission of ultrasound waves, reflection of echoes, tissue absorption and acoustic attenuation properties of tissues, transducer characteristics and piezoelectric material types, near field and far field calculations, diameter and frequency response of transducers, transducer design principles, Doppler Effect and blood velocity calculations.

Chapter 4 introduces k-Wave toolbox and simulation results for different body (geometry and acoustic properties) and source configurations.

Chapter 5 is on experimental studies conducted using tissue mimicking phantoms. First, phantom preparation methodology is introduced. Next, experiments conducted using a commercial ultrasound system with 16 channel phased array transducer are

presented. The pulse-echo signals acquired using the experimental system and calculated using k-Wave toolbox are comparatively displayed.

CHAPTER 2

ULTRASOUND THEORY

This chapter is prepared to describe the basics of the ultrasound theory. Basics of ultrasound mechanism, ultrasound physics and formulations of ultrasound phenomena is discussed here. This chapter also aims to give an overview about ultrasound starting from the beginning. The idea of emitting sound waves in a medium and observing its echo is elaborated including its history, background physical phenomenon, formulations, advantages and usages in daily routine.

2.1 Basics Of Ultrasound

Ultrasound is similar to the other audible soundwaves in its physical properties, except that humans cannot hear it. The range varies from person to person but in general, human ear can detect the frequencies between 20 Hz to 20 kHz (Figure 10). Ultrasound is defined by the American National Standards Institute as "sound at frequencies greater than 20 kHz." Ultrasound devices operate with frequencies from 20 kHz up to several gigahertzes.

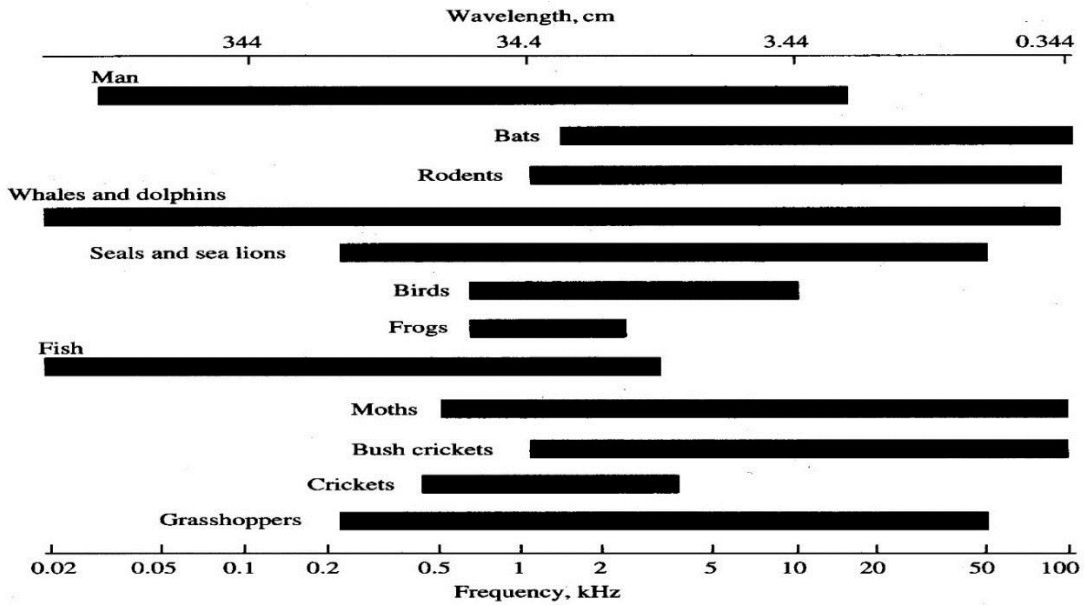

Figure 10: Animal sensitivity to sounds at different frequencies [14].

2.2 History Of Ultrasound

The origins of sonography can go back to the ancient Greek philosophers. Pythagoras (c.570–c.495 BC) who conducted experiments on the sounds produced by vibrating strings and invented the so-called Sonometer to study sounds [15]. In addition, Aristotle (384–322 BC) discovered that the propagation of sound requires a medium. and studied how its properties affect the transmission [15].

In a paper given in 1842, Austrian physicist Christian Doppler described the change in frequency of a wave (or other periodic event) for an observer moving relative to its source. However, the first milestone towards modern ultrasonography was achieved by Pierre Curie (1859–1906) and Jacques Curie (1856–1941) by the discovery of the piezoelectric effect. This phenomenon describes the creation of electric potential by compression of crystals and the reverse process, crystals deforming upon applying electrical charge [15]. Ultrasound can be generated by a so-called transducer that converts electrical energy into acoustic and vice versa. The discovery of the piezoelectric effect and materials made it possible to develop ultrasound transducers.

A transducer is made of piezoelectric materials that deform when an electric signal is applied and produce a potential when deformed mechanically [16].

Underwater sonography, gained major momentum after the sinking of the Titanic (1912) and World War I (1914). After all, it was the French physicists Paul Langevin (1872–1946) and the Russian researcher Constantin Chilowsky (1880–1958), who developed a high frequency ultrasonic echo-sounding device called 'hydrophone' that allowed to detect underwater objects and submarines [17]. This technique, sound navigation and ranging (SONAR), finally became practical during World War II. Industrial uses of ultrasound began in 1928 with the suggestion of Soviet Physicist Sokolov that it could be used to detect hidden flaws in materials. Medical uses of ultrasound through the 1930s were confined to therapeutic applications such as cancer treatments and physical therapy for various ailments. Diagnostic applications of ultrasound began in the late 1940s through collaboration between physicians and engineers familiar with SONAR [18].

2.3 Medical Ultrasound

Ultrasound signals and resulting data reflected waves can also be used for medical diagnostic and imaging purposes. Detected echoes allow the monitoring and examination of different body tissues using high frequency ultrasound waves. This technic is capable of producing real-time images of soft body tissues and even can be used to show 3D organs, fetus movement during pregnancy or blood flow in the vessels.

The ultrasound image is obtained using the reflected waves from the soft body tissues. The amplitudes of the echo signals and the traveling times of the ultrasonic sound wave through the body provide the necessarily information to reconstruct an ultrasound image.

A handheld portable device called *probe* or *transducer* produces ultrasonic sound waves using the piezoelectric effect. Created ultrasound waves travel through soft

body tissues and reflected waves captured by two-way transducers. The transducer converts the echoes into electrical signals and by means of an algorithm an image is constructed and displayed on a screen. High frequency ultrasonic imaging (Figure 11) has found many applications in clinical and preclinical imaging [19].

Although some research on mice states that ultrasound signal exposure can cause lung damage [20], ultrasound is known as non-invasive, relatively safe and advantageous imaging technique compared to the other medical imaging methods [21].

Using abdominal ultrasound applications, organs and soft body tissues such as liver, pancreas, kidneys and spleen can be examined and imaged, fat, tumor, bone and gas in the body can be differentiated. Obstetric ultrasound images monitor unborn baby's health, sex and potential problems during pregnancy. Another usage of ultrasound, which is called Doppler ultrasound, measures blood flow, blood pressure and shows blocked veins in the body.

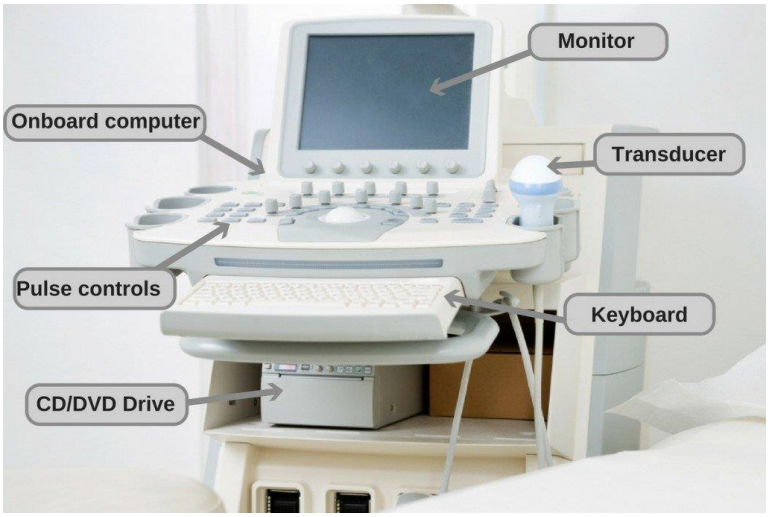

Figure 11: An ultrasound imaging system and its components [22].

2.4 Diagnostic And Therapeutic Ultrasound

Diagnostic ultrasound is a medical imaging technique, which uses high frequency pulse-echo algorithms to evaluate images of structures inside the body. These are non-invasive, low power (<100 mW/cm^2), high frequency (1–10 MHz) techniques. Acoustic waves used for diagnostic applications are so low in intensity or power that they do not impart change to the physicochemical properties of the tissue [23]. The amount of energy that reaches a specific site is dependent upon characteristics of the ultrasound (frequency, intensity, and amplitude, focus and beam uniformity) and the tissues through which it travels [24].

Ultrasound is also used in the medical industry as a therapeutic tool. Low intensity (~1 W/cm^2) ultrasound is used as a deep-heating agent and ultrasound with higher intensities (~10 W/cm^2) can be used to treat oncological diseases. Finally, significantly higher power intensities (10^3 W/cm^2) are used in short duration pulses to modify body tissues [23].

In pulse echo ultrasound imaging systems, different frequency ranges are used for examination of different parts of the body. For example, operation frequencies of 3–5 MHz are used for abdominal areas. Frequency range 5–10 MHz is used for small and superficial parts. For the skin or eyes frequencies rise up to 10–30 MHz [25]. Therapeutic ultrasound works at higher frequency ranges and used mainly for pain treatment or to increase the effect of drugs on the cured tissue. Internal body tissues can be stimulated by mechanical and thermal approaches employing ultrasound's heating and vibrating effects [26].

2.5 Ultrasound System Parameters

Ultrasound imaging systems include detection, calculation and display of acoustic echo signal energy reflected from different tissues within the body. Different tissue

structures in the body have different ultrasonic parameters that causes the ultrasound signal scatter, transmit or reflect.

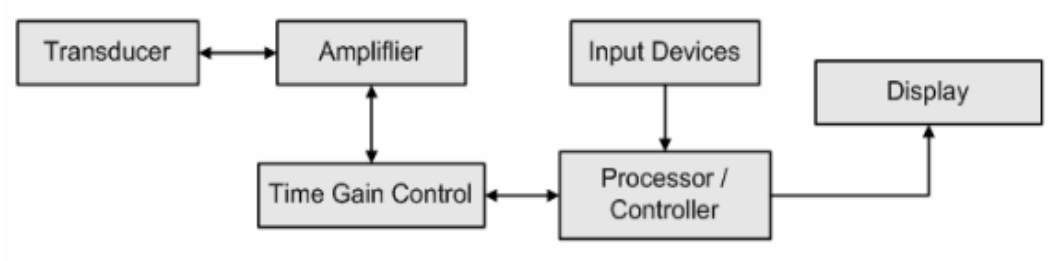

Figure 12: Block diagram of pulse echo ultrasound imaging system [27].

Figure 12 shows the block diagram of a pulse echo imaging system. The system basically consists of transducer, amplifier, time gain control unit, processor and a display [27].

2.5.1 Ultrasound Wave Equation

While an ultrasound exposure propagates through the soft body tissues, it results in a sinusoidal vibration, compression and rarefaction inside the medium. The amplitude of a wave can be expressed as peak excess pressure (Pa) that is the maximum difference between the rest pressure in the medium and the pressure induced by the wave [28]. Basics of the wave equation terminology and formulations can be found elsewhere [29].

Conservation of mass and Newton's Second Law simplifies the wave equation in the case of an ideal, homogeneous medium and in one-dimensional case the following wave equation is obtained:

$$\frac{\partial^2 U}{\partial X^2} = \frac{1}{C^2} \cdot \frac{\partial^2 U}{\partial t^2} \tag{2.1}$$

Where *c* is the speed of sound and the term *U* symbolizes any physical property that characterizes the propagation of perturbation [29]. For example, the acoustic pressure as a function of location (*x*) and time (*t*). Here $U = U\ (x \pm ct)$ and (+), (–) signs represents the direction of the wave movement.

The linear acoustic wave equation is obtained under three basic condition. First, the medium is assumed as compressible, second, the medium has inertia and the third, acoustic parameters of the medium effects the propagation. This relation is expressed as an equation of state or pressure-density relation [30]. Customizing the wave equation into the three dimensional medium gives

$$\nabla^2 U = \frac{1}{C^2} \cdot \frac{\partial^2 U}{\partial t^2} \tag{2.2}$$

Fourier series solution says that any wave similar function can be represented as sum of simple periodic trigonometrical functions. Complex exponentials could also be used as a solution due to Euler's identity. Therefore,

$$\mathrm{U} = Ae^{j[\omega t - kx]} = \mathrm{A}\big[\cos(\omega \mathrm{t} - \mathrm{kx})\big) + \mathrm{j}\sin(\omega \mathrm{t} - \mathrm{kx}))] \tag{2.3}$$

where angular frequency is

$$\omega = 2\pi f = \frac{2\pi}{T} \tag{2.4}$$

Here, *k* is called wave number and calculated from harmonic wave equations as

$$k = \frac{2\pi}{\lambda} \tag{2.5}$$

2.5.2 Transmission, Reflection and Refraction

One of the most important acoustic properties, which makes it possible to obtain biomedical images, is reflection and refraction. While an ultrasound signal travels

through two mediums with different acoustic properties, some of its energy is transmitted into the second medium and some of its energy is reflected back or redirected in different directions (Figure 13). Reflected waves are called echo signals. The signal detection probability and ultrasound echo quality at the transducer side increases when the incident angle converges to the normal of the boundary [31].

Snell's Law describes the reflection and refraction characteristics of ultrasound (will be examined in detail in Chapter 3).

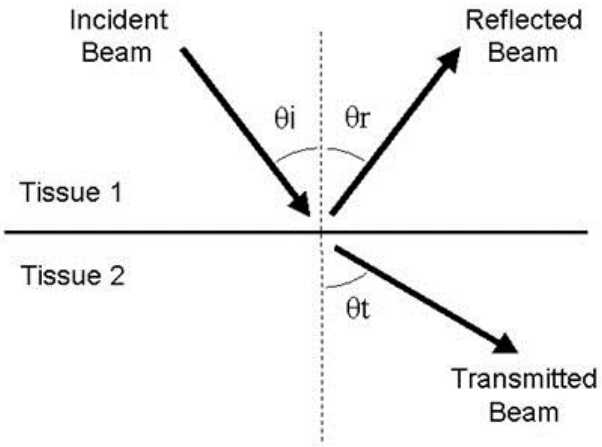

Figure 13: Reflection and transmission conditions [34].

In the Figure 13, θ_i, θ_r and θ_t represents the angles of incident, reflected and transmitted beams respectively. In addition to transmission, reflection and refraction there are different interactions that effect the ultrasound imaging such as scattering and attenuation [34].

2.5.3 Scattering

While reflection takes place at interfaces of infinite size, scattering takes place at small objects with dimensions much smaller than the wavelength [32]. The scattering from particles much less than a wavelength is normally referred to as Rayleigh scattering. Reflection actually is an important example of specular scattering [33].

Scattering means that the part of the incident wave that is reflected will be spread or scattered over a large range of angles [34].

Ultrasound transducers are developed to detect also very low-level scattered echoes. At biomedical imaging, scattering can be observed in most of the human tissues especially in blood, where the red blood cells have much smaller diameter than the wavelength of clinical ultrasound range [32].

2.5.4 Attenuation

The incoming ultrasonic signal, which propagates in the soft body tissues, is attenuated because of ultrasound absorption, reflection, refraction and scattering concepts. Amplitude, energy or intensity of the pressure wave decreases during transmission and the signal fades down according to ultrasonic parameters of tissue. This lost energy is converted to heat that causes the unwanted effects of ultrasound [35].

Reflection and refraction losses at tissue interfaces depend on the impedance mismatch at the interfaces [36]. In general, the acoustic pressure amplitude and intensity amplitude of ultrasound signal decreases exponentially during signal propagation and for most of the mediums, attenuation linearly depends on signal frequency.

CHAPTER 3

PHP APPLICATIONS FOR MEDICAL ULTRASOUND

This chapter is prepared to introduce the applications related to basics of ultrasound physics. Basic relations are converted into a series of ultrasound applications by means of PHP based online codes. The main purpose of generated applications is to show the acoustic parameters and ultrasound phenomena in visual way and to develop in-class student interaction. One can reach the applications from all over the world using World Wide Web and can regenerate the different conditions or repeat the virtual experiments using online PHP based applications.

Following eight applications are dedicated to assist students comprehend the ultrasound theory. Different tissue types are examined to understand the acoustic parameters and ultrasonic conditions inside the body. Exact formulations and relations are applied into the codes to get information and to show realistic images and diagrams. RGB codes of tissue color used in applications was chosen according to the Slicer Group's generic anatomy colors work for medical image computing to obtain realistic visuals [38].

Throughout the applications, transmission of ultrasound signal and reflection of echoes inside the body are studied, tissue absorption and acoustic attenuation conditions examined while an ultrasound wave travels through the body. Transducer characteristics and piezoelectric material types, near field (Fresnel Zone) and far field (Fraunhofer Zone) calculations, diameter and frequency response of transducer and transducer design topics also given in the form of PHP applications. Some other ultrasound applications also prepared such as Doppler Effect and blood velocity

calculations. Finally, using ultrasound formulations and developed software background, A-mode ultrasound and the image generation process related applications prepared to understand the biomedical imaging modalities and whole ultrasound system.

3.1 Application 1: Snell's Law

When an ultrasonic wave passes obliquely between two materials with different acoustic properties, its direction and speed are changed. The beam direction is bent and reflection occurs.

The wave returning to the first material is called as reflected wave (or echo) and the wave traveling into the second material is called as transmitted wave (or refracted wave). When an ultrasound wave encounters the interface between two materials, the refracted wave into the second material is moving faster or slower according to the materials' acoustic parameters and this causes the wave to bend. Snell's Law explains the relation between velocity of ultrasound and travel direction as follows:

$$\frac{C_1}{\sin\theta_i} = \frac{C_2}{\sin\theta_T} \tag{3.1}$$

where C_1 and C_2 are the ultrasound speed of waves in the two mediums respectively, θ_i is the angle of incidence and θ_T is the angle of transmission which are measured relative to the normal to the boundary.

Since Snell's law is directly related to the incident angle and the velocity of sound inside the tissue, prepared application needs to use sound speed database to calculate and draw the transmission angle and direction of propagating wave. For different tissue types, Table 2 is used as a database file.

Table 2: Sound speed - tissue/material type relations [29], [37].

Tissue Type	**Sound Speed m/sec**
Lung	950
Fat	1450
Water	1480
Brain	1550
Spleen	1565
Kidney	1570
Heart	1570
Blood	1575
Muscle (along the fibers)	1575
Muscle (across the fibers)	1590
Liver	1590
Eye	1650
Skin	1730
Bone axial (shear waves)	2800
Bone axial (longitudinal waves)	4080

Generated codes also paint and display the tissue fields in accordance with realistic tissue colors. Color code table (Table 3) is used to pick futuristic RGB colors.

Table 3: RGB color codes of tissue types used in applications from Slicer Group [38].

Tissue Type	RGB Codes
Lung	rgb(197,165,145)
Fat	rgb(230,220,70)
Brain	rgb(250,250,225)
Spleen	rgb(157,108,162)
Kidney	rgb(185,102,83)
Heart	rgb(206,110,84)
Blood	rgb(216,101,79)
Muscle	rgb(192,104,88)
Liver	rgb(221,130,101)
Eye	rgb(194,142,0)
Skin	rgb(177,122,101)
Bone	rgb(241,214,145)

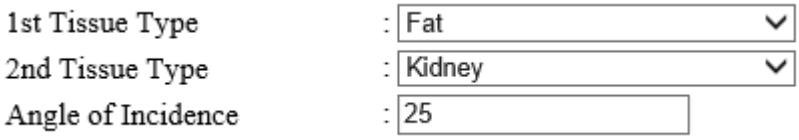

Figure 14: Data input screen of Application 1.

In the first application, one can choose the tissue types from push menu buttons and enter in the angle of incidence as degrees from the page above. After data input completion application runs, automatically calculates tissue conditions, acoustic relations and Snell's Law, builds the tissue structure and color then finally prints out the resulting relations as an interactive tool.

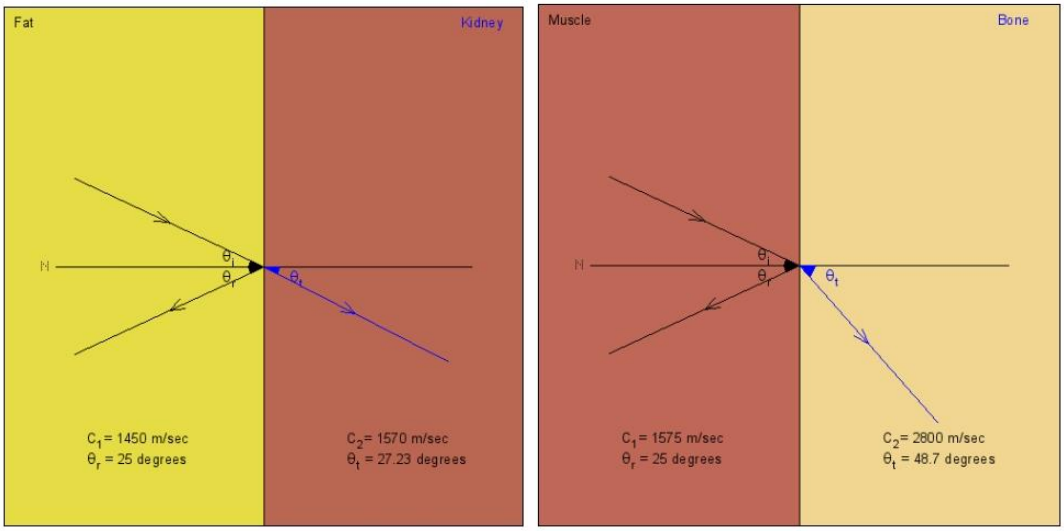

Figure 15: Results of Application 1: Snell's law. (left) Result for conditions as given in Figure 14. (right) Muscle-bone condition to show the transmission angle more clearly.

3.1.1 Critical Angle

If an ultrasound wave passes obliquely from one media to another media that has different acoustic properties, then part of its energy is reflected. The incidence angle will be equal to the reflection angle. The remaining energy will penetrate the second medium in the form of transmitted wave.

If we increase the angle of incidence, then the transmission angle also increases. According to the Snell's law, for a specific incidence angle no ultrasound energy is transferred to the second medium and we obtain θ_T =90°. For this incidence angle, the transmitted wave can only move along the boundary. The incidence angle at which refraction causes no ultrasound to enter in the second medium is called as the *critical angle* θ_C. By means of Snell's law (θ_T=90°)

$$\theta_c = \sin^{-1}[\frac{c_1}{c_2}] \tag{3.2}$$

Application 1 calculates the critical angle for different tissue types and prints them out automatically if available. Generated software behaves properly if angle of

incidence is above or below from the critical angle. If critical angle is not available, (ultrasound wave speed inside the first medium is much greater than the second medium) then application prints out NAN instead of critical angle.

For example, for Brain to Bone transition, the critical angle is calculated and printed as 22.32 degrees which is actually $\sin^{-1}(1550/4080)$. If angle of incident is greater than the critical angle, then no ultrasound signal can pass into the bone region.

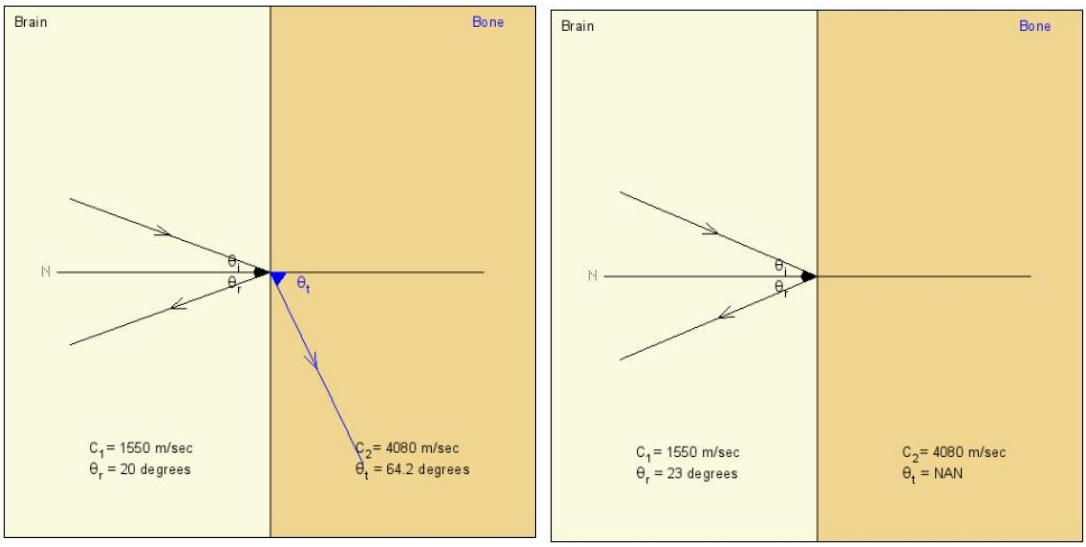

Figure 16: Results of Application 1: Critical angle. Critical angle is 22.32 degrees. Left figure shows the case when $\theta_i < \theta_C$, right figure shows the case when $\theta_i > \theta_C$.

3.1.2 Reflection and Transmission Coefficients

Different tissue types have different acoustic properties. The speed of ultrasound "c" in the medium and the density of the medium "ρ" are characteristically values and their product gives an important property for ultrasound imaging, which is defined as acoustic impedance and formulated as $Z = \rho c$.

For an ultrasound wave incident perpendicularly upon an interface, the pressure reflection coefficient (R_p) and the transmission coefficient (T_p) is found by using the

boundary conditions that the pressure and particle velocity should be continuous across the boundary [39].

$$R_\rho = \frac{Z_2 - Z_1}{Z_2 - Z_1} \qquad T_\rho = \frac{2Z_2}{Z_1 + Z_2} \qquad T_\rho = R_\rho + 1 \tag{3.3}$$

where Z_1 and Z_2 are the acoustic impedances of the two media respectively.

The continuity of velocity and pressure states that the normal components of the ultrasound velocity and pressure must be equal on both side of the interface. So the reflection and the transmission coefficients can be written as follows under oblique incident conditions [4]

$$R(\theta_i) = \frac{\rho_2 c_2 \cos(\theta_i) - \rho_1 c_1 \cos(\theta_t)}{\rho_2 c_2 \cos(\theta_i) + \rho_1 c_1 \cos(\theta_t)} \tag{3.4}$$

$$\mathrm{T}(\theta_\mathrm{i}) = \frac{\rho_2 c_2 \cos(\theta_i)}{\rho_2 c_2 \cos(\theta_i) + \rho_1 c_1 \cos(\theta_\mathrm{t})} \tag{3.5}$$

Application 1 also calculates reflection and transmission coefficients even for the oblique conditions. Total output of Application 1 is as follows for Heart to Blood transition when $\theta_i = 23°$.

1st Tissue Type : Heart

2nd Tissue Type : Blood

Angle of Incidence : 23

Calculate

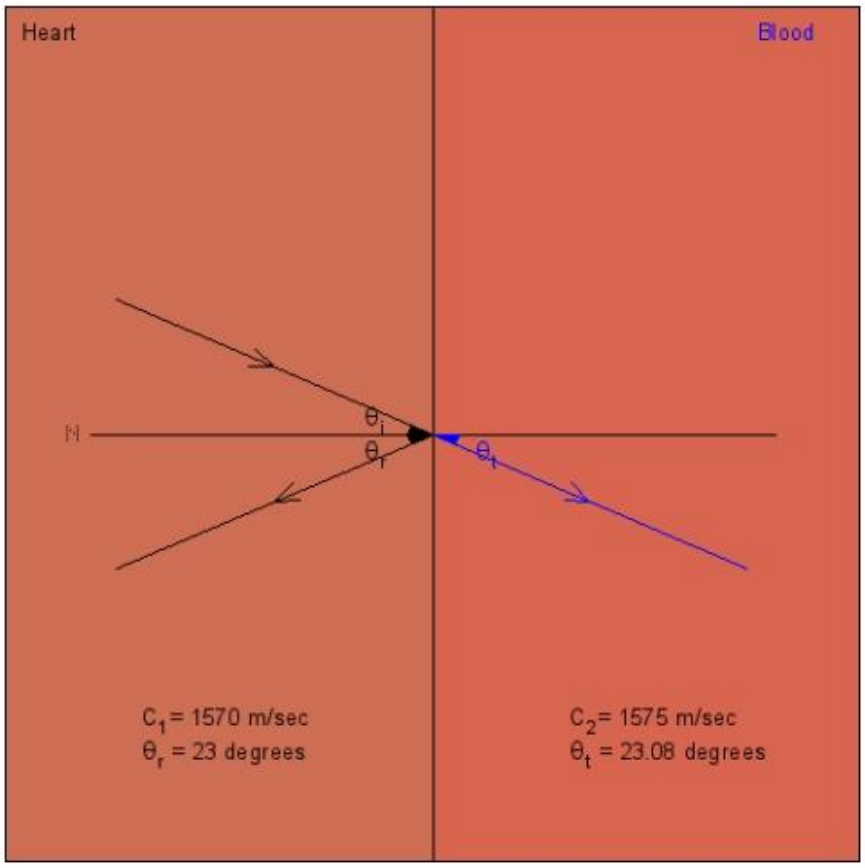

Critical Angle : 85.33

$$R(\theta_i) = \frac{\rho_2 c_2 \cos(\theta_i) - \rho_1 c_1 \cos(\theta_t)}{\rho_2 c_2 \cos(\theta_i) + \rho_1 c_1 \cos(\theta_t)} = 0.00636$$

$$T(\theta_i) = \frac{2\rho_2 c_2 \cos(\theta_i)}{\rho_2 c_2 \cos(\theta_i) + \rho_1 c_1 \cos(\theta_t)} = 1.00636$$

Figure 17: Results of Application 1: Input, output and calculations of Application 1 for heart-to-blood transition.

Note that T - R=1, and this direction dependent relation is formulating the energy conservation.

3.2 Application 2: Multiple Tissue Transmission

If there are more than two cascaded media -like inside the real human body-, the same Snell's rule, reflection and transmission calculations affect the incoming wave. Each different tissue type changes the direction and amplitude of the ultrasound according to its acoustic properties. New transmission, reflection angles and coefficients are calculated using acoustic impedance of every tissue and angle of incidence. This process continues for every transition layer one by one.

3.2.1 Amplitude Reflection and Transmission Coefficients:

If we arrange the equations (3.4) and (3.5) inserting the acoustic impedance values then we obtain

$$R = \frac{Z_2 \cos\theta_i - Z_1 \cos\theta_T}{Z_2 \cos\theta_i + Z_1 \cos\theta_T} \qquad T = \frac{2Z_2 \cos\theta_i}{Z_2 \cos\theta_i + Z_1 \cos\theta_T} \qquad (3.6)$$

To calculate reflection and transmission coefficients and draw the related figures, Application 2 and 1 need to use acoustic impedance database. For different tissue types, Table 4 is used as a database file.

Table 4: Acoustic impedance - tissue type relations [29], [37].

Tissue Type	**Acoustic Impedance kg/(sec· m ^{2})] × 10 ^{6}**
Lung	0,26
Fat	1,38
Water	1,48
Brain	1,60
Spleen	1,65
Kidney	1,65
Heart	1,64
Blood	1,66
Muscle (along the fibers)	1,68
Muscle (across the fibers)	1,69
Liver	1,69
Eye	1,72
Skin	1,99
Bone axial (shear waves)	5,32
Bone axial (longitudinal waves)	7,75

For the second application, different tissue types are again selectable from the push menu buttons and angle of incidence can be entered in degrees from the interface as shown in the Figure 18.

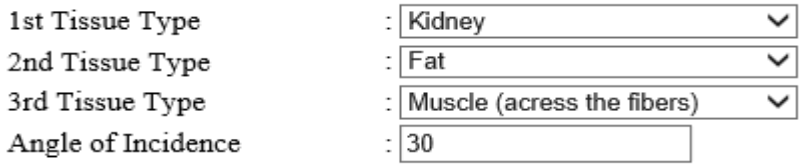

Figure 18: Data input screen of Application 2.

After completing the data input, application automatically calculates tissue conditions, acoustic relations and Snell's Law for multiple tissue condition. Application finally builds the tissue structure and prints out the resulting calculations as an interactive tool.

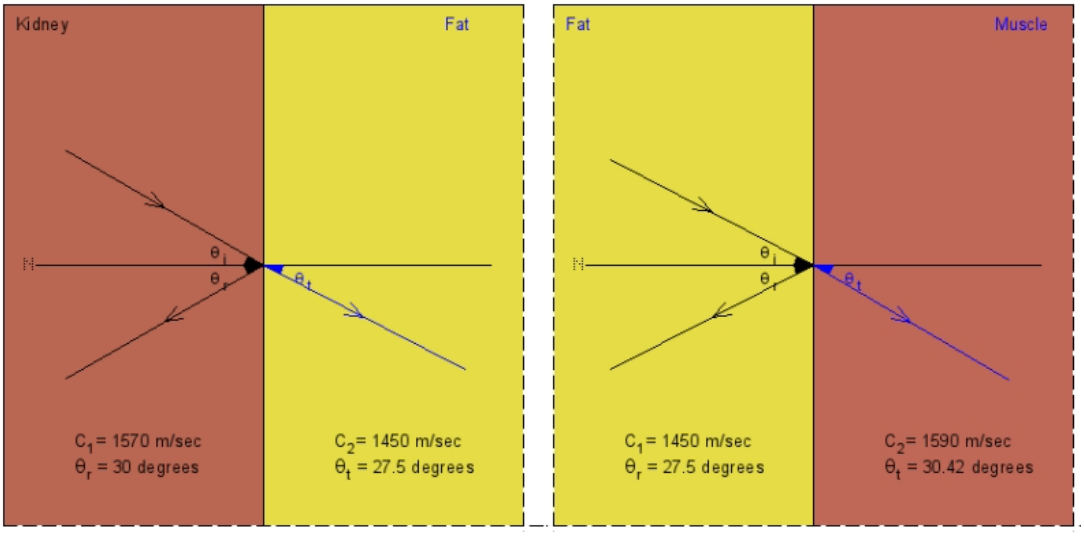

Figure 19: Results of Application 2: Outputs for the input values given in Figure 18.

3.3 Application 3: Intensity Reflection and Transmission Coefficient

Ttransmission and reflection coefficients were given in (3.6). Under special conditions where $\theta_i = \theta_T = 0$ one can obtain:

$$R = \frac{Z_2 - Z_1}{Z_2 + Z_1} \qquad T = \frac{2Z_2}{Z_2 + Z_1} \tag{3.7}$$

Above conditions also called as *perpendicular* or *normal incidence*. The pressure is related to the acoustic impedance (P = Zu) and the relation between the intensity and pressure is described as $I = P_0^2/2Z$. Intensity (W/m^2) is the amount of power through a cross-sectional area.

The intensity reflection and transmission coefficients are calculated as follows:

$$R_I = \frac{I_R}{I_i} = \frac{P_R^2}{2Z_1} . \frac{2Z_1}{P_i^2} = \frac{P_R^2}{P_i^2} = R^2 = \left(\frac{Z_2 - Z_1}{Z_1 + Z_1}\right)^2 \tag{3.8}$$

$$T_I = \frac{I_T}{I_i} = \frac{P_T^2}{2Z_2} . \frac{2Z_1}{P_i^2} = \frac{Z_1}{Z_2} . \frac{P_T^2}{P_i^2} = \frac{z_1}{z_2} . T^2 = \frac{4Z_1 Z_2}{(Z_2 + Z_1)^2} \tag{3.9}$$

Application 3 uses the relation between acoustic impedance and intensity transmission and reflection coefficients. Initial reference intensity is given as 30 W/m^2. Different tissue types are selectable from the push menu buttons and tissue width can be entered from the interface below. After completing data input application automatically calculates the transmission and reflection coefficient intensities for every different surface layer and goes on to next surface. Finally, application builds and draws the resulting calculations as an interactive tool.

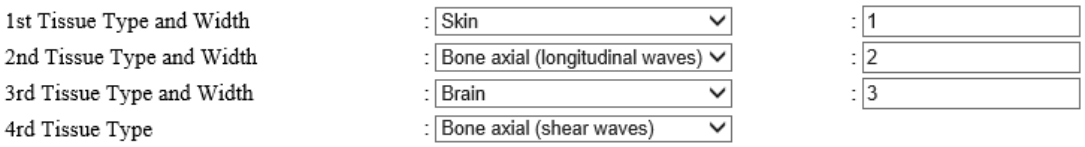

Figure 20: Data input screen of Application 3.

Application calculates the intensity reflection and transmission coefficients for every surface layer one-by-one. Output values of the first surface are used as inputs for the second surface calculations and iterations go on both for transmitted and reflected waves inside and outside direction. For example, intensity reflection coefficient I_{r3} which is actually the echo intensity from the deeper tissue, is found after 5 level of calculation. For Application 3, the attenuations inside the tissues are neglected.

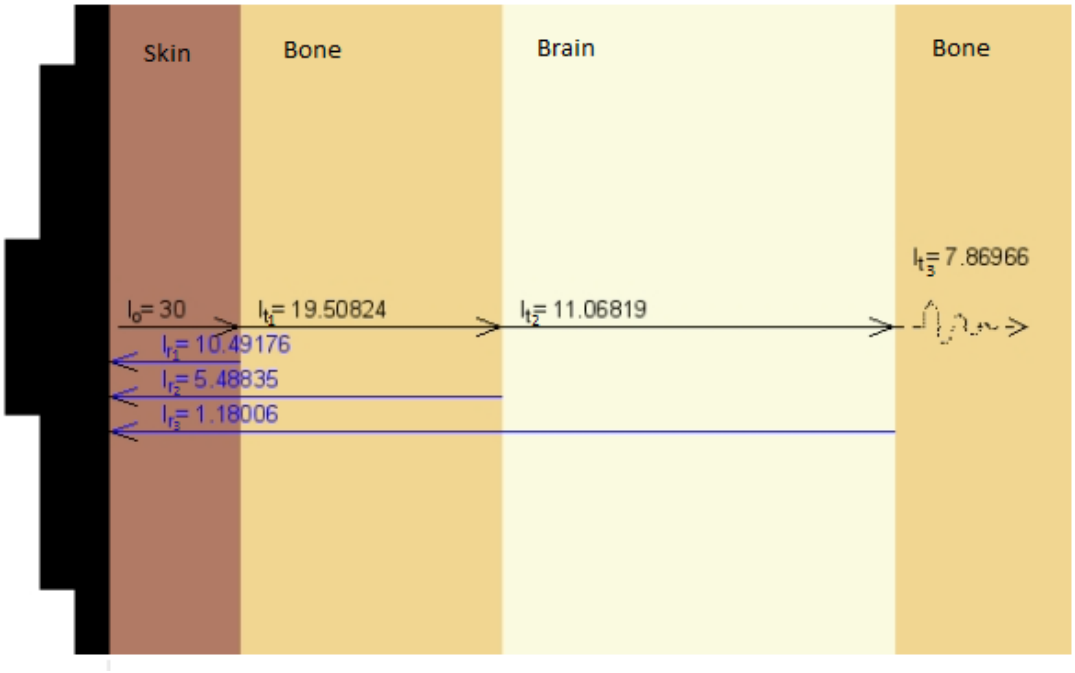

Figure 21: Results of Application 3: transmitted and reflected intensities.

Above application shows that we would only get almost 35% of the incident intensity into the brain if we were trying to use ultrasound to image the brain even for the half way. This is one reason that ultrasound is not used to image the adult brain, but it is used in infants where the skull is not yet calcified [40].

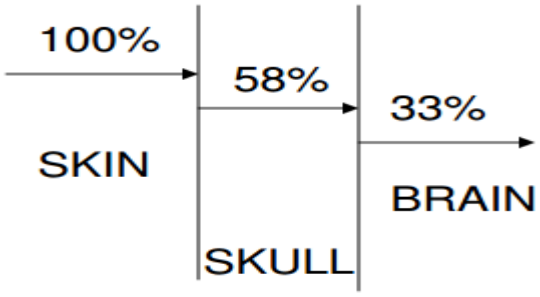

Figure 22: Intensity loss while trying to image the brain

Figure 22 is from PNT Wells [40] that completely validates the results of Application 3.

3.3.1 A-Mode Ultrasound

The simplest version of ultrasound imaging methods is A-Mode or Amplitude Mode ultrasound. Transducer generates a single narrow ultrasound beam and it goes on the straight path inside the tissues. Reflected waves are detected by the same transducer and echo positions are figured on the ultrasound screen as a function of travel distance. Scan results displayed 2D on the ultrasound screen. On the screen, *x* axis represents the depth or half way travel distance and *y* axis represents the amplitude of the scanned echo signals.

In biomedical imaging, A-mode ultrasound scan can be used to measure tissue or material length. For example, ophthalmologists can use it to measure the diameter of the eye ball or to find the optic nerve (Figure 23).

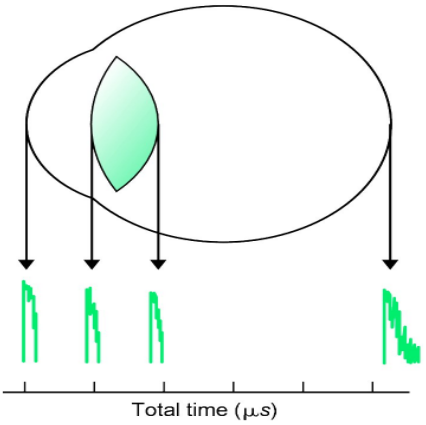

Figure 23: A-Mode Ultrasound Usage: Eye histogram uses echoes from cornea and retina surfaces [41].

Detection time difference between the two successive echo signals, which are generated on the same tissue walls, is used to calculate the thickness of that tissue. One should keep in mind that total wave distance is twice of the tissue thickness. The depth *S* is calculated as a function of ultrasound velocity in the tissue (c) and the time difference as:

$$S = c(t_1 - t_0)/2 \tag{3.10}$$

Where, t_1 and t_0 are final and initial time values respectively.

For the calculations of A-Mode Ultrasound part of the third application, attenuation inside the tissues are neglected and no gain factor (TGC) are applied at the receiver side. Physical equipment, connections or interferences are not considered. In addition, each medium is assumed homogeneous. To demonstrate more realistic plots, random Gaussian background noise is added to the application graphs as shown in Figure 24.

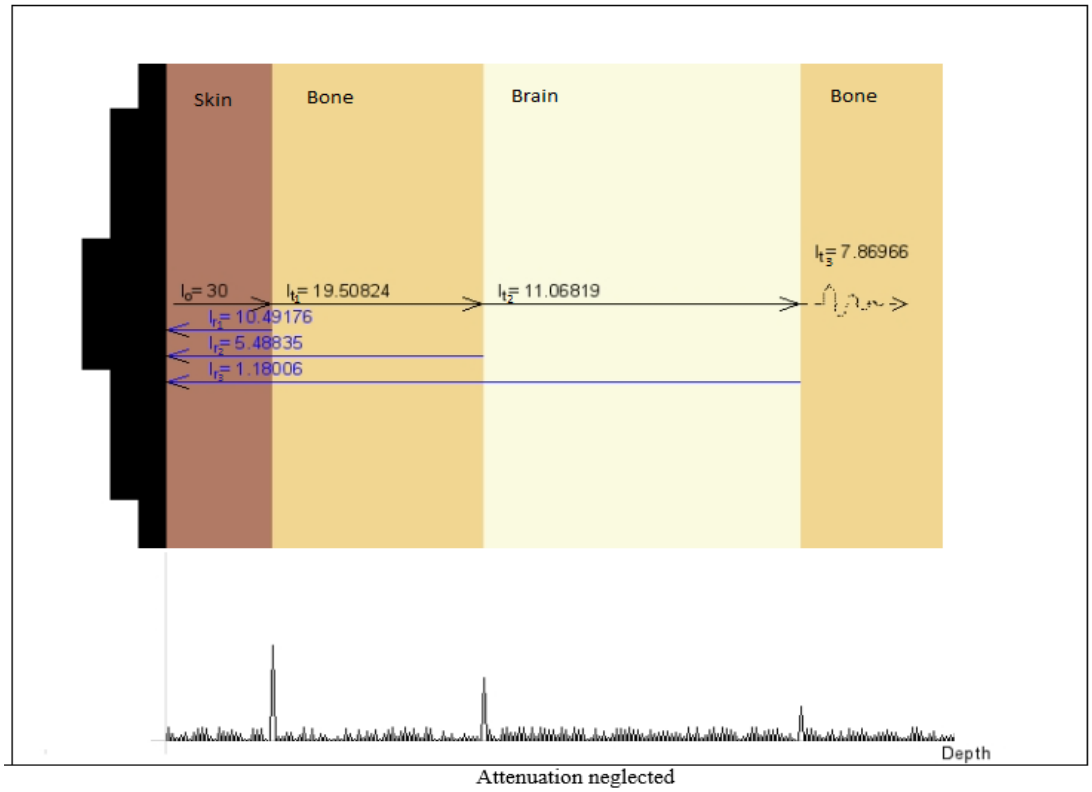

Figure 24: Results of Application 3: A-mode ultrasound response from four-layer tissue geometry. Fourth tissue is used to get the third echo and behaves as a perfect attenuator medium.

3.4 Application 4: Attenuation of Ultrasound

When an ultrasound signal travels inside a tissue some part of ultrasound energy of the signal is lost from the signal in the form of heat by reflection, scattering and absorption phenomena. This kind of energy lost in the tissue is called as attenuation.

From experimental results, we learn that the ultrasound energy of an acoustic signal which travels inside the homogeneous medium decreases with the travel distance of the ultrasound signal inside the medium. The amplitude of ultrasound signal also decreases with the travel distance. This intensity or energy decrement is exponential and loss is defined in decibels (db). The acoustic wave pressure exponentially decreases as function of travel distance and at a given distance x it is calculated using the initial value P_0 . The pressure amplitude as a function of position is given as

$$P(x) = P_0 e^{-\alpha x} \tag{3.11}$$

The attenuation coefficient α (db/cm) is a characteristic acoustic parameter and depends on the properties of the medium in which the ultrasound signal propagates. The intensity variation is expressed as

$$I(x) = I_0 e^{-2\alpha x} = I_O e^{-\mu x} \tag{3.12}$$

$$\alpha \text{ (db/cm)} = -\frac{1}{x} 10\log_{10}\left(\frac{|p|^2}{{P_0}^2}\right) = -\frac{1}{x} 20\log_{10}\left(\frac{p}{P_0}\right) = 8.686\alpha \tag{3.13}$$

For low frequency ultrasound applications, the relation between the frequency and attenuation coefficient are given as follows:

$$\alpha (f) = af^b \tag{3.14}$$

where *a* and *b* are empirical constants that depend on the tissue type. For soft body tissues, *b*=1 and attenuation increases almost linearly with the increasing frequency [29] where

$$\alpha(f) = \alpha f \tag{3.15}$$

For bone and water, the above expression is experimentally described as

$$\alpha(f) = \alpha.f^2 \tag{3.16}$$

Table 5: Relation between frequency and ultrasound attenuation coefficient. α_1 is the attenuation coefficient at 1 MHz, υ denotes the frequency [18].

Tissue	*Frequency Variation*	*Material*	*Frequency Variation*
Blood	$\alpha = \alpha_1 \times \nu$	Lung	$\alpha = \alpha_1 \times \nu$
Fat	$\alpha = \alpha_1 \times \nu$	Liver	$\alpha = \alpha_1 \times \nu$
Muscle (across fibers)	$\alpha = \alpha_1 \times \nu$	Brain	$\alpha = \alpha_1 \times \nu$
Muscle (along fibers)	$\alpha = \alpha_1 \times \nu$	Kidney	$\alpha = \alpha_1 \times \nu$
Aqueous and vitreous		Spinal cord	$\alpha = \alpha^1 \times \nu$
humor of eye	$\alpha = \alpha_1 \times \nu$	Water	$\alpha = \alpha_1 \times \nu^2$
Lens of eye	$\alpha = \alpha_1 \times \nu$	Caster oil	$\alpha = \alpha_1 \times \nu^2$
Skull bone	$\alpha = \alpha_1 \times \nu^2$	Lucite	$\alpha = \alpha_1 \times \nu$

Table 6: Attenuation coefficients for 1 MHz ultrasound used in Application 4 [18].

Material	*α (dB/cm)*	*Material*	*α (dB/cm)*
Blood	0.18	Lung	40
Fat	0.6	Liver	0.9
Muscle (across fibers)	3.3	Brain	0.85
Muscle (along fibers)	1.2	Kidney	1.0
Aqueous and vitreous	0.1	Spinal cord	1.0
humor of eye		Water	0.0022
Lens of eye	2.0	Caster oil	0.95
Skull bone	20	Lucite	2.0

Note that, during the wave propagation inside the body tissues, frequency dependency for the attenuation coefficient is governed by f^n where n is typically in the range 1.1 to 1.5 [42].

Application 4 aims to comprehend the relations between the tissue types, ultrasound frequency and ultrasonic attenuation. Tissue types, which specifies the acoustic attenuation coefficients, can be selectable from the push menu buttons and frequency values can be given manually as program inputs to analyze different conditions.

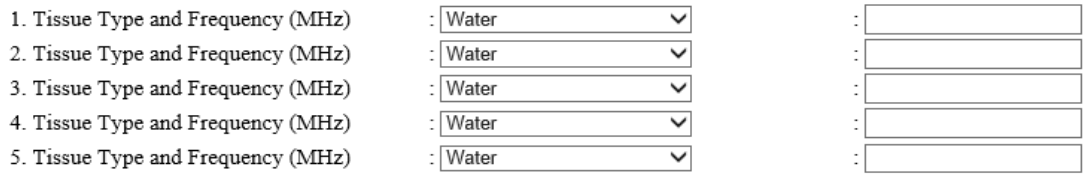

Figure 25: Data input screen for Application 4.

One can choose five different tissue or material types at once and give the frequency values between 1 to 10 MHz respectively.

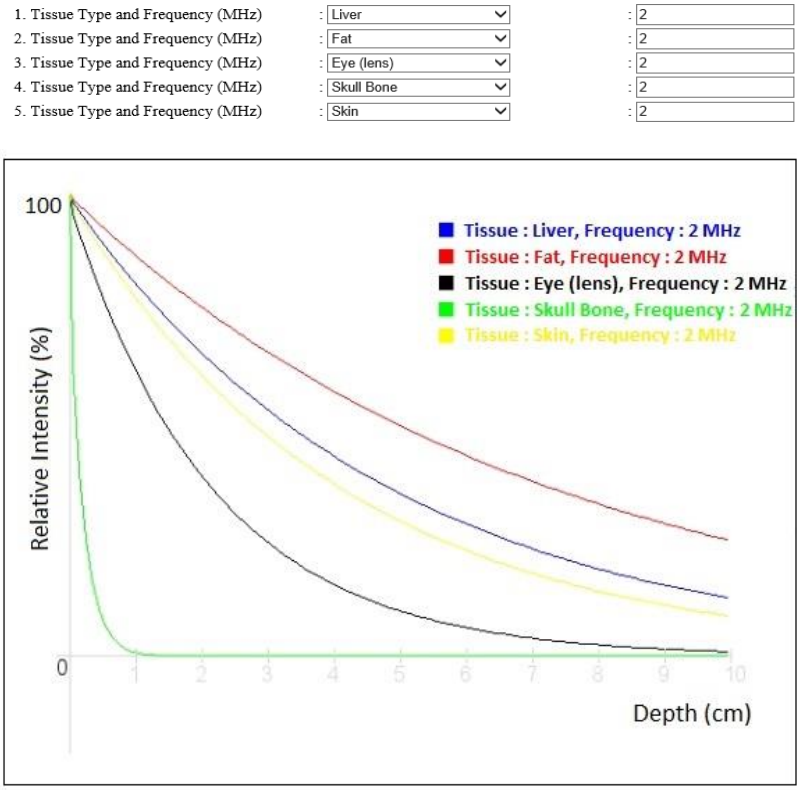

Figure 26: Application 4 results: attenuation characteristics under different tissue types (different attenuation coefficients) and same frequency (2 MHz) conditions.

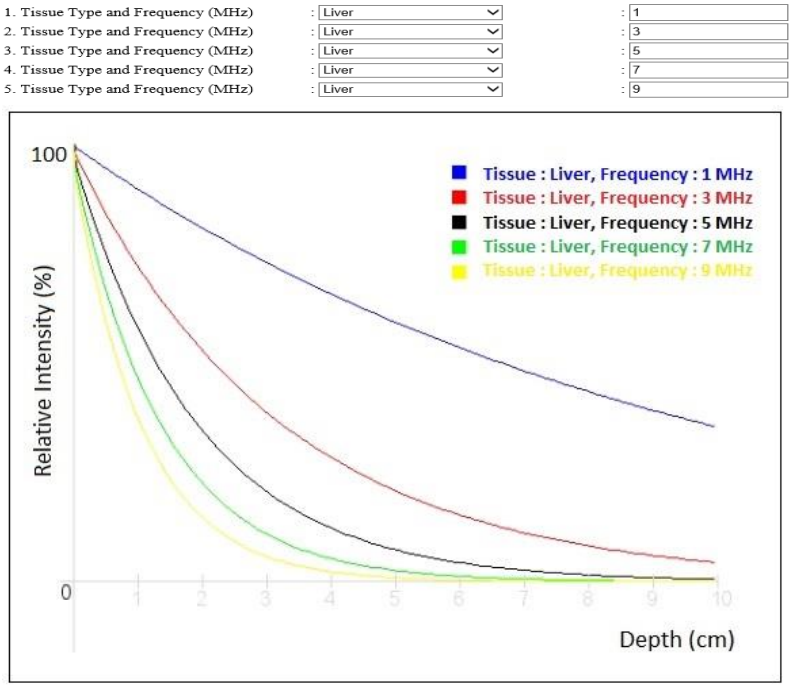

Figure 27: Results of Application 4: attenuation characteristics under the same tissue type (liver; α=0.9 db/cm) and different frequency conditions.

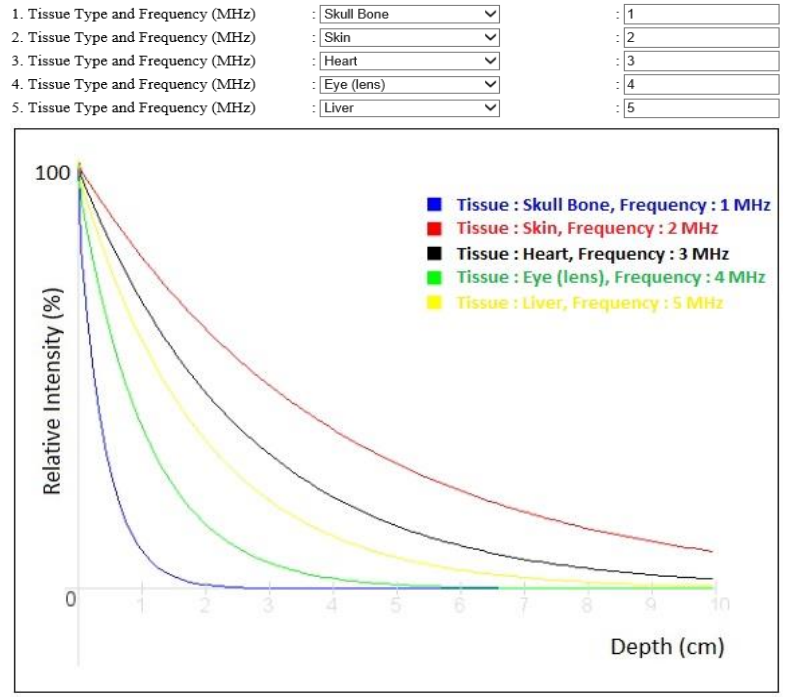

Figure 28: Results of Application 4: different tissue types and frequency responses.

3.5 Application 5: Piezoelectric Transducers

The piezoelectric effect is defined as a pressure to electric or electric to pressure transformation, and is a characteristic of certain crystals. Curie brothers discovered the piezoelectric effect in 1880 [43]. When a pressure is applied to the crystals, they produce an electrical voltage between the crystal poles. The meaning of "piezo" is pressure and while a pressure is applied to a piezoelectric crystal mechanical energy is converted to electrical energy. This concept is called as piezoelectric effect.

Similarly, voltage application across the crystal surfaces cause deformation of the crystal. Depending on the applied voltage polarity, the resulting effect can be in the form of compression or extension. This deforming effect, called as "*converse piezoelectric effect"*, and is used to generate an ultrasonic signal from a transducer [18].

While an oscillating voltage is applied into a certain crystal, the thickness of the crystal vibrates with certain frequency and if that material is in contact with an object, the vibrations produce an acoustic pressure wave into that object. Crystal behaves as an ultrasonic transducer due to the piezoelectric effect [44].

An ultrasonic transducer is commonly comprised of three layers: the piezoelectric crystal, which is located in the middle; an impedance matching layer facing the medium; and a backing layer that absorbs the energy transmitted to the backside of the transducer [29].

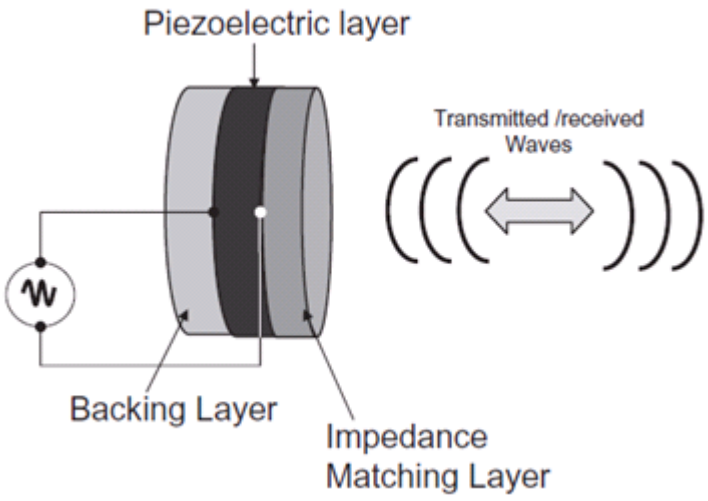

Figure 29: Piezoelectric transducer structure [29].

3.5.1 Transducer Design

The main purpose of designing a proper transducer is to adjust the material and geometry as efficient as possible for the desired usage. One of the most important transducer design concerns is the operating frequency. The piezoelectric crystal shows its most efficient response at the resonance frequency.

The resonance frequency is determined by the thickness or width of the piezoelectric crystal, which is actually the crystal's natural oscillation frequency. Also reversely, one can achieve the most efficient ultrasound operation at a given stable frequency by adjusting the transducer size or piezoelectric crystal width. The resonant frequency operation is obtained when piezoelectric crystal thickness is equal to half the wavelength of the desired ultrasound signal. A piezoelectric material of half-wavelength thickness resonates at a frequency v [18].

$$v = \frac{c}{\lambda} = \frac{c}{2t} \tag{3.17}$$

where c is the ultrasound velocity and t is the thickness of the piezoelectric crystal

Another important issue, the designer should keep in mind while producing an ultrasound transducer, is impedance matching. Since the acoustic impedance of the

piezoelectric material is different from the body tissue, in the ultrasound system the energy transmission from transducer to body is inefficient. The energy is lost in the form of heat and reflection. The impedance matching layer aims to find a solution for this non-desirable effect.

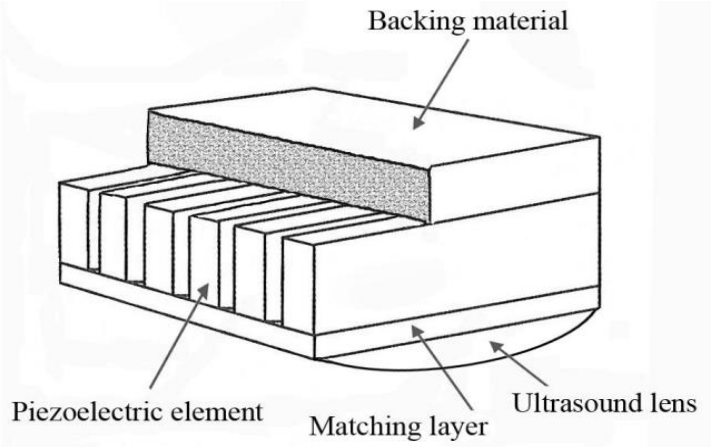

Figure 30: Detailed view into an ultrasound transducer [45].

Let the thickness of the matching layer attached to the piezoelectric element is L, which fulfills the condition L = (2 n - 1) λ/4 (where *n* is an integer number and λ is the wavelength within this layer). A 1/4 λ thickness, called as quarter-wavelength, maximizes energy transfer from the ultrasound transducer to the body tissue. An odd multiple would perform the same function, but the greater thickness of material would increase attenuation. Therefore, a single one-quarter wavelength thickness commonly is used for the matching layer [18].

Under the following condition, the intensity transfer coefficient equals to 1. This situation states that all acoustic energy will be transferred from the piezoelectric crystal to the body tissue without any loss in ideal conditions.

$$Z = \sqrt{Z_{piezo}\, Z_{medium}} \tag{3.18}$$

where Z is acoustic impedance of the matching layer.

The matching layer material has an acoustic impedance value between the values of the piezoelectric material and the tissue. There is usually more than one layer, where each layer has an acoustic impedance value closer to the acoustic impedance of the tissue [45].

Other remarkable considerations while designing an ultrasound transducer are backing and insulating issues. Without a backing material present, the element can oscillate with maximum amplitude [46]. The backing or dumping material decreases the ringing effect of the piezoelectric crystal at the transducer side. The backing material is located behind the crystal and reduces the excessive oscillation. This effect causes the piezoelectric component to produce and capture shorter pulse length sharp ultrasonic waves and enhances axial resolution. After design completion, transducer should be insulated to prevent from electric, acoustic, thermal or outside noise effects.

At Application 5, different piezoelectric materials such as PVDF, PZT-5H, PbTiO3, PMN-PT crystal are examined. Since each of the piezoelectric crystals has different acoustic parameters, the response, purpose and transducer design for the most efficient uses are also different.

Table 7: Acoustic properties of piezoelectric materials used in Application 5 [47].

Properties	PVDF	PZT-5H	$PbTiO_3$	$LiNbO_3$ crystal	PMN-0.33PT Crystal
d_{33} (10^{-12} C/N)	-33	593	60	23	2820
k_t	0.12-0.15	0.51	0.49	0.49	0.58
k_{33}	–	0.75	0.51	-	0.94
$\varepsilon_{33}^S/\varepsilon_o$	5-13	1470	180	28	680-800
c(m/s)	2200	4580	5200	7400	4610
ρ(kg/m^3)	1780	7500	7660	4640	8060
Z_a (Mrayl)	3.9	34.4	39.8	34	37.1
Curie temp (°C)	100	200	260	1150	150

Application 5 uses the piezoelectric material acoustic parameter database. The information for that database was taken out from the above table.

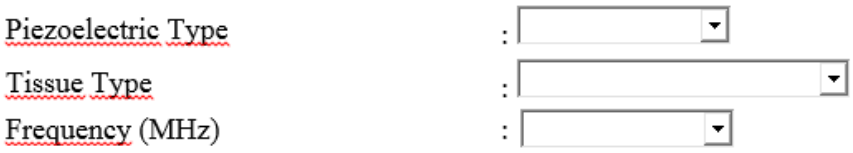

Figure 31: Data input screen Application 5.

Developed PHP code calculates and prints out the results according to the predefined frequency value and chosen piezoelectric material type. Acoustic parameters of the matching layer are also calculated by means of piezoelectric material and tissue properties. Program also evaluates the necessary thickness of the piezoelectric material for the most efficient ultrasound response.

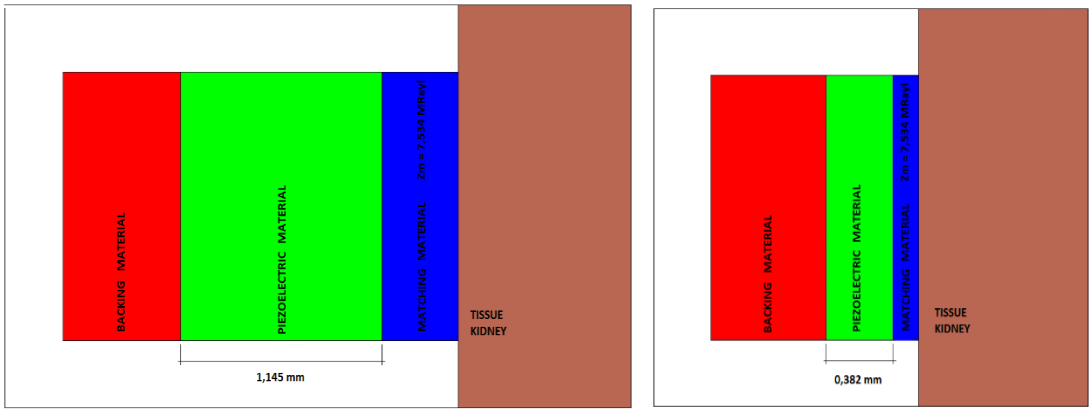

Figure 32: Results of Application 5: effect of frequency for the most efficient operation. Piezoelectric crystal type: pzt-5h, tissue type: kidney, frequencies: (left) 2 MHz and (right) 6 MHz respectively.

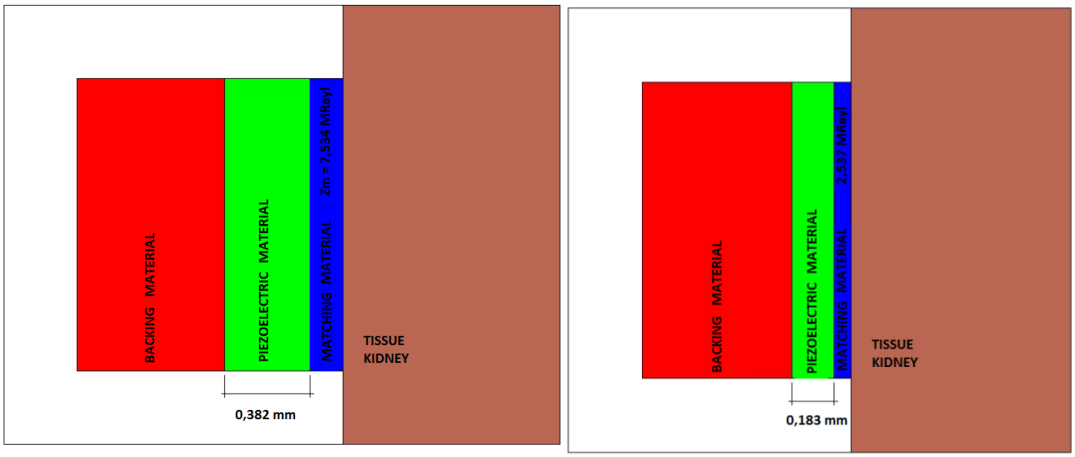

Figure 33: Results of Application 5: effect of piezoelectric material type. Tissue type: kidney, frequency: 6 MHz, piezoelectric crystal types: (left) pzt-5h and (right) pvdf respectively.

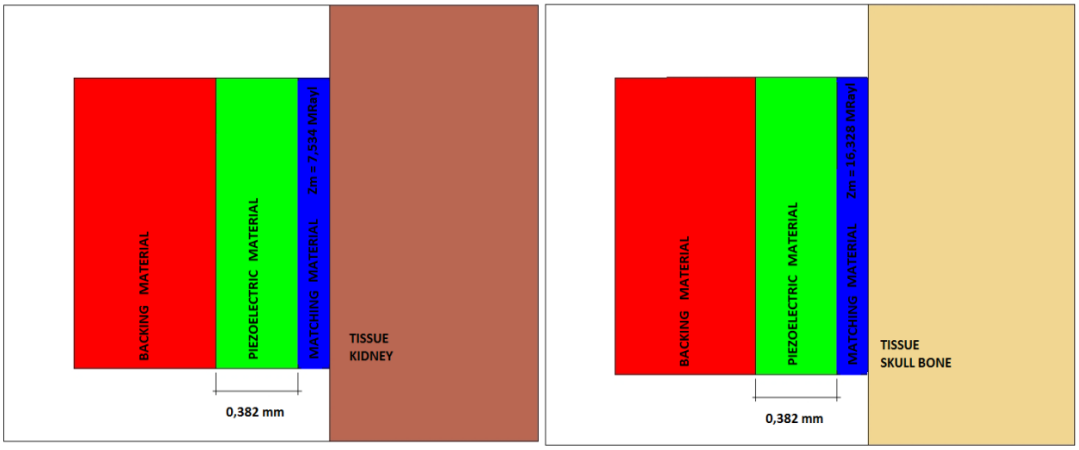

Figure 34: Results of Application 5: effect of tissue type. Frequency: 6 MHz, piezoelectric crystal type: pzt-5h, tissue types: (left) kidney and (right) skull bone respectively.

3.6 Application 6: Near Field (Fresnel Zone) And Far Field (Fraunhofer Zone) Calculations

Ultrasound transducers produce a beam profile, which is generally composed of two main regions with different wave behavior and acoustic characteristics. The near field or Fresnel Zone is known as the zone, which is located close to the transducer area. Because of the variations in intensity, the near field characteristics are affected by the interference effects. In medical ultrasound, the points we want to image is located in the near field of the probe. The source is located close to the array [48]. The length of the near field is often termed the transition distance.

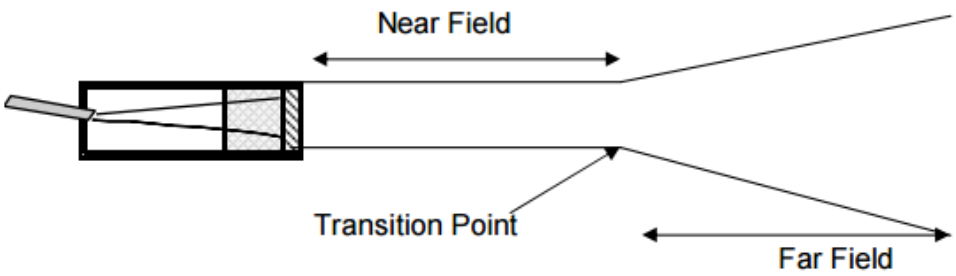

Figure 35: Near field and far field zones of an ultrasound transducer [49].

As seen from the Figure 35, the outer beam zone or the rest of the region beyond the near field is called as “far field”. Ultrasound intensity in this region decreases with distance and pressure amplitude variation in this region is less according to the near field [50].

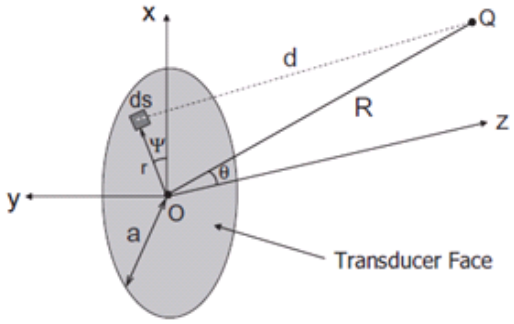

Figure 36: Acoustic field of a disc source [29].

The relative axial intensity at point z for a given disc source is defined as:

$$\frac{I}{I_0} = sin^2\left[\frac{\pi}{\lambda}\left\{(a^2 + z^2)^{1/2} - z\right\}\right] \tag{3.19}$$

where a is the radius of disc, λ is the wavelength in the medium, I_0 is the maximum axial intensity at source side and I is the axial intensity at distance z.

If we plot the normalized intensity value (I/I_0) versus $\lambda z/a^2$ maximum and minimum values occur at the following locations:

$$z_{max} = \frac{4a^2 - \lambda^2(2m+1)^2}{4\lambda(2m+1)} \qquad m = 0,1,2,\ldots(\sin = \pm 1) \tag{3.20}$$

$$z_{min} = \frac{a^2 - \lambda^2 n^2}{2n\lambda} \qquad n = 1,2,3,\ldots(\sin = 0) \tag{3.21}$$

Normalized maximum intensity defined as (Z_{NF}) and given by

$$Z_{NF} = \frac{4a^2 - \lambda^2}{4\lambda} \tag{3.22}$$

For n=1, $a^2 \gg \lambda^2$ (i.e., the source is much bigger than the wavelength) (Fresnel zone)

$$D = Z_{NF} = \frac{a^2}{\lambda} \tag{3.23}$$

Up to this point, the field's intensity changes very rapidly. Within the Fresnel zone, most of the ultrasound energy is confined to a beam width no greater than the transducer diameter [29].

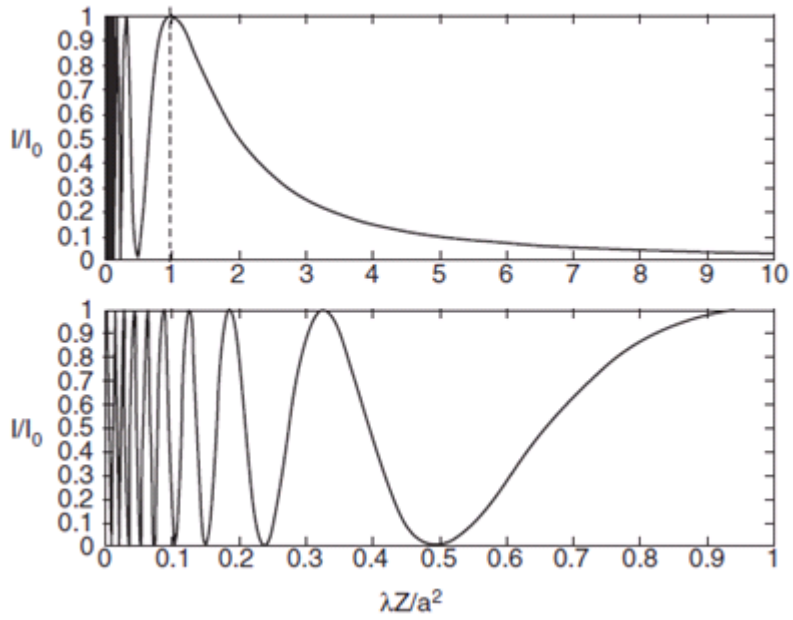

Figure 37: Normalized intensity (I / I_0) vs. normalized distance $\lambda z/a^2$ plot for a disc source. (down) zoom in [0:1] for near field observation [29].

Beyond the Fresnel zone, some of the energy escapes along the periphery of the beam to produce a gradual divergence of the ultrasound beam that is described by

$$\theta = sin^{-1}\left(\frac{0.61\lambda}{a}\right) \tag{3.24}$$

where θ is the Fraunhofer divergence angle in degrees [18].

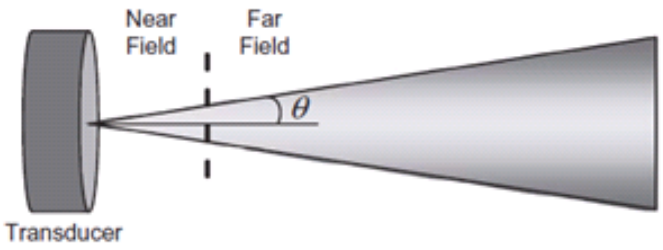

Figure 38: Conic approximation to understand far field behaviors [29].

As a result, we can conclude that:

- The distance of the near field or Fresnel zone expands if you increase the transducer diameter, decrease wavelength or increase wave frequency.

– The beam divergence in the far field or Fraunhofer zone decreases if you increase the transducer diameter, decrease wavelength or increase frequency.

Application 6 uses the Fresnel (near field) and Fraunhofer (far field) zone equations, calculates the near field distance, Fraunhofer divergence angle and plots the results according to given tissue type, frequency and transducer diameters.

Figure 39: Data input screen of Application 6.

Tissue types can be selected from the push menu buttons and other inputs can be manually entered. The aim of the Application 6 is to comprehend the zone relation between variable frequency, transducer size and tissue type.

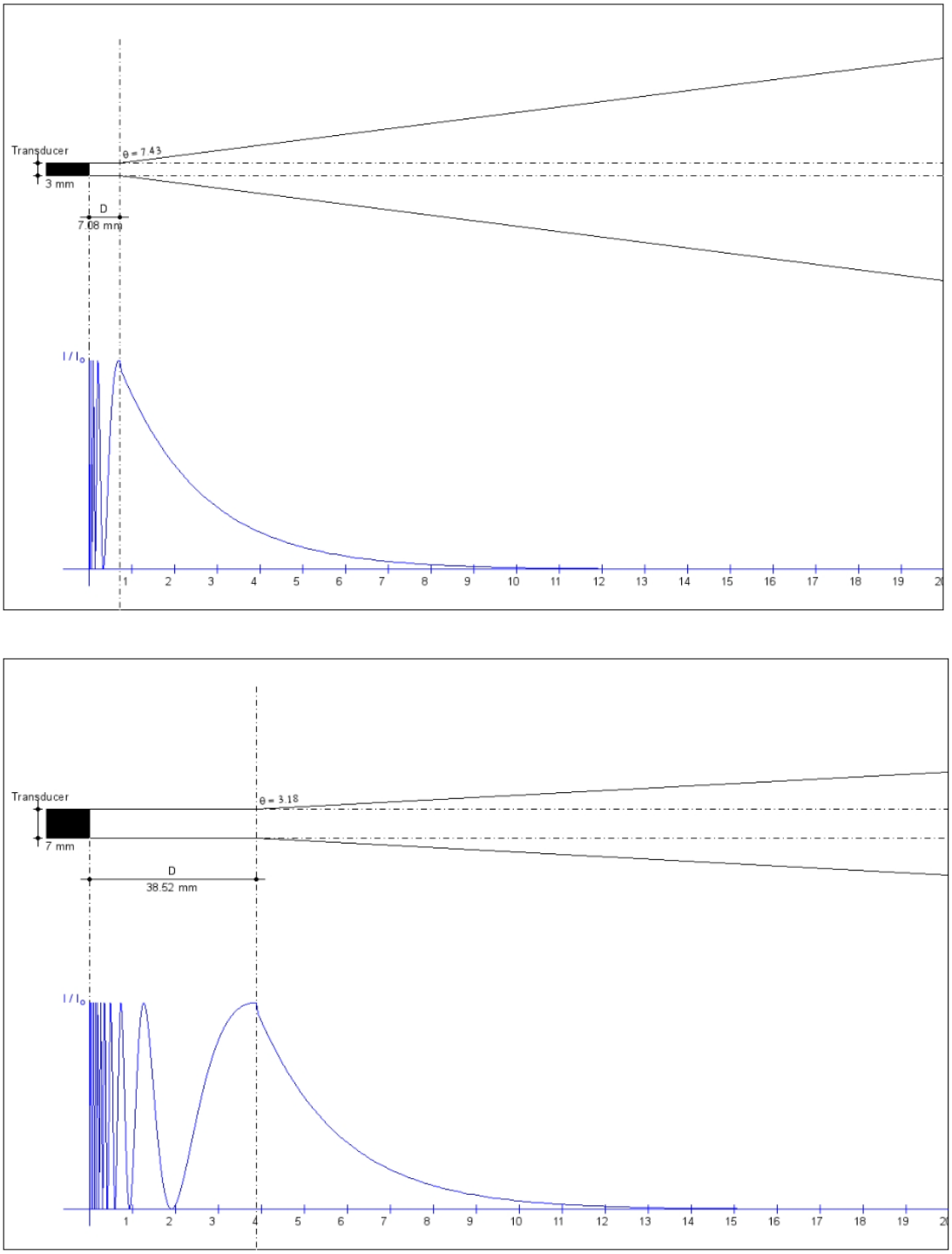

Figure 40: Results of Application 6: near field – far field calculation and plots effect of transducer diameter. Tissue types: liver, frequencies: 5 MHz, transducer diameter: (above) 3 mm and (below) 7 mm.

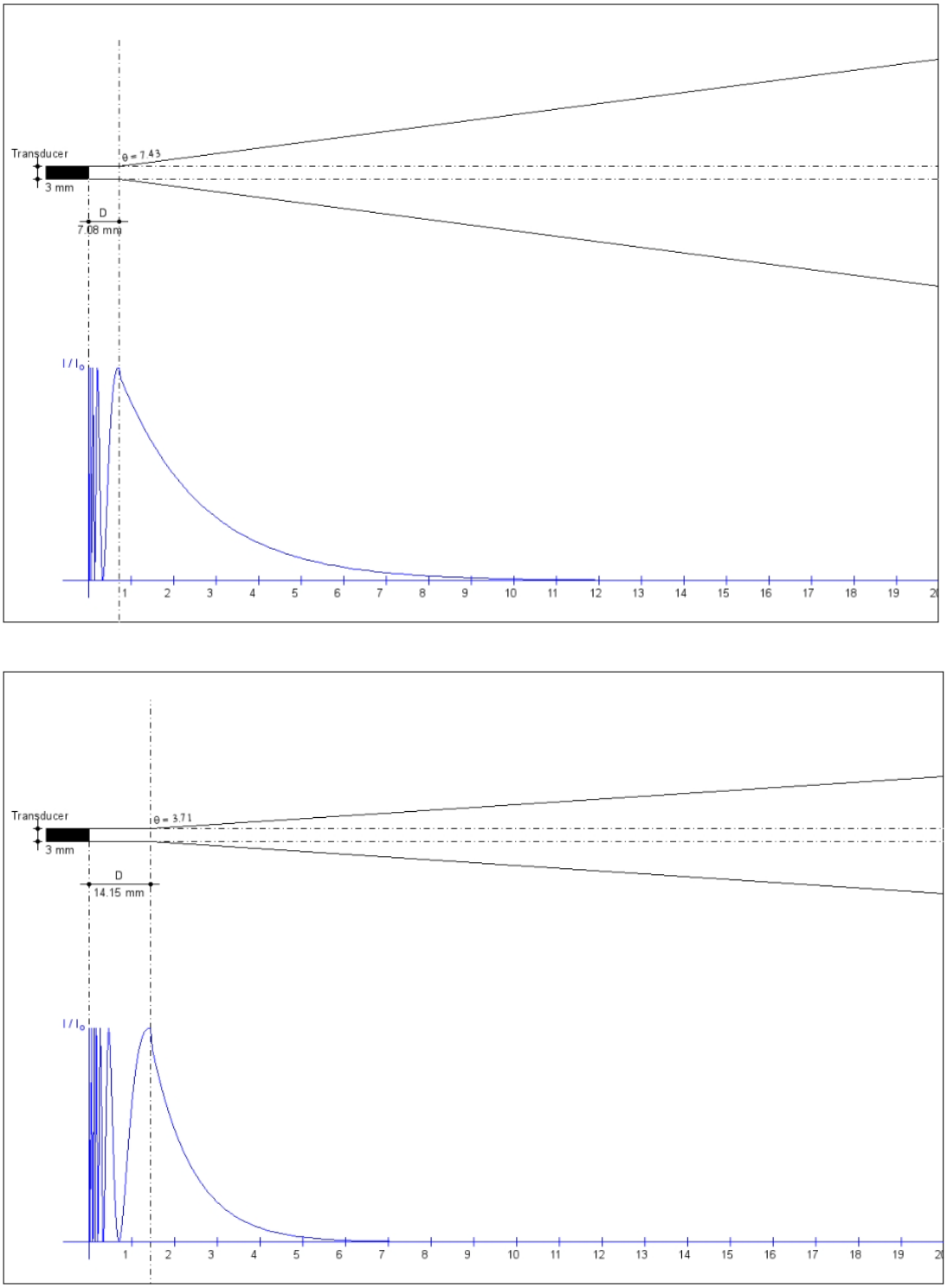

Figure 41:Results of Application 6: near field – far field calculation and plots. Tissue types: liver, transducer diameters: 3mm, frequency: (above) 3 MHz and (below) 10 MHz.

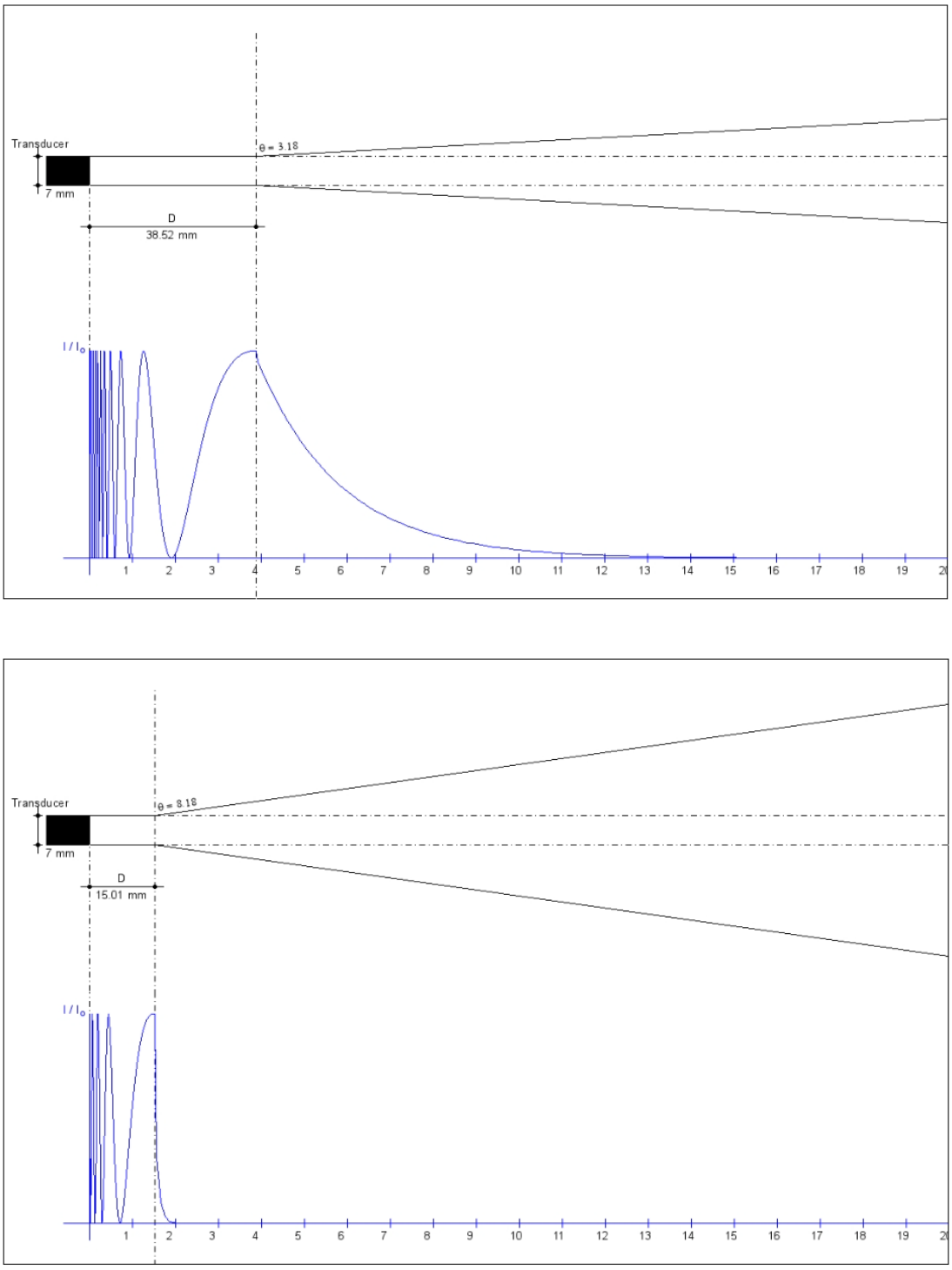

Figure 42:Results of Application 6: near field – far field calculation and plots. Effect of tissue type. Frequencies: 5 MHz, transducer diameters: 7 mm, tissue type: (above) liver and (below) bone.

3.7 Application 7: Doppler Effect

The Doppler Effect is defined as the frequency change of a propagating wave for an observer moving with respect to its source or vice versa. Austrian physicist Christian Doppler, 1842, first described it [51]. If the signal source is moving toward the observer like an approaching ambulance siren, each of the consecutive signal wave is emitted from a position closer to the observer than the previous wave. Therefore, each of the incoming wave takes less time than the previous wave to arrive the observer. Conseqntly, the wavelength of the wave decreases or the frequency of the wave increases relatively [52].

Reversely, if the signal source is going away from the observer like an ambulance siren, each of the consecutive signal wave is emitted from a position farther from the observer than the previous wave. Therefore, each of the incoming wave takes more time than the previous wave to arrive the observer. Because of the increment in the duration between two consecutive signal waves at the observer side, the wavelength increases or the frequency of the wave decreases relatively. The distance between consecutive wave fronts is then increased, so the waves "spread out" [54].

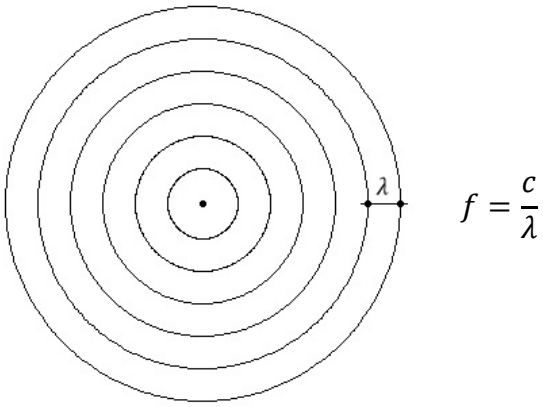

Figure 43: A normally propagating wave from stable source with the frequency.

$f^{\prime\prime} = \frac{c}{\lambda^{\prime\prime}}$

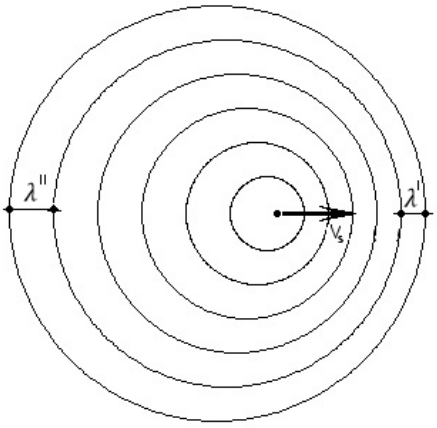

$f^{\prime} = \frac{c}{\lambda^{\prime}}$

Figure 44: A moving wave source with the velocity v.

In Figure 43, the wave propagation of stable source condition can be seen. When the sound source moves to right with the velocity v (Figure 44), the wavelength and frequency of propagating wave changes according to the observer. The new frequency values are calculated in (3.25) and (3.26)

$$f^{\prime} = \frac{c}{\lambda^{\prime}} = \frac{c}{\lambda - vT} = \frac{c}{(c-t)T} = \frac{c}{c-v} f \qquad (3.25)$$

$$f^{\prime\prime} = \frac{c}{\lambda^{\prime\prime}} = \frac{c}{\lambda + vT} = \frac{c}{(c+v)T} = \frac{c}{c+v} f \qquad (3.26)$$

In Application 7, the Doppler Effect and the change in frequency due to the source movement is examined. The wave frequency (*f*) and the speed of motion (*v*) can be manually entered. Velocity of speed in the air (*c*) is roughly accepted as 300 m/s for the applications. Motion of direction is also adjustable from left to right or right to left respectively.

Figure 45: Data input screen of Application 7.

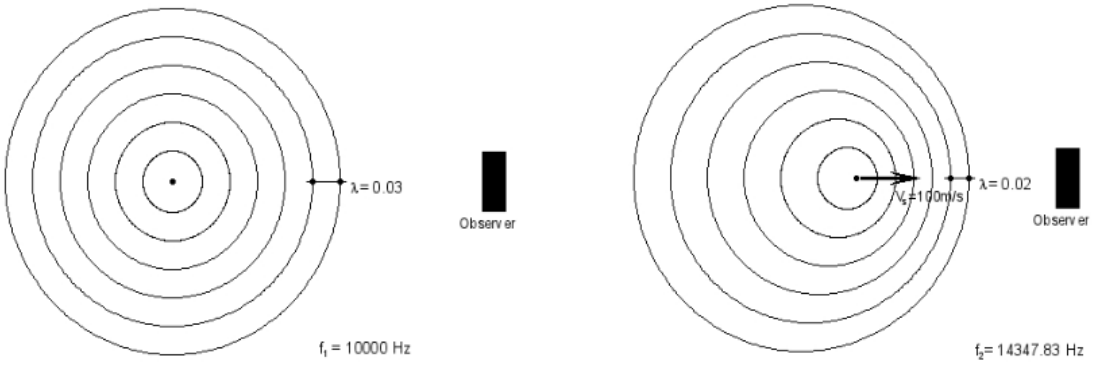

Figure 46: Results of Application 7: Effect of direction. Frequency: 10 kHz, motion speed: 100 m/s, movement direction: left to right.

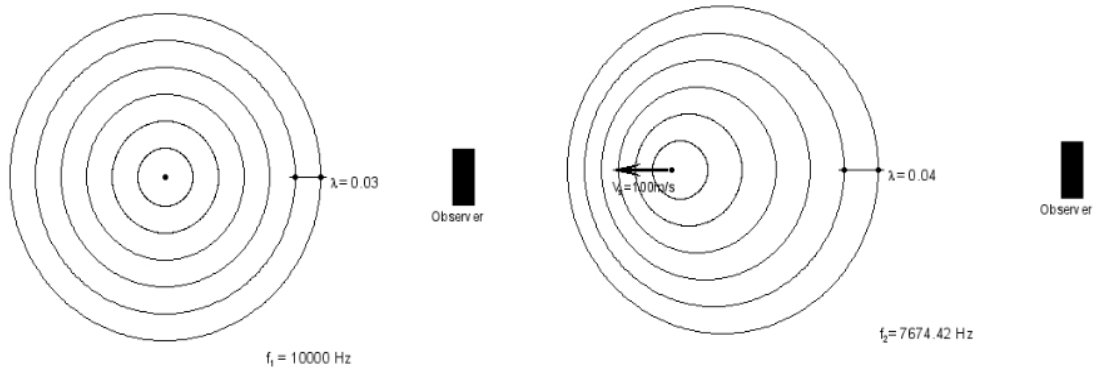

Figure 47: Results of Application 7: effect of direction. Frequency: 10 kHz, motion speed: 100 m/s, movement direction: right to left.

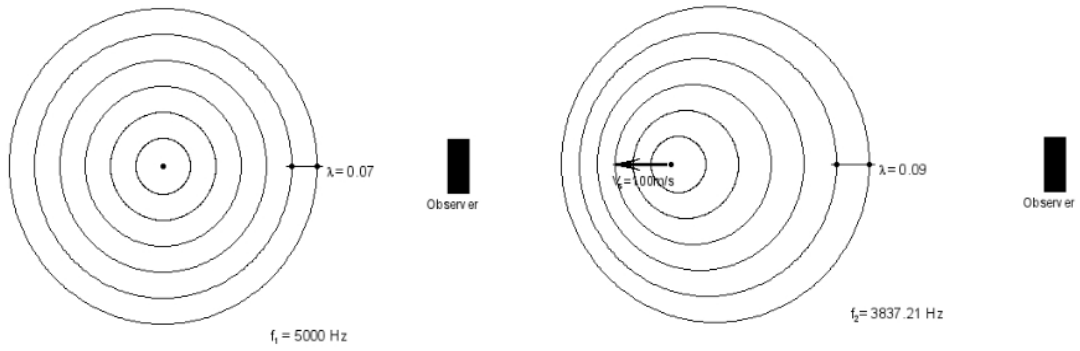

Figure 48: Results of Application 7: Effect of frequency. Frequency: 5 kHz, motion speed: 100 m/s, movement direction: right to left

.

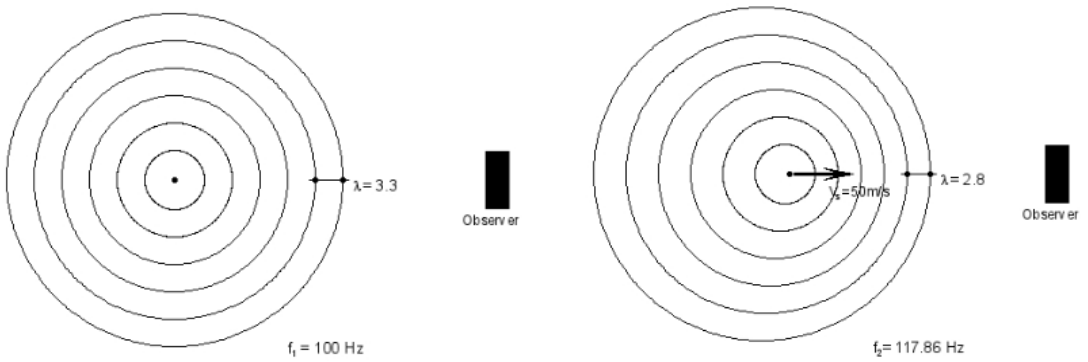

Figure 49: Results of Application 7: Effect of motion speed. Frequency: 100 Hz, motion speed: 50 m/s, movement direction: left to right.

3.8 Application 8: Doppler Effect Applications

The Doppler frequency calculations in the previous application is given under the specific condition where ultrasound beam is parallel to the motion of the direction. In general situation, ultrasound signal obliquely approaches and hit a moving object with a sonation angle θ. This condition can be used to calculate the blood velocity in the vessel or volumetric blood flow.

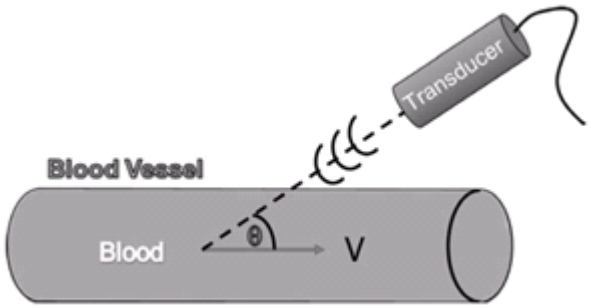

Figure 50: Oblique examination with sonation angle **θ** of blood flow [29].

An ultrasonic transducer transmits waves toward a blood vessel through which blood flows with an instantaneous speed V. The angle between the acoustic beam and the blood vessel's axis is θ [29].

Under these conditions, the shift in frequency Δf is

$$\Delta f = \frac{f_0 \cdot 2V \cos\theta}{c} \tag{3.27}$$

As seen from the above formulations, Doppler frequency depends on the blood velocity, ultrasound frequency and Doppler angle. Moreover, Doppler frequency also depends on the direction of blood flow and ultrasound probe [54].

A negative sign in this expression would imply that the object is moving away from the ultrasound source and detector and that the frequency of detected ultrasound is shifted to a lower value [18].

Velocity of blood in the vessel is:

$$V = \frac{\Delta f \cdot C}{2 f_0 \cos\theta} \tag{3.28}$$

Assume the vessels are cylindrical tubes and the cross-sectional area (A) of the vessel is

$$A = \pi \left(\frac{d}{2}\right)^2 \tag{3.29}$$

The volumetric flow (Q) is

$$Q = VA \tag{3.30}$$

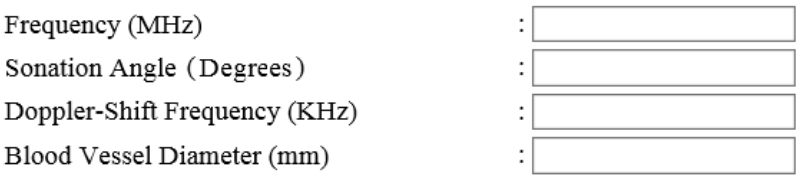

Figure 51: Data input screen of Application 8.

Application 8 applies the oblique Doppler formulations above and calculates the blood velocity in the vessel according to manually given Doppler frequency, sonation angle and Doppler-shift frequency values. Application also calculates the volumetric flow depending on the blood vessel diameter input.

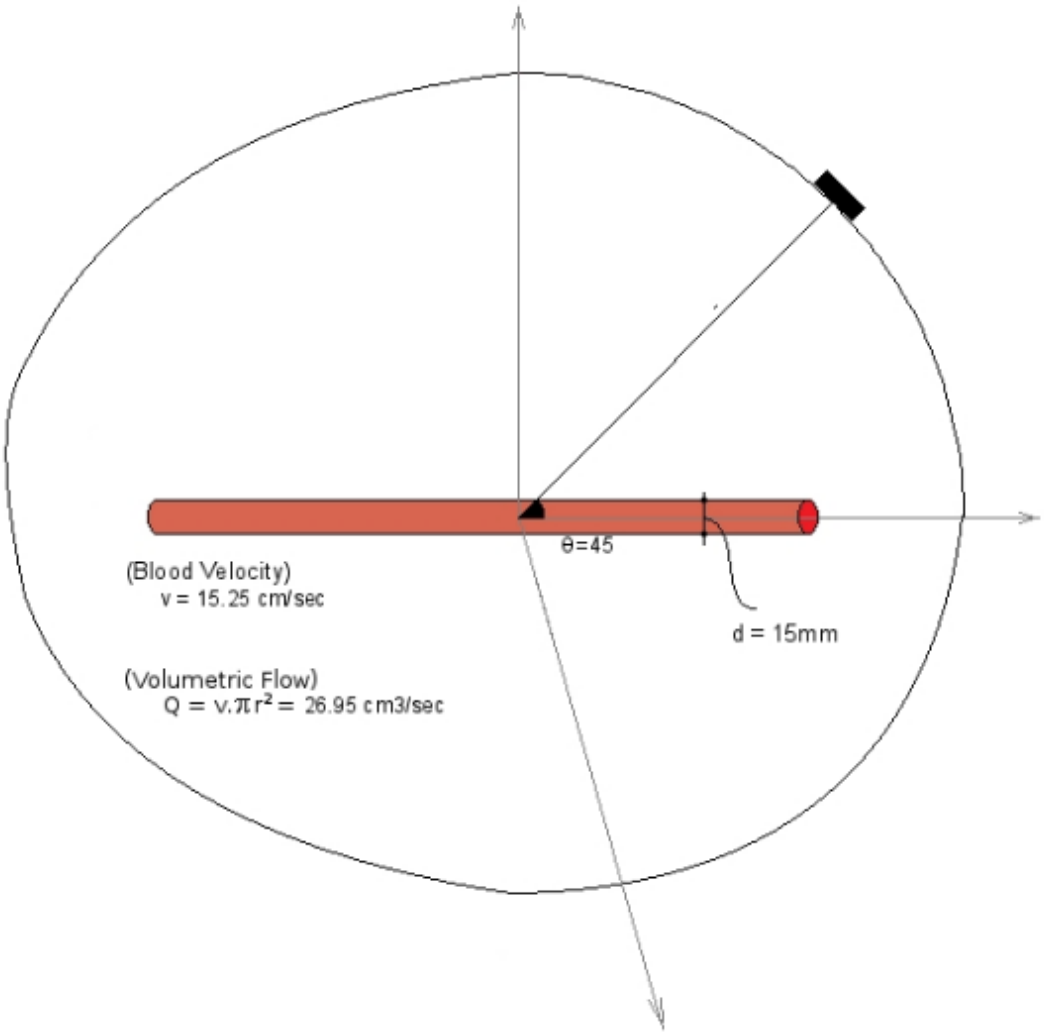

Figure 52: Application 8 results: frequency: 10 MHz, sonation angle: 45, blood vessel diameter: 15 mm, Doppler-shift frequency: 1.4 kHz.

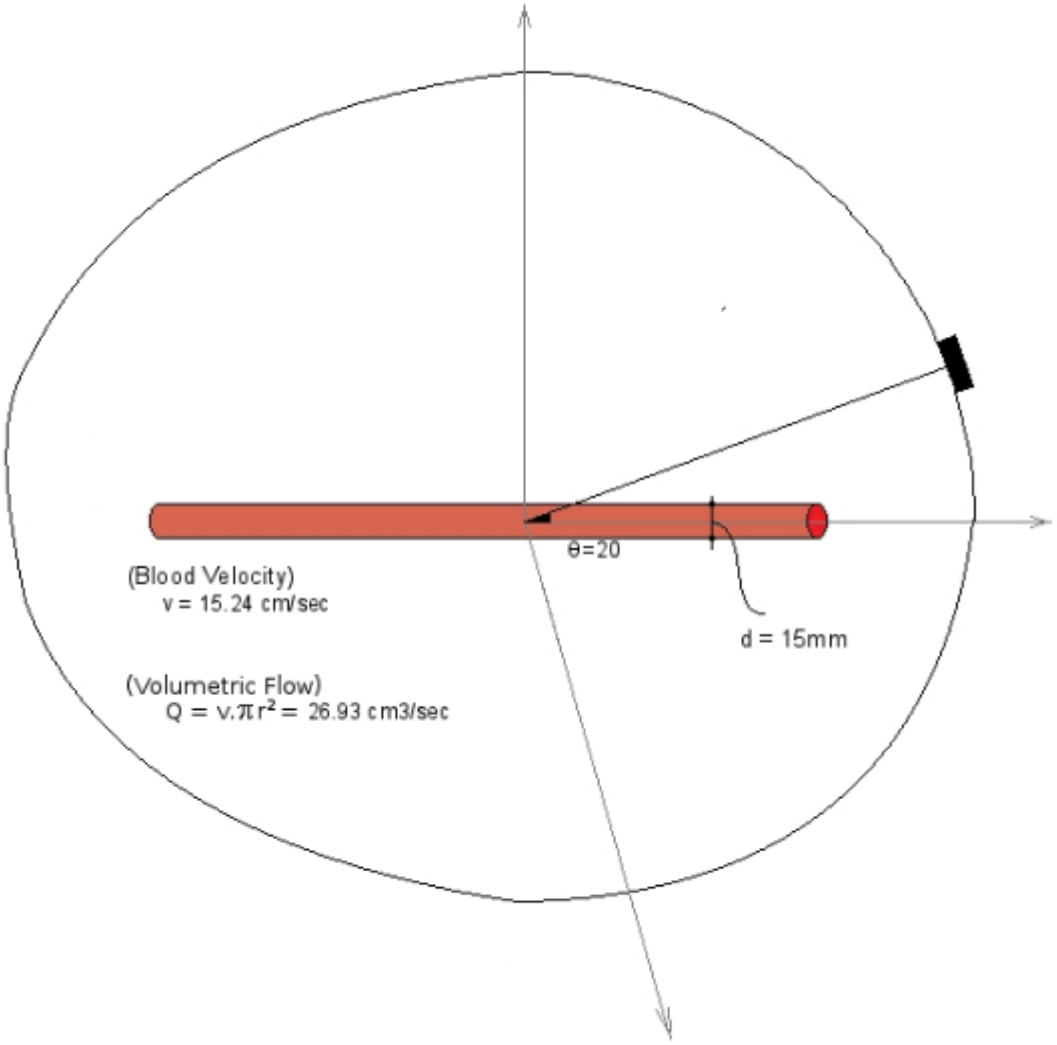

Figure 53: Application 8 results: effect of sonation angle. frequency: 10 MHz, sonation angle: 20, blood vessel diameter: 15 mm, Doppler-shift frequency: 1.86 kHz

Note that if the sonation angle is changed from 45° to 20°, Doppler-shift frequency also changes from 1.4 kHz to 1.86 kHz because of the changing relative movement conditions. Similar observations can be done by using Application 8 parameters and results.

3.9 Application 9: Medical Ultrasound System Applications

This section present a PHP based application for the whole ultrasound system using The Medical Ultrasound System (MUS) Application is prepared to model complete ultrasound system by using components of software codes prepared at previous applications and obtain images. Another purpose of MUS Application is to create body like geometry and work on a realistic medium.

Once the scenario desired to examine is decided and corresponding geometry is created according to the tissue locations, then PHP code run. Application calculates all related relative transmission and reflection intensities depending on the given initial reference intensity I_0. Entire values of resulting matrix are built one by one for every tissue surface and is calculated under the effect of attenuation.

To create a body model, application allows user to choose different tissue types with different acoustic parameters. Tissue locations and center point of the tissues can manually be positioned inside the background. Edge of the square and diameter of the circle in the background area, in other words, sizes of the tissues are adjustable. Tissues can be put close or far from each other to present their cascaded positions in the body and intersection or continuity phenomenon can be created and examined using the generated tissue geometry.

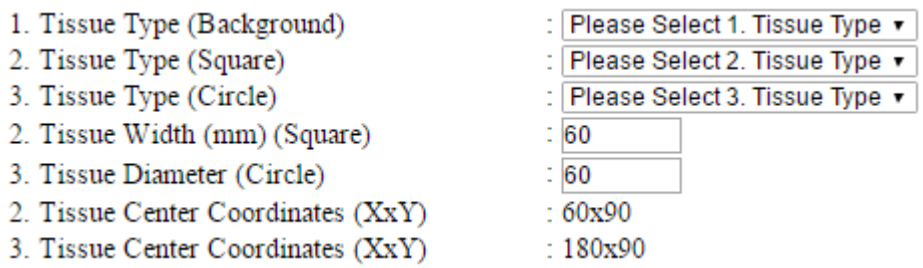

Figure 54: Data input screen of ultrasound imaging system (MUS) application.

Here the first tissue is background, the second tissue is the square object and the third tissue is the circle object.

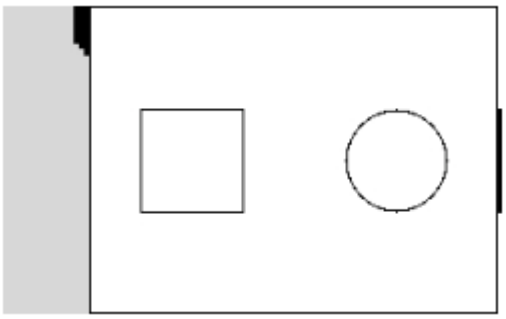

Figure 55: Initial coordinates and size of the MUS application Lcation coordinates: left up corner: (0,0) right down corner: (240,180).

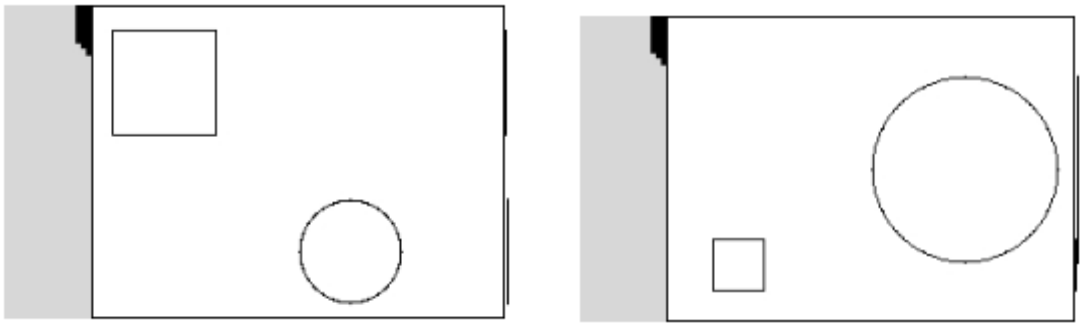

Figure 56: Different allocations of tissues in the MUS application.

(left) edge of square: 60 mm, diameter of circle: 60 mm
center of square: (42x44), center of circle: (150x141)
(right)edge of square: 30 mm, diameter of circle: 110 mm
center of square: (42x146), center of circle: (175x90).

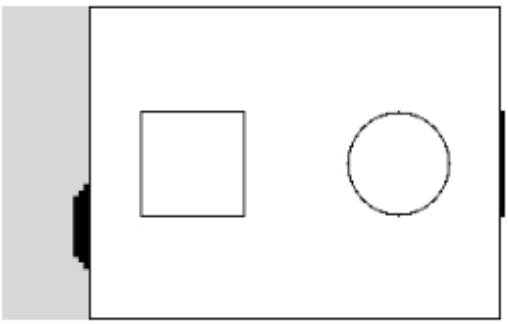

Figure 57: Different allocations of transducer in the MUS application.

For the application input, center locations of the tissues are given by just a mouse click. In addition to the tissue location and size adjustment, place of the transducer is also adjustable on the y-axis freely. One can scan the overlapping points or single tissues one by one changing the transducer position. The simulated transducer scans the x-axis linearly using its 16 channels scanning algorithm.

For the application usage, firstly, the tissue types should be chosen, then size of the tissues and the transducer position must be entered. Once the MUS geometry is set, the application automatically generates the final plot and starts to scan the corresponding path.

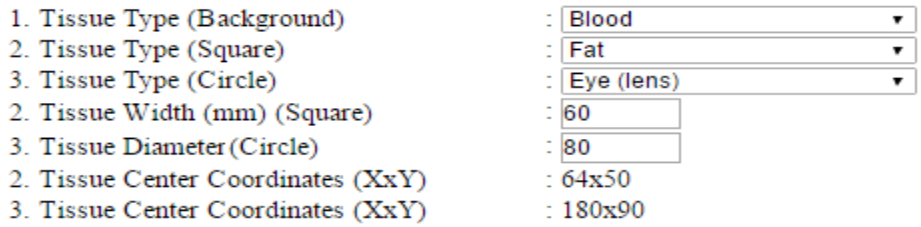

Figure 58: MUS application data input screen under specific conditions.

For every scan path, transducer generates an ultrasound signal with initial intensity I_0. Application calculates the transmission and reflection intensities corresponding to the penetrated tissues along every single scan route. All acoustic intensity formulations and effect of tissue specific attenuations applied and calculated. Then according to the calculations, reflected echo intensity values are collected. Finally returning time and echo intensity values matrix is built up. This process is repeated 16 times along the y-axis to simulate the16 channel linear array transducer. So application scans both x-axis and y-axis for every single run. At the transducer side, reflected data are collected over rectangular scan path by means of echo calculation and channel scan algorithms.

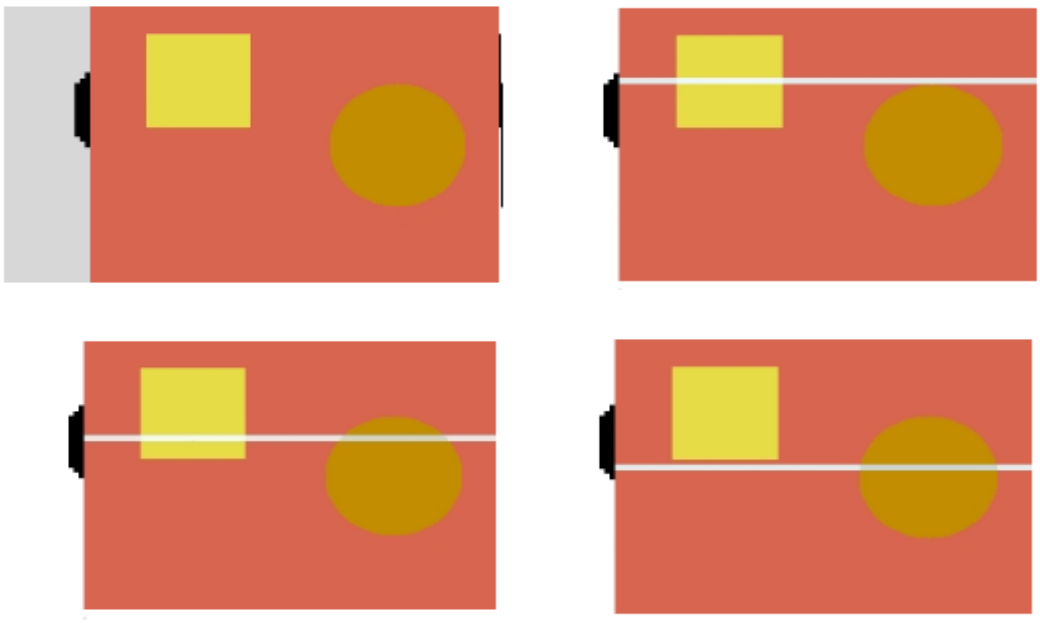

Figure 59: MUS application geometry and scan path under the conditions given in Figure 58.

Upper left graph of Figure 59 shows the generated RGB codes and geometry. Upper right graph is the first linear scan path (1/16), bottom left figure is the eighth of sixteenth linear scan path and the final linear scan path (16/16) can be seen at bottom right.

As shown in Figure 59, the first scan line scans and calculates two tissue condition: the background (blood) and square (fat) tissues. The eight scan line penetrates all of the three objects (blood, fat, eye) creating and calculating blood-fat-blood-eye-blood path. For every surface transition, application calculates the reflection under the effect of attenuation, related returning echo time and returning relative intensity values are collected as a matrix form to build images.

In a real ultrasound system, electrically excited piezoelectric materials vibrate as a function of variable input voltage and by means of this oscillating motion, pressure waves are created and transferred into the body. Dual mode transducers behave as a generator and detector. Transferred ultrasound signal are reflected, transmitted and attenuated inside the body because of the acoustic characteristics, surface transitions

and inhomogeneities inside the different tissues. The reflected echo signals are detected by transducer on the body.

Pressure waves are captured by transducer and converted back into voltage values by means of the reverse piezoelectric effect. These pulse echo signals are processed to obtain ultrasound based biomedical images of the human body.

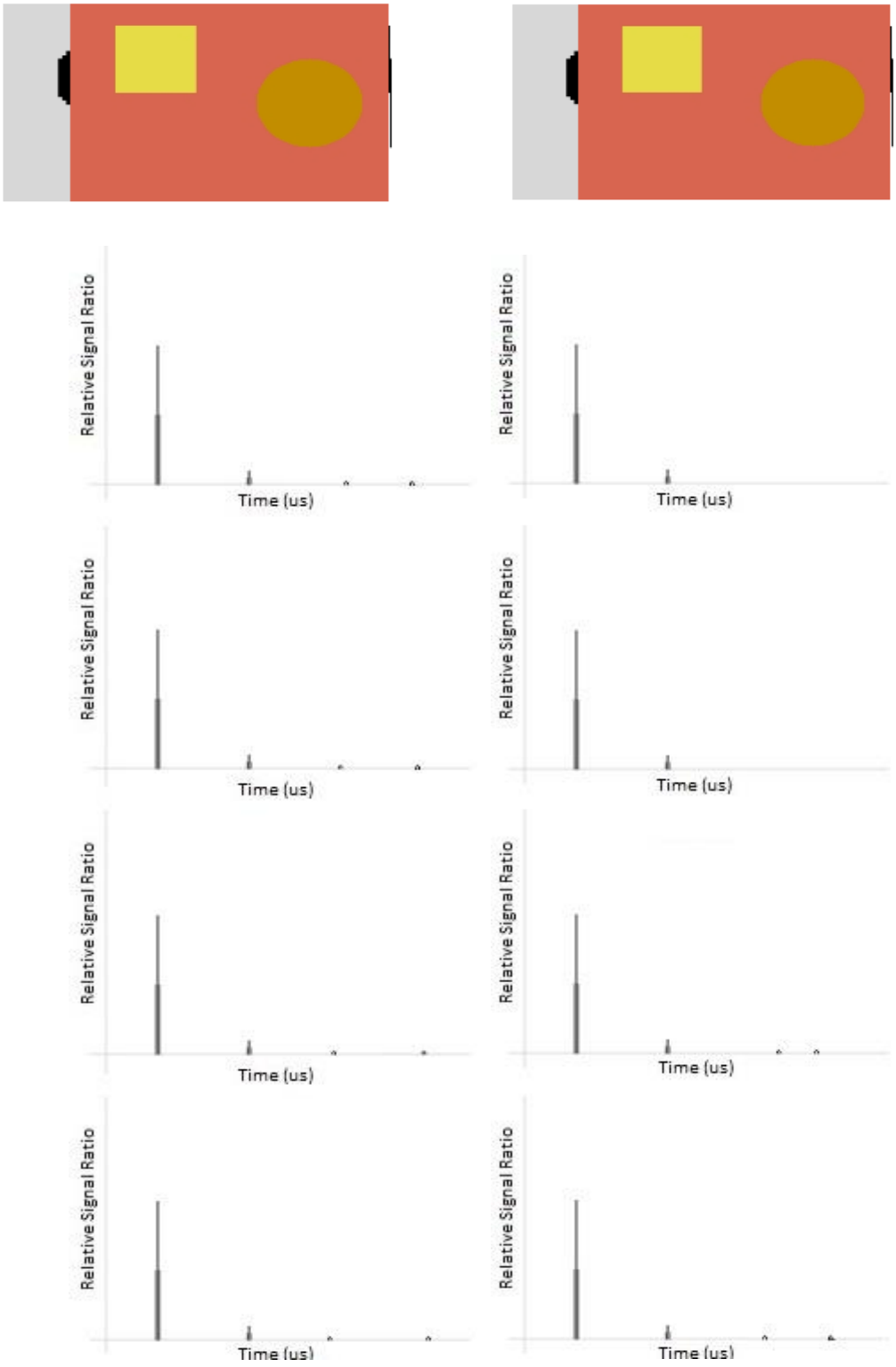

(a) (b)

Figure 60: MUS application results: (a) Scan 1-to-4 (b) Scan 5-to-8.

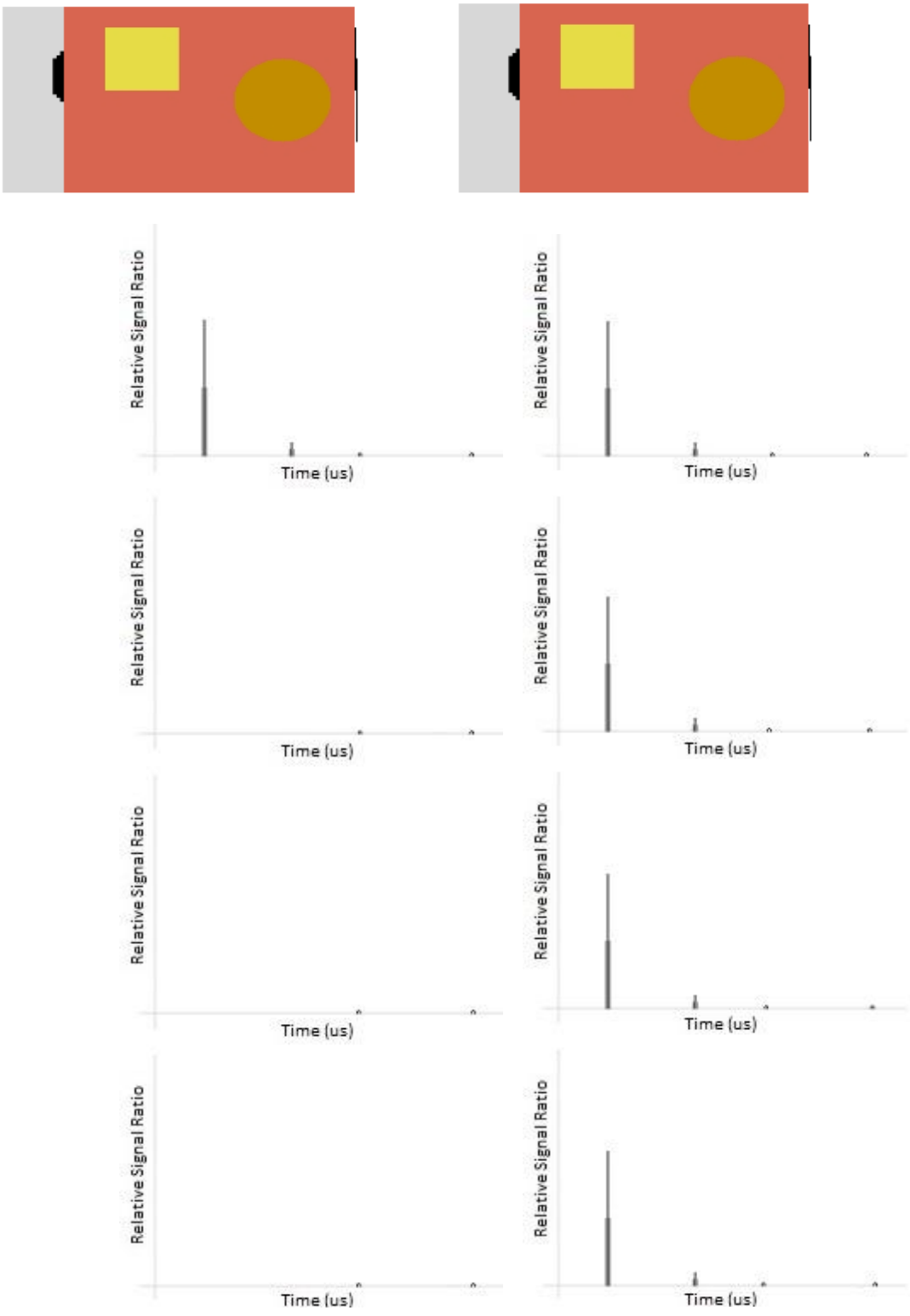

(a) (b)

Figure 61: MUS application results: (a) Scan 9-to-12. (b) Scan 13-to-16.

The MUS Application scans 16 paths like a 16-channel linear array transducer. The returning time and magnitude of each echo signal is processed and related visual outputs are plotted. The plotted graphs are actually A-mode ultrasound outputs. The application also printouts the calculated echo intensity and travel time values to make some observations.

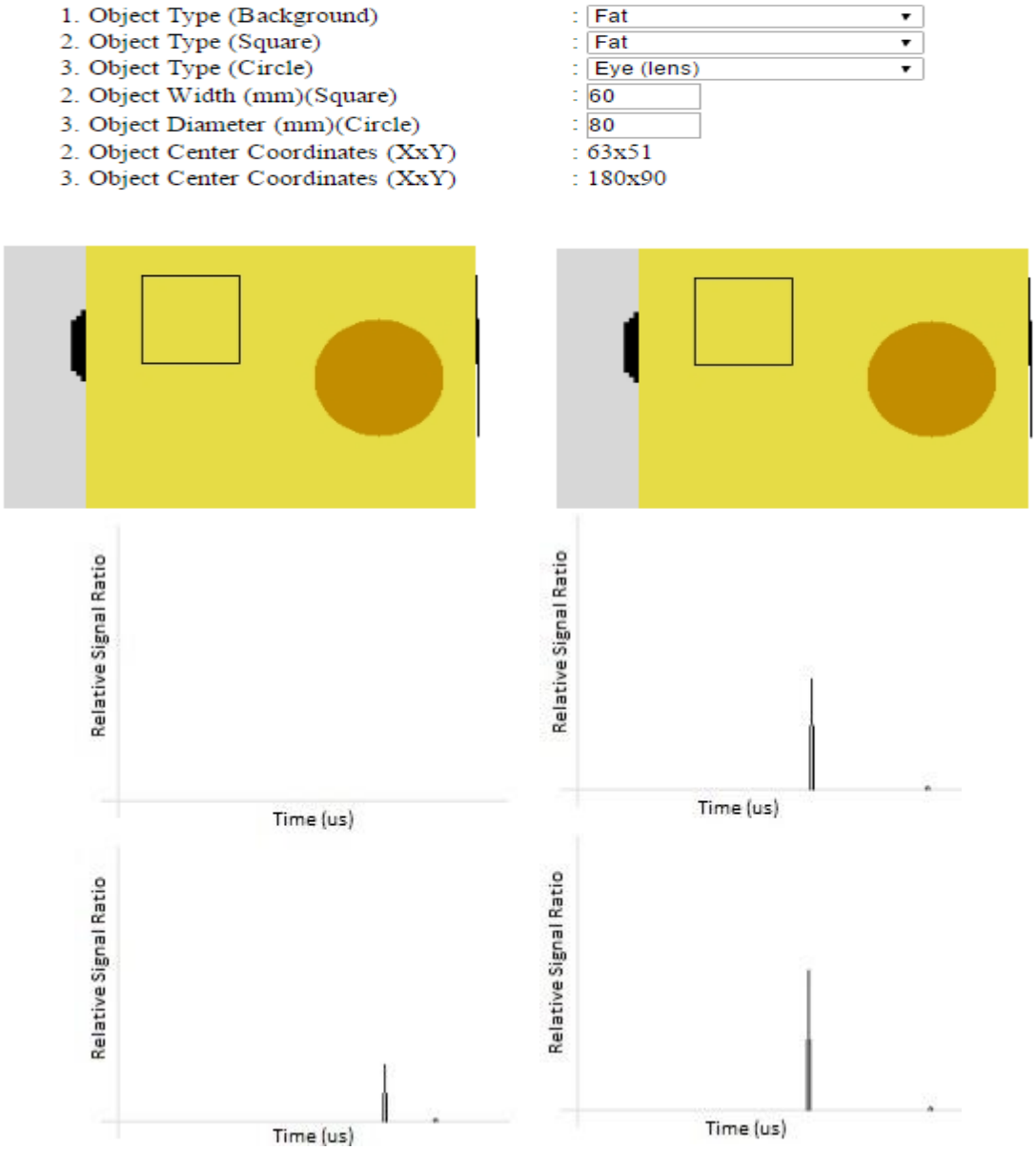

Figure 62: MUS application results: effect of distance and circular object. First, fifth, tenth and fifteenth scan results are plotted for observations.

3.9.1 B-mode Ultrasound

B-mode or brightness mode ultrasound is a technique of ultrasound imaging. The echo magnitude from each point in the field of view not simply displayed on a graph, instead the amplitudes are mapped to the grey level, or brightness, of the corresponding pixel in the image [55].

The largest echo amplitude produces the most shinny brightness or maps to whiter colors, no echo detected areas are mapped to the black and intermediate echo amplitudes mapped to different shades of gray.

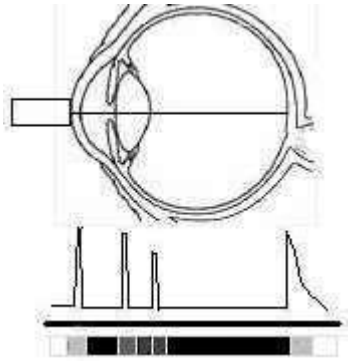

Figure 63: The A-mode and B-mode ultrasound scan visuals of an eyeball. ophthalmologic ultrasound [53].

Figure 64: MUS application results: B-mode ultrasound graph.

The MUS Application also plots the B-Mode Ultrasound graphs. Above figure shows the resulting graph of B-Mode scan according to the related tissue allocation.

3.9.2 Time Gain Compensation (TGC)

While an acustic wave propagates inside the body, the intrensity and power of the signal fades down exponentionally due to attenuation. So the deeper tissues can reflect weaker echoes and normally undetectable or unmeaningful ultrasonic information can be obtained from the deeper tissues. Received weak echoes artifically magnified at trancducer side to compensate this effect. This process is called as Time Gain Compensation (Figure 65).

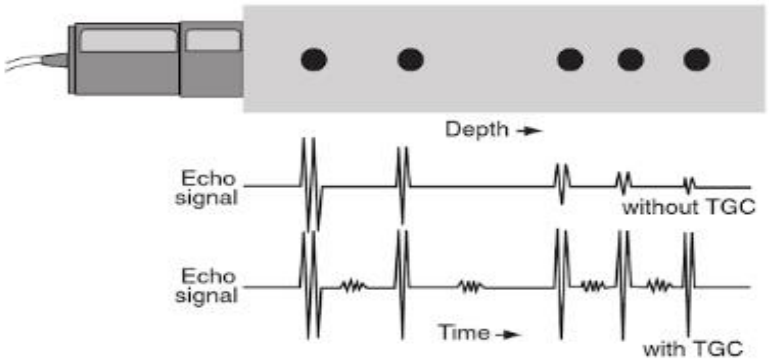

Figure 65: Time gain compensation (TGC) [56]

Several kinds of gain algorithms can be generated and applied into the detected echo signal to amplify the reflections. Plotted signals magnified with the echoes of the amplifiers. Maybe the most basic and simply useful TGC alghorithm is linear TGC. The depth of the tissues can be calculated by means of travel time of the returning echoes. Echo signal amplification is implemented by a linear multiplier which increases the measured voltage value as a function of travel time.

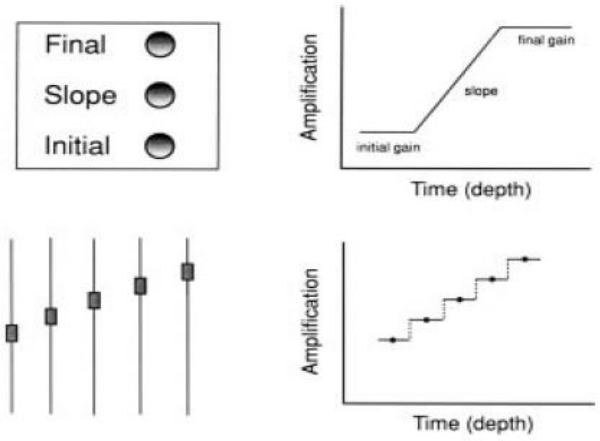

Figure 66: Three-knop and linear time gain compensation [18]

The MUS Application also uses the time gain compensation algorithm to make some observations and to obtain comparative results. After trials of linear and distance square algorithms, the most effective and distinguishable results are taken by natural exponential function. An exponential function, which depends on frequency and distance, actually removes the effect of attenuation and transmission loss.

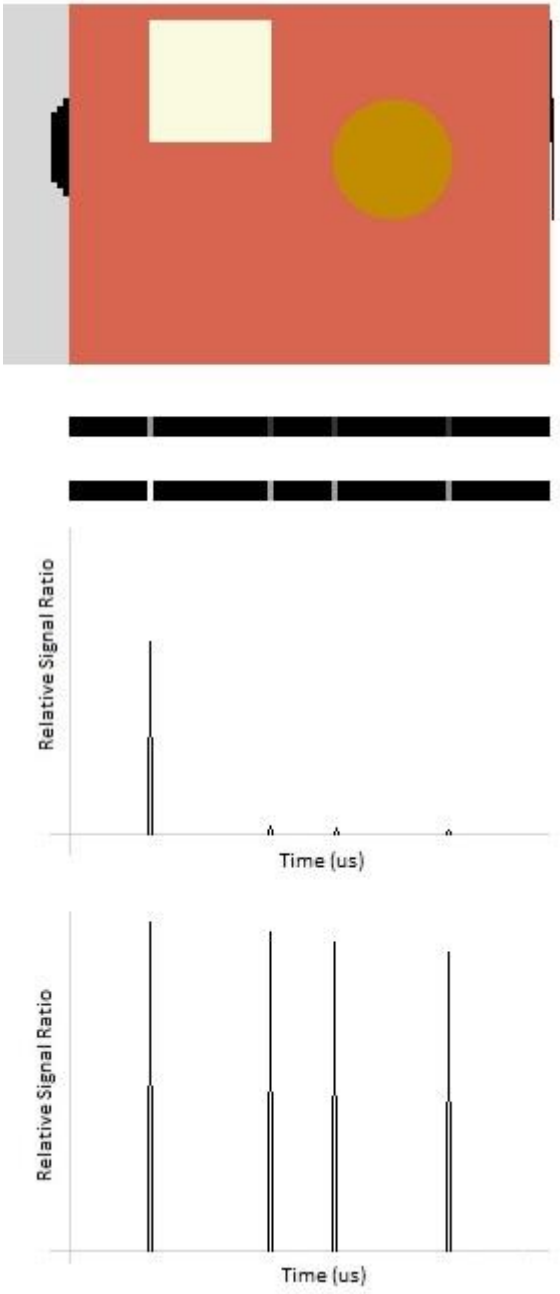

Figure 67: MUS application results: B-mode and A-mode ultrasound results without (above) and with (below) TGC algorithm.

3.9.3 Backprocessing and Image Reconstruction

The prepared MUS Application has also a reverse mode. For the MUS Application output, the software produces graphical results, and in addition, the software also prints out the corresponding returning intensity and travel time in CSV format for every scan line and every captured reflection or echo.

For every scan line or channel, The MUS Application calculates and prints 10 values in A;B;C;D;E;F;G;H;I;J format where the first five entries are travelling times of the captured echoes and the other five are the calculated relative intensity values from the tissue and boundary intersections. MUS Reverse Calculation (MUSr) Application uses its back computation algorithm and solves the reverse problem. MUSr Application has tissue specific acoustic properties database. Once the CSV formatted data inputs are given to the MUSr Application, the software starts calculations accepting that the first tissue (background) is blood and the second tissue is fat. A comparison is made and if the result is not valid then application changes the second tissue to liver, kidney, brain, muscle… one-by-one and compare the results. If result is provided and related tissues are discovered, then application passes to the next step. If not, the software changes the first tissue to fat, liver, kidney, brain, muscle… one-by-one and attempts to find the second tissue again changing tissues and calculating related conditions. For the twelve tissue types this procedure is repeated maximum 12*12 times for every echo signal. When the calculated result and the program input taken from the MUS Application is matched, the MUSr algorithm reconstructs the image using position information and color codes of related tissues.

1. Tissue Type : Fat
2. Tissue Type : Eye (lens)
3. Tissue Type : Kidney
2. Tissue Width (mm) : 60
3. Tissue Diameter : 60
2. Tissue Center Coordinates (XxY) : 88x126
3. Tissue Center Coordinates (XxY) : 180x90

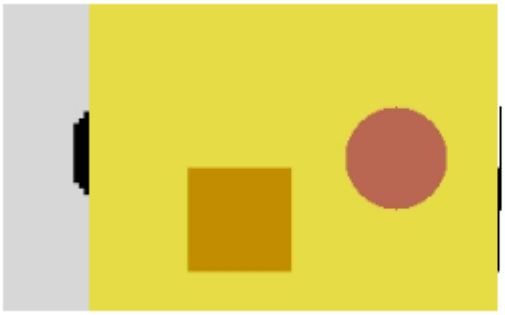

Figure 68: MUS application geometry under specific conditions.

Please enter results table :

```
9;0.00020710396812;0.00028315396331236;0;0;0.001574598477564 3;2.5077874575211E-5;0;0;0.0003663274167
9374;0.00011272827991792
10;8.0E-5;0.00015272727272727;0.0001977012356053 4;0.0002725900939834 3;0.1087045471586;2.665518651329
E-5;4.4460574088149E-6;7.5411987947277E-8;0.0003148054361718 5;3.4328231373178E-7
11;8.0E-5;0.00015272727272727;0.0001987711678410 5;0.0002716837182678 3;0.1087045471586;2.665518651329
E-5;4.3053912898407E-6;8.1286684883989E-8;0.0003149689926919 5;3.7804086090324E-7
12;8.0E-5;0.00015272727272727;0.0002003197497345 3;0.0002703718622688 9;0.1087045471586;2.665518651329
E-5;4.1096410514151E-6;9.0609374340411E-8;0.0003152057185865;4.3467529178437E-7
13;8.0E-5;0.00015272727272727;0.0002024089801568 8;0.0002686020046499 6;0.1087045471586;2.665518651329
E-5;3.8595776277922E-6;1.0490335783087E-7;0.0003155250913899 1;5.2475584673709E-7
14;8.0E-5;0.00015272727272727;0.0002051410658307 2;0.0002662875626460 1;0.1087045471586;2.665518651329
E-5;3.5553840133225E-6;1.2705165932584E-7;0.000315942735059 8;6.7130067090802E-7
15;8.0E-5;0.00015272727272727;0.0002086937757815 8;0.0002632779421143 9;0.1087045471586;2.665518651329
E-5;3.1953927059832E-6;1.6298925884768E-7;0.0003164858244790 4;9.2470649610969E-7
16;8.0E-5;0.00015272727272727;0.0002134169278996 9;0.0002592768005111 5;0.1087045471586;2.665518651329
E-5;2.7726042685061E-6;2.2697453737042E-7;0.0003172078349939 1;1.4155100741346E-6
```

Enter

Figure 69: MUSr application data input screen. Resulting values taken from MUS application outputs under figure 68 conditions.

1;Fat;160.738639716;Kidney;38.522720568;Fat;81.477279432
2;Fat;157.639320225;Kidney;44.72135955;Fat;75.27864045
3;Fat;155.281585811;Kidney;49.436828378;Fat;70.563171622
4;Fat;153.467001677;Kidney;53.065996646;Fat;66.934003354
5;Fat;152.089428526;Kidney;55.821142948;Fat;64.178857052
6;Fat;151.08633541;Kidney;57.82732918;Fat;62.17267082
7;Fat;150.419601085;Kidney;59.16079783;Fat;60.83920217
8;Fat;150.066740906;Kidney;59.866518188;Fat;60.133481812
9;Fat;150.016671299;Kidney;59.966657402;Fat;60.033342598
10;Fat;150.267862505;Kidney;59.46427499;Fat;60.53572501
11;Fat;58;Eye;60;Fat;32.828095708;Kidney;58.343808583;Fat;30.828095708
12;Fat;58;Eye;60;Fat;33.715728753;Kidney;56.568542495;Fat;31.715728753
13;Fat;58;Eye;60;Fat;34.962988331;Kidney;54.074023338;Fat;32.962988331
14;Fat;58;Eye;60;Fat;36.622844919;Kidney;50.754310162;Fat;34.622844919
15;Fat;58;Eye;60;Fat;38.783626468;Kidney;46.432747065;Fat;36.783626468
16;Fat;58;Eye;60;Fat;41.603921946;Kidney;40.792156109;Fat;39.603921946

Result :

Figure 70: MUSr application results: back processed image reconstruction

If there is an unexpected echo signal arrived or kind of anomaly inside the tissues, then the MUS Reverse Calculation Application cannot match the detected echo with its database conditions. In real world, this kind of behavior can be observed because of a tumor or a foreign object inside the body. Under these conditions, the MUSr Application calculates the position of anomaly, reconstruct the geometry and paints the related region into green to attract the technician or student's attention as seen below.

Figure 71: MUSr application results: unknown image reconstruction

CHAPTER 4

k-WAVE SIMULATIONS

k-Wave open source acoustics toolbox for MATLAB is very useful and powerful instrument for ultrasound simulations [13]. k-Wave is specially designed for time domain simulation of 1D, 2D or 3D acoustic pressure wave propagation. It can be used for the analysis of linear or nonlinear wave propagation. The material distribution and properties can be arbitrarily assigned while employing power law acoustic absorption.

In this part of the study, k-Wave is used to simulate 2D ultrasound wave propagation. The accuracy of solutions is assessed by comparing the results using analytical solutions. A simulation study for a specific body geometry and transducer configuration is used to compare the received signals with the experimental data (as described in Chapter 5)

4.1 Theory

The numerical model is based on the solution of first-order partial differential equations, which are equivalent to a generalized form of the Westervelt equation. The equations are solved using a k-space pseudospectral method, where spatial gradients are computed using the Fourier-collocation method, and temporal gradients are computed using the finite difference approximation. Mass conservation equation, momentum conservation equation and the pressure-density relation can be brought together as follows [57]:

$$\frac{\partial u}{\partial t} = -\frac{1}{\rho_0}\nabla p, \tag{4.1}$$

$$\frac{\partial \rho}{\partial t} = -\rho_0 \nabla . u - u . \nabla \rho_0, \tag{4.2}$$

$$p = c_0^2(\rho + d . \nabla \rho_0 - L\rho), \tag{4.3}$$

Where p is the sound pressure, d is the acoustic particle displacement, c_0 is the signal sound speed, ρ is the ambient density, u is the acoustic particle velocity, ρ_0 is the ambient density, ρ is the acoustic density, L is the loss operator and defined as

$$L = \tau \frac{\nabla}{\partial t}(-\nabla^2)^{\frac{y}{2}-1} + \eta(-\nabla^2)^{\frac{(y+1)}{2}-1} \tag{4.4}$$

For modeling the power law absorption, it is convenient to define L as a derivative operator based on the fractional Laplacian [57]. τ and η are the absorption and dispersion proportionality coefficients. $\tau = -2\,\alpha_0 {c_0}^{y-1}$, $\eta = 2\,\alpha_0 {c_0}^{y}\tan(\pi y/2)$, α_0 is the power law prefactor and y is the power law exponent.

These partial differential equations (4.1), (4.2) and (4.3) are solved using a k-space pseudospectral method, where spatial gradients are computed using the Fourier-collocation method, and temporal gradients are computed using the finite difference approximation.

4.2 Comparison Between k-Wave And Analytical Solution

To assess the accuracy of k-Wave simulations, analytical solution of pressure distribution generated by a point source in a homogeneous medium is calculated. For the same source and material configuration, pressure distribution is solved numerically using k-Wave.

In the homogeneous medium, equations (4.1), (4.2) and (4.3) can be simplified as follows:

$$\frac{\partial u}{\partial t} = -\frac{1}{\rho_0}\nabla p, \tag{4.5}$$

$$\frac{\partial \rho}{\partial t} = -\rho_0 \nabla . u, \tag{4.6}$$

$$p = c_0^2 \rho, \tag{4.7}$$

Where p is the sound pressure, c_0 is the signal sound speed, ρ is the ambient density, u is the acoustic particle velocity, ρ_0 is the ambient density, ρ is the acoustic density.

In the analytical solution, equations (4.5), (4.6) and (4.7) were combined together and the second order wave equation is obtained:

$$\nabla^2 p - \frac{1}{{c_0}^2}\frac{\partial^2 p}{\partial t^2} = 0 \tag{4.8}$$

In the simulation study, a point source is placed in the middle of the homogeneous medium. Assuming unbounded, acoustically homogeneous medium, the acoustic pressure distribution for a medium with density ρ and velocity c satisfies the following equation.

$$\nabla^2 p + k^2 p = -\rho Q(r)\delta(r - r_0) \tag{4.9}$$

where r is the field point and r_0 is the source point.

$$P(R) = \frac{W_0 \rho Q}{4} {H_0}^2(kR) \tag{4.10}$$

Here $R=\sqrt{r^2 + {r_s}^2 - 2rr_s\cos(\theta - \theta_s)}$ is the distance of the source (r^s, θ^s) to any point (r, θ), ${H_0}^2(.)$ is the zero order Hankel function of the second kind and $w_0 = kc$. To compare the analytical and k-Wave results, relative errors are calculate as given below:

$$e_{magnitude} = \frac{|\phi_{analytical}| - |\phi_{numerical}|}{|\phi_{analytical}|} \tag{4.11}$$

$$e_{phase} = \left|\arg(\phi_{analytical}) - \arg(\phi_{numerical})\right| \tag{4.12}$$

Both k-Wave and analytical solutions are calculated on a regular grid of 40000 mesh elements (grid size is 0.5 mm).

4.2.1 Time Step Error Between Numerical and Analytic Solution

In this section, numerical solutions obtained by k-Wave are compared with the analytical solutions for three different time steps. For this study, the medium is chosen homogeneous and sound speed inside the medium is assume as 1500 m/s. Acoustic source is chosen as a point source and it produces 1 Pa, 1 MHz sinusoidal pressure wave. Space between the square shaped mesh elements was 0.50 mm and mesh size was 100×100 (Figure 72).

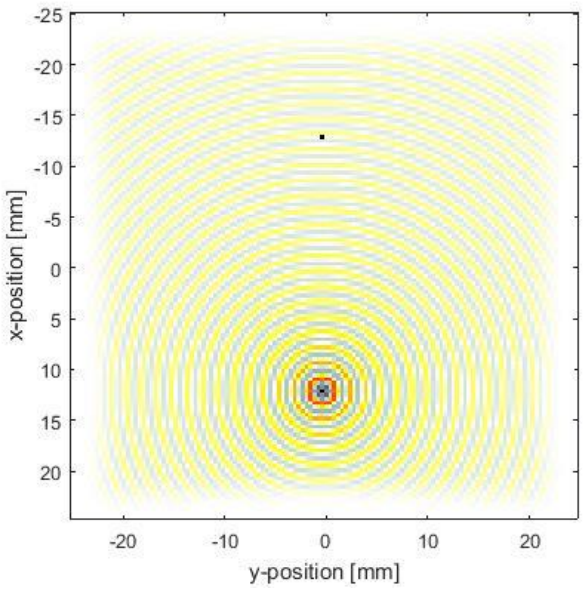

Figure 72: Pressure distribution generated by point source in k-Wave.

Three different time steps are chosen as 1 ns, 25 ns and 100 ns. Under these conditions, simulations are made and normalized acoustic pressure waves calculated at 25 mm distance from the source are shown (Figure 73, 74 and 75). The error between the analytical and numerical solutions are also presented in the same figures.

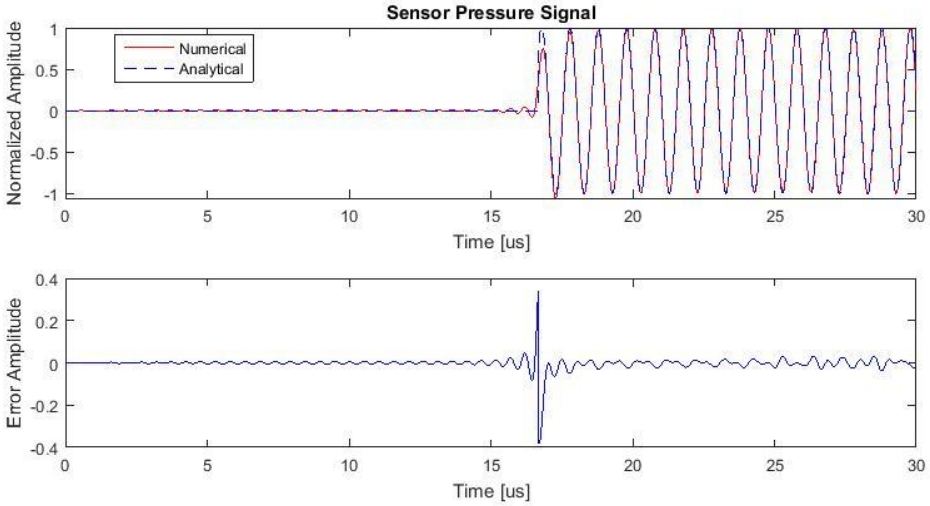

Figure 73: Analytical and numerical solutions for a sinusoidal acoustic point source (1 Pa, 1 MHz) in a homogeneous medium. Phase errors between analytical and numeric solutions are shown in the lower figure. Time step in numerical solutions is 1 ns.

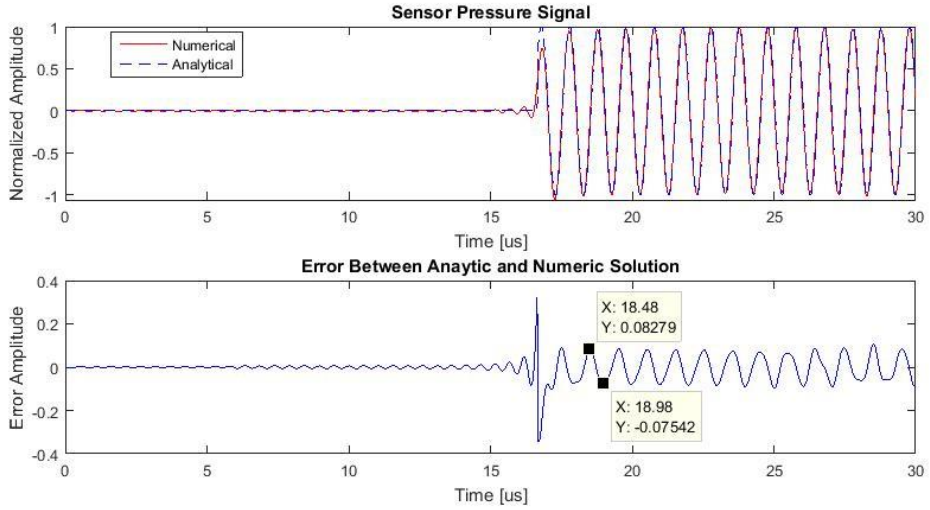

Figure 74: Analytical and numerical solutions for a sinusoidal acoustic point source (1 Pa, 1 MHz) in a homogeneous medium. Phase errors between analytical and numeric solutions are shown in the lower figure. Time step in numerical solutions is 25 ns .

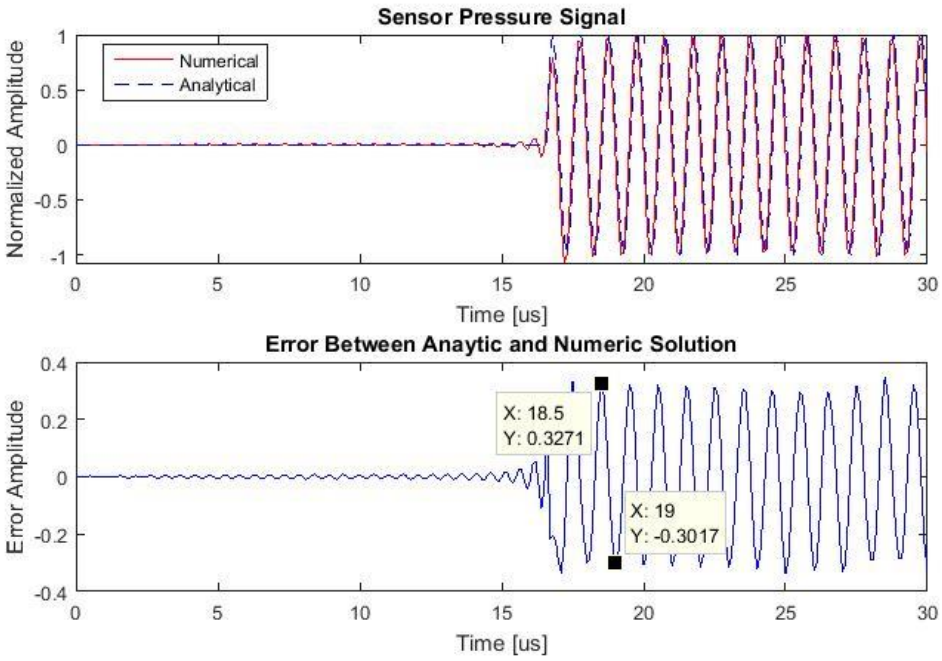

Figure 75: Analytical and numerical solutions for a sinusoidal acoustic point source (1 Pa, 1 MHz) in a homogeneous medium. Phase errors between analytical and numeric solutions are shown in the lower figure. Time step in numerical solutions is 100 ns.

The phase errors between the analytical and numeric solutions are found as 31 %, 7.5% and below 1 % for 100 ns, 25 ns and 1 ns, respectively. Consequently, the time step is chosen as 25 ns for the rest of the numerical calculations, since the error is acceptable (7.5 %) and calculations are obtained in shorter time.

4.2.2 Spatial Discretization Error Between Numerical and Analytic Solution

In this section, numerical solutions are compared with analytical solutions for two different mesh sizes. The body and source configuration is same as given in the previous section.

Two different meshes are used: 100×100 and 400×400. The corresponding grid sizes are 0.5 mm and 0.125 mm, respectively. The latter mesh is assumed as the reference mesh which produces solutions with acceptable accuracy (since the corresponding

grid size is $1/12^{th}$ of the wavelength [13]). Under these conditions, simulations are done and normalized acoustic pressure waves measured at 25 mm distance from the source are shown in Figure 76.

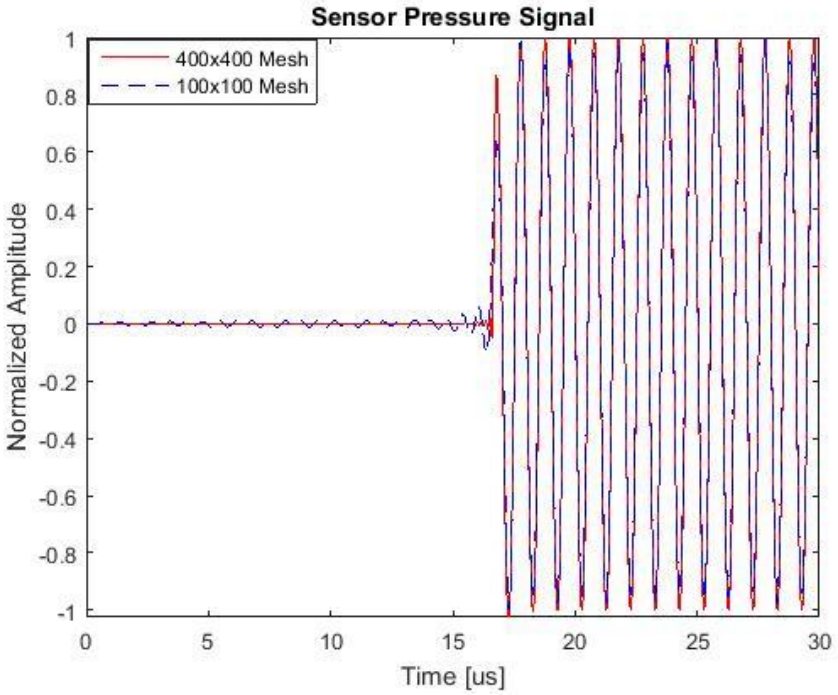

Figure 76: Effects of grid size on the accuracy of solutions. Acoustic pressure waves measured at the sensor position (25 mm away from the point source) for 100×100 and 400×400 mesh sizes.

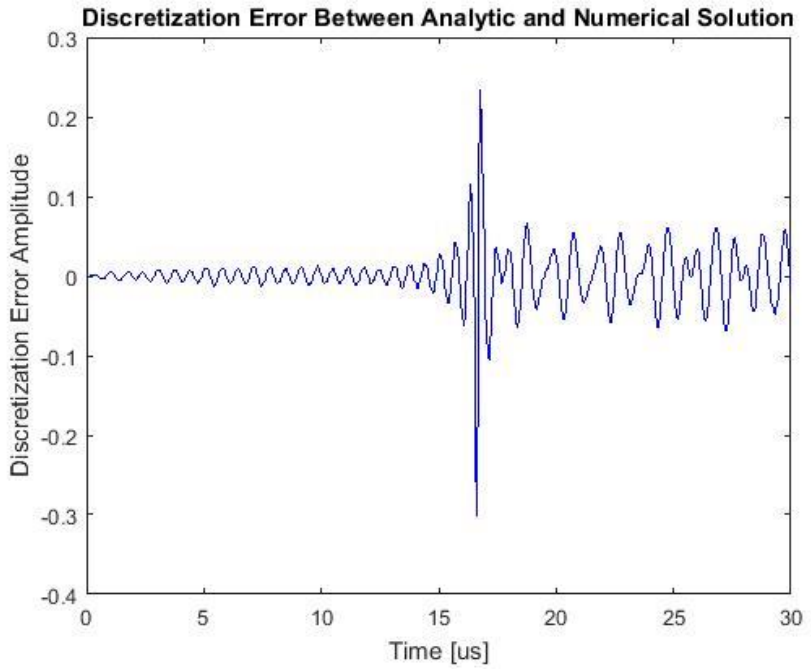

Figure 77: Phase error between acoustic pressure waves calculated in 100×100 and 400×400 mesh sizes.

The phase error between the pressure wave solutions calculated for 100×100 mesh size and 400×400 mesh size is calculated and shown in Figure 77. Maximum error relative to the solutions obtained by the fine mesh is found as 7 %. Since the error is under 10 % and the results are obtained in a shorter time, a grid size of 0.5 mm (corresponding to 100×100 mesh size) is used in heterogeneous k-Wave simulations.

4.3 Simulation Procedure

In the beginning of the k-Wave simulations, program inputs are defined. Each mesh element's shape is rectangular. Width and height of each rectangular mesh element are first defined. After mesh element description, the simulation geometry needs to be specified. Simulation geometry is defined by three matrices, each of which describes the acoustic properties of the medium. These properties are density, acoustic velocity and attenuation coefficient of each mesh element. Inhomogeneities

within the simulation region are specified by the given values of each matrix element.

After providing the medium's geometry and acoustic properties, monopole source matrix is created which has the same column and row numbers with the simulation domain matrices. In the monopole source matrix, all values of the elements are zero except the elements which correspond to the point source locations. Value of these elements are set one. Note that these point sources represent the piezoelectric elements of the transducer. Once the transducer position is set, the pressure excitation waveform type is defined for each of the point source elements. The initial pressure excitation type is defined as any arbitrary waveform such as sinusoidal, Gaussian pulse, square wave etc.

To define sensor locations and the geometry of the sensors, the same procedure with the point source is applied and corresponding matrices are set. In addition, simulation duration and time step are defined so that the time vector is formed. Lastly, boundary condition type is defined as Perfectly Matched Layer (PML). PML absorbs the pressure wave's normal component according to the following formulas.

$$\frac{\partial u}{\partial t} = -\frac{1}{\rho_0}\nabla p - \alpha . u \tag{4.13}$$

$$\frac{\partial \rho_{\mathrm{x}}}{\partial t} = -\rho_0 \frac{\partial u_{\mathrm{x}}}{\partial x} - \alpha_{\mathrm{x}}\rho_{\mathrm{x}}, \tag{4.14}$$

$$\rho = c_0^2 \sum \rho_{\mathrm{x,y,x}}, \tag{4.15}$$

where equation (4.14) is representation of equation (4.5) for each Cartesian direction, and $\alpha = \{ \alpha_1, \alpha_2, \alpha_3 \}$ is the anisotropic absorption in Np/m, which is only nonzero within the PML.

These inputs defining the acoustic properties and geometry of the medium, point source and sensor positions, time vector are given as input parameters for the "kspaceFirstOrder2D" function. This function takes these inputs and solves the pressure distribution for each time step according to the Westervelt equation.

4.4 Simulating The Phantom Experiment

For the preparation of phantom experiment, first a fixed experiment geometry is created. Size and shape of the background, square and circle objects define the boundaries and represents three different type of objects with different acoustic properties.

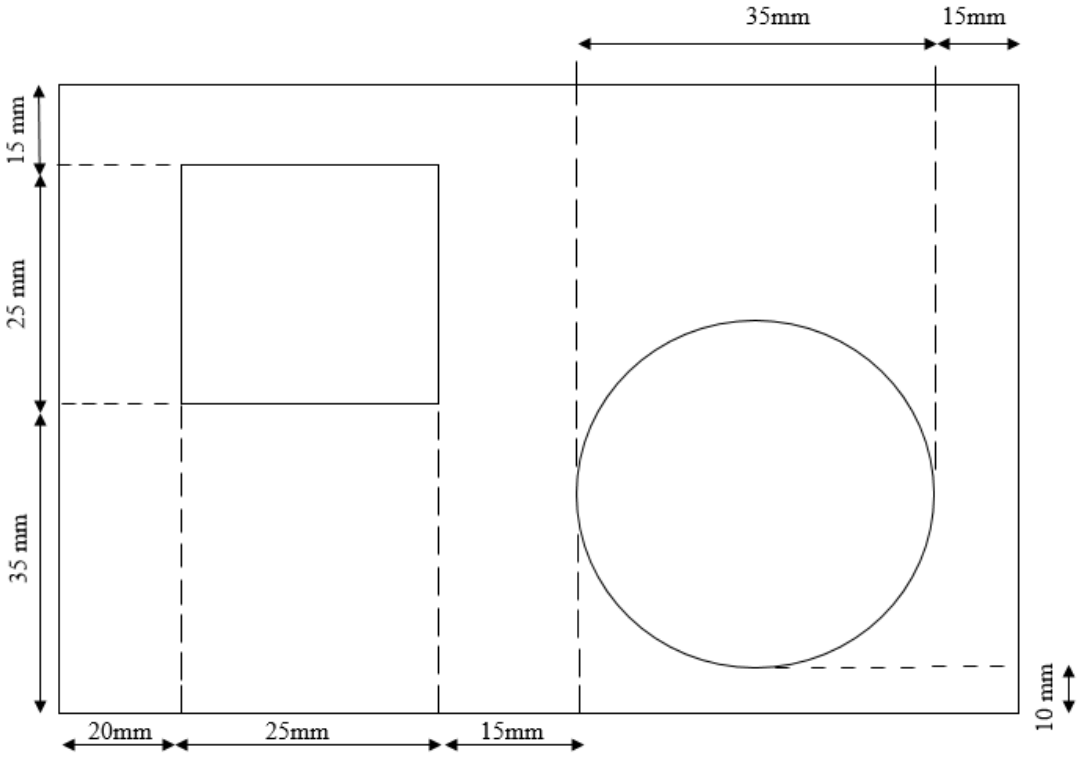

Figure 78: The body geometry created for comparing the k-Wave solutions and experimental data.

The density, attenuation coefficient and acoustic signal speeds within the objects are taken according to the values given in Table 9. In this simulation, dimension of the simulation domain was 75 mm x 110 mm. This 2D simulation domain is divided into 33000 mesh element. Each mesh element's shape is assumed square (0.5 mm x 0.5 mm). The resulting absorption coefficient distribution is shown in Figure 79.

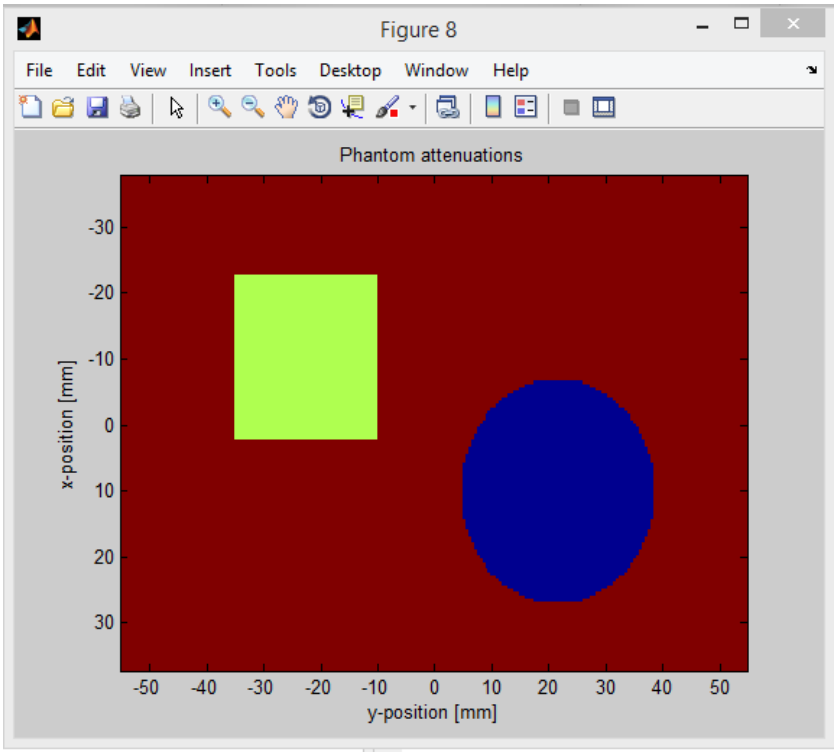

Figure 79: Created geometry and acoustic conditions for k-Wave simulations

Simulation duration is chosen as 150 microseconds and while the time step is 25 nanoseconds. Boundary condition of this simulation is the absorbing boundary condition. Computational domain wis enclosed by the Perfectly Matched Layer so that propagating acoustic waves do not reflect from the boundaries and fully absorbed.

In this simulation, 1 period sinusoidal acoustic pressure wave is generated by 16 point source element. Space between these elements is 1 mm, same as the distance between each piezoelectric element in the Imasonic Transducer [58] used in the experimental study (Chapter 5). These elements generate 1 MPa pressure wave. Reflected waves are recorded by 16 sensor elements, which are placed at the location of the 16-point sources. In order to get a clear reflected wave from the boundary of square region, the transducer is placed in the upper left edge starting from the 5th mesh element (2.5 mm from the top boundary). The propagation of acoustic pressure at three different time intervals is shown in Figure 80.

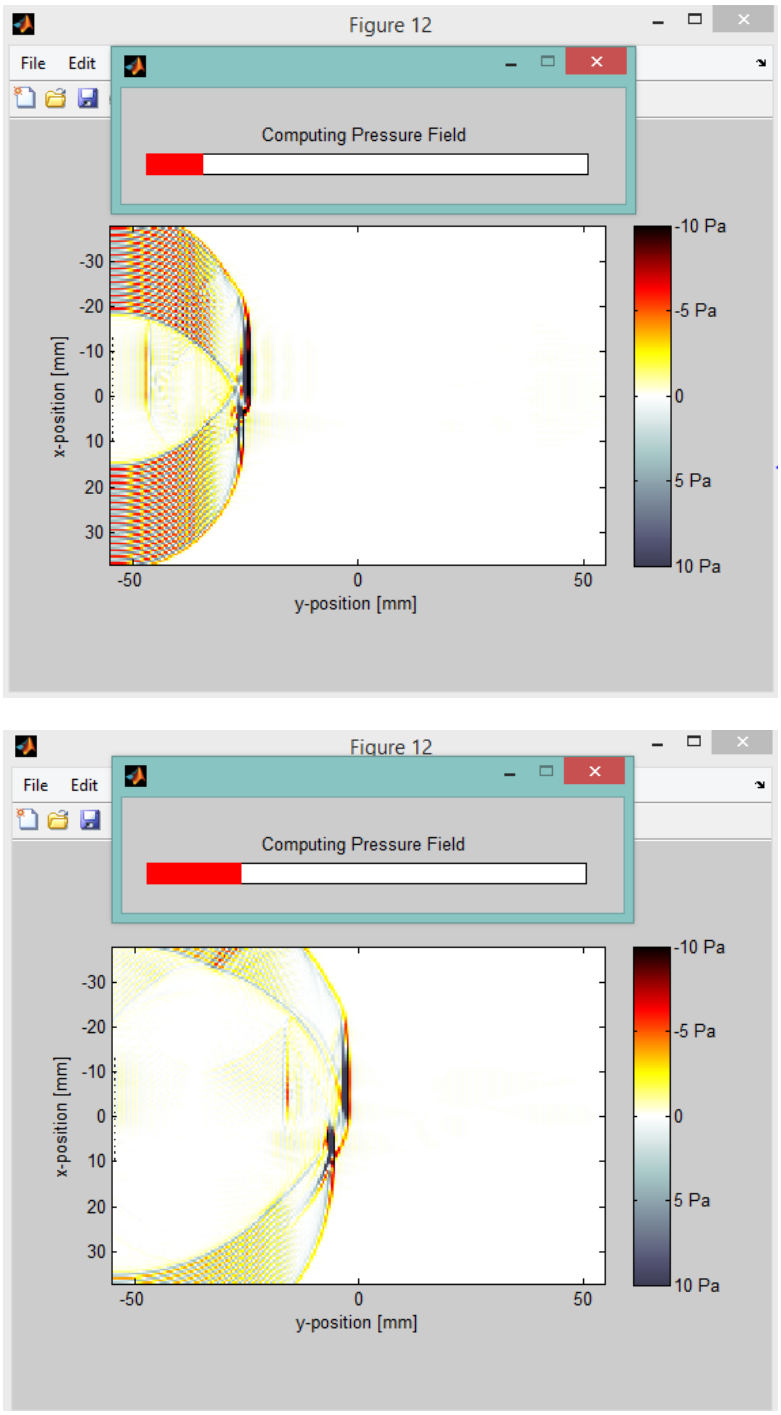

Figure 80: Representation of propagation of pressure wave at k-Wave simulation

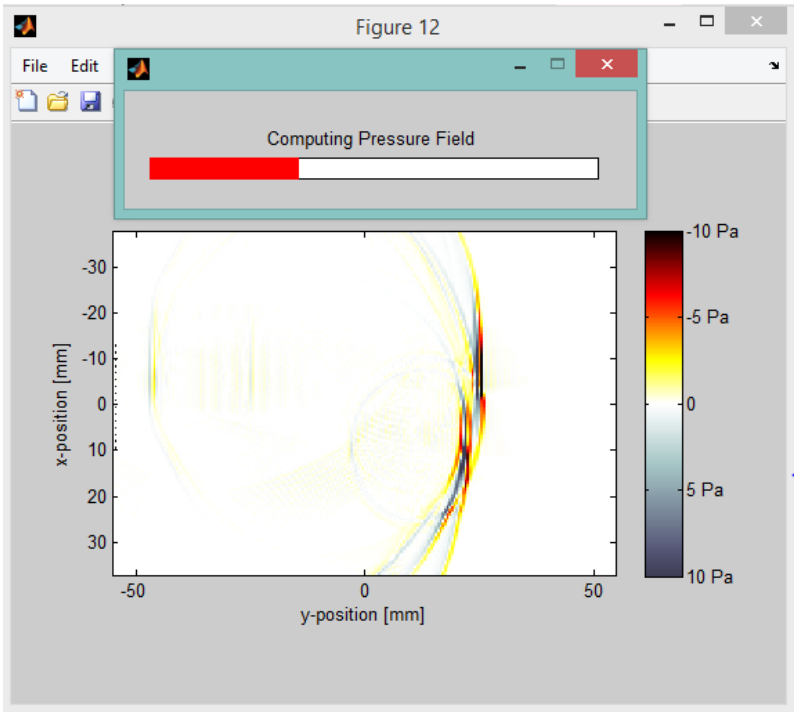

Figure 80 (continued)

CHAPTER 5

EXPERIMENTAL RESULTS

In this part of the thesis study, experimental results obtained by tissue mimicking phantoms and an experimental ultrasound system with 16-channel phased array transducer are presented. The core of this study is phantom preparation process. The experimental studies are to be performed in the scope of medical ultrasound. Consequently, phantoms should mimic the acoustic properties of biological tissues. Once the phantoms are prepared, pulse-echo signals are acquired and the resultant waveforms are shown for the selected ultrasound beam direction. The phantom preparation procedure and data acquisition stages presented in this thesis can be the basis of future educational experimental studies in the field of biomedical engineering.

5.1 Phantom Preparation

Ultrasonic phantoms are experimental objects prepared for tissue mimicking purpose that simulate the acoustic properties of tissues. Phantoms are in general used for training and calibration of ultrasound systems [59].

The acoustic properties of human body tissues such as attenuation of sound, reflection and transmission coefficients, and sound wave propagation inside the body can be experimentally analyzed by specially designed ultrasound phantoms. Human organs and body tissues can be modeled by artificially prepared tissue equivalent phantoms. In the literature, multitudes of techniques and tissue-mimicking materials have been proposed to prepare phantoms [28].

This kind of tissue like medical phantoms are mostly used for clinical or experimental purposes, such as biopsy training, development of new system, probe, devices and for comparison of experimental data with computer models. Acoustic properties, attenuation, scattering coefficients, ultrasound speed, reflection and transmission calculations can be modeled and characterization of ultrasound systems can be expressed using biological tissue mimicking materials.

Prepared materials 1) should provide the acoustic properties of biological tissues, 2) should have high stability around room temperature for a long period, 3) must not contain toxic materials, and 4) should be easy to produce [60].

The most often-used bulk matrix materials for mimicking soft tissue are based on: aqueous suspensions, agarose, gelatin, magnesium-silicate, oil gel, polyacrylamide gel, polyurethane resin, polyvinyl alcohol (PVA), polyester resin, epoxy resin, polysaccharide gels TX-150 and TX-151, polyacrylamide, and Room-Temperature-Vulcanizing (RTV) silicone [61].

Agarose based gel phantoms used in the experiments were approximately prepared according to the methodologies and ratios described in [62]. In this thesis study, three different material composition is developed to form an inhomogeneous body phantom (circular and rectangular inhomogeneities in a rectangular background area). Table 8 shows the ingredients of the three compositions.

Table 8: Raw materials and ratios used in experiments.

	Background	**Circle Object**	**Square Object**
Ethanol	130 ml	48 ml	-
Tri-distilled water	220 ml	82,5 ml	144,65 ml
NaCl	2,18 gr	1,5 gr	1,125 gr
Agarose	3,3 gr	4,5 gr	1,91 gr
Gelatin	10 gr	7 gr	5,9 gr
Formaldehyde	-	-	0,35 ml

Agarose is a gelling agent that provides the phantom with the necessary firmness. Ethanol and chloride of sodium quantities affects the electrical permittivity and the conductivity respectively [62]. Formaldehyde used as hardener is added to increase cross-linking[63].

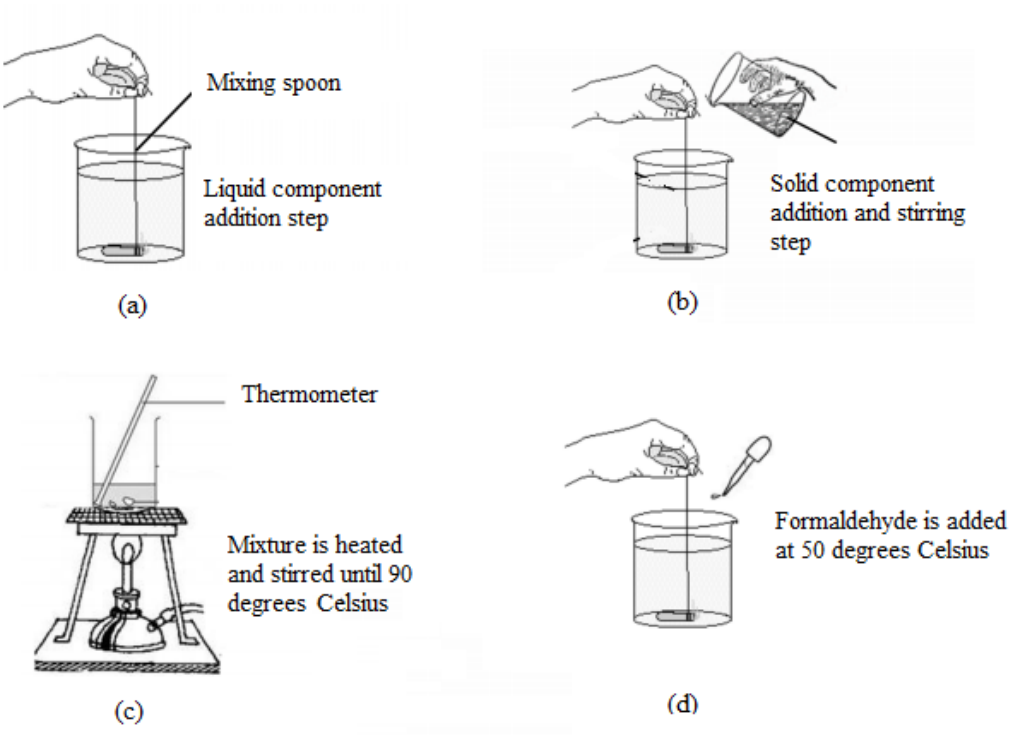

Figure 81: Preparation steps of experiment specific gel objects.

The preparation procedure is shown in Figure 81. Background and circular object ingredients are weighed and mixed according to the proportions in Table 8. First, the liquid components are mixed then the solid components aredissolved into the mixture. After that, the mixture is heated and stirred until about 90°C to reach the melting temperature. Heating process should be slow and controlled so that no air bubble occurs which causes undesired echo signals and errors during ultrasonic experiments. Square object is prepared in the same way; in addition, formaldehyde is injected at the cooling phase as a final step when the phantom mixture is about 50°C as shown in the Figure 81 (d).

Figure 82: Half completed acoustic gel object.

For the acoustic gel object production, first the background object is prepared and molded. After the cooling and hardening process at room temperature, the circular and square objects are prepared and molded into their spaces as shown in Figure 82.

After preparing the phantoms and 3D geometry is set, the related physical and acoustic properties of each phantom is measured one-by-one by means of the real ultrasound system and the remaining phantom samples. Samples were stored within separate volumetric containers. After measuring their net weights, the density of gel objects are calculated from the ratio of mass (m) to sample volume (V). Sound speed and attenuation values are measured using Imasonic ultrasound system kit [58] (Figure 83). Since we measured the travelling distance (x) and echo time (t) of the propagating wave, speed of sound within the gel objects could be calculated by $c = x/t$ formula. Attenuation of gel objects is measured by taking results from different points of the sample. The received signal attenuation at different distances gives the attenuation coefficient in db/cm. Finally, acoustic impedances of the gel objects were calculated via $Z=dc$ formula. After these calculations and measurements, the acoustic property of each phantom is obtained and presented in Table 9.

Table 9: Measured acoustic properties of phantoms used in experiments.

	Density (gr/cm^3)	**Sound Speed (m/sec)**	**Acoustic Impedance $kg/(sec\cdot m^2)\times 10^6$**	**Attenuation (db/cm)**
Background	1,002	1547	1,550	0,744
Circular Inhomogeneity	0,888	1752	1,556	0,656
Square Inhomogeneity	0,979	1637	1,602	0,703

5.2 Experiments

Figure 82 shows the geometry of half-completed phantom. Fully completed phantom pictures are not shown because of the low contrast between inhomogeneities and the background. After phantom preparation, ultrasonic measurements are acquired using a commercial research system Imasonic Open System Ultrasound kit (Figure 83). The system uses16-element phased array transducer of the same firm [58]. The specifications of the transducer are: Element pitch: 1 mm, inter element spacing: 0,35 mm, total active region: 15,65 mm, and center frequency (6 db) is 1 MHz.

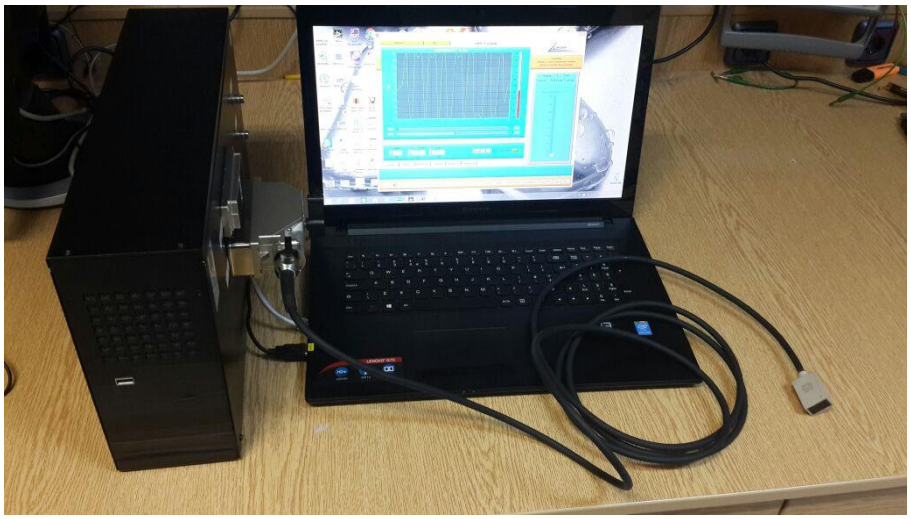

Figure 83: Imasonic, open 179, ultrasound system kit and 16-channel, cdc12184-3, linear array transducer

The block diagram prepared for ultrasound experiments is shown in Figure 84. To minimize the effect of air between the transducer and gel object and get close the matching layer conditions, acoustic measurements are made in a water tank. Collected acoustic information and experimental data are transferred and processed in MATLAB.

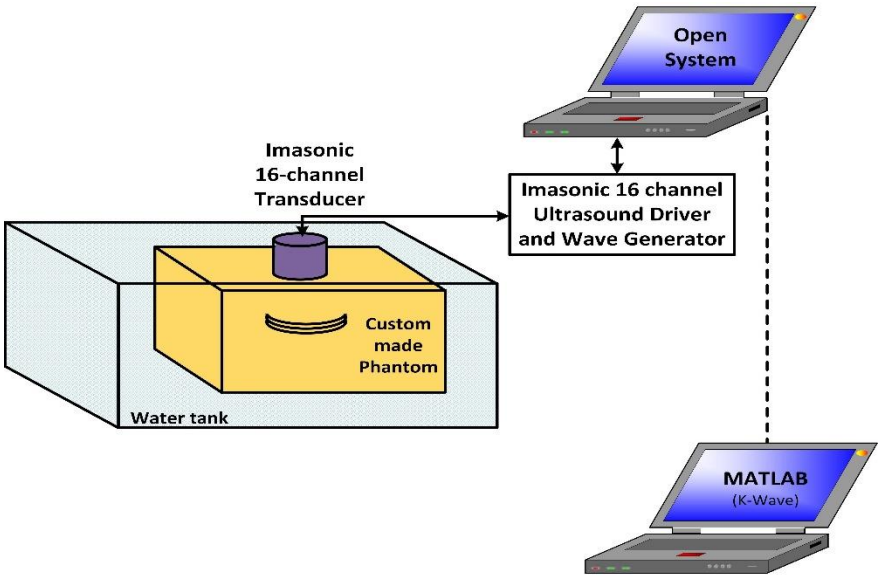

Figure 84: Block diagram of the system used in ultrasound experiments.

To excite the linear array, no special effort is made to generate a specific beam profile. Each element of the transducer is driven by 100 V (peak to peak) at 1 MHz (single cycle). Consequently, an ultrasound wave of about 2 cm beam width is generated inside the phantom. Figure 85 shows the phantom and transducer location (Figure 85). In the receive mode, data is acquired from 16 channels. Data recorded from the second element (channel) is displayed.

To obtain better plots and minimize the external effects such as measurement noise and errors due to the interferences, acoustic scan data is collected with an averaging algorithm. Imasonic Ultrasound System [58] supplies this algorithm itself. In the experiments, 500 samples are used for averaging and for every single scan path, the region is scanned 500 times. The summary of resulting echo magnitudes are divided by 500 in the time domain.

5.3 Results and Comparison

The aim of this section is to present the results of PHP application, k-Wave simulations and experimental results for a specific body geometry and acoustic property configuration.

The geometry and conditions of the PHP Application, created in Chapter 3 is customizable. The software is specialized and re-coded using the conditions given in Figure 78. Inhomogeneity sizes, shapes and locations are fixed according to the related geometry. Phantom specific acoustic properties, which are calculated and given in Table 9, are manually embedded into the PHP codes to generate the exact geometry.

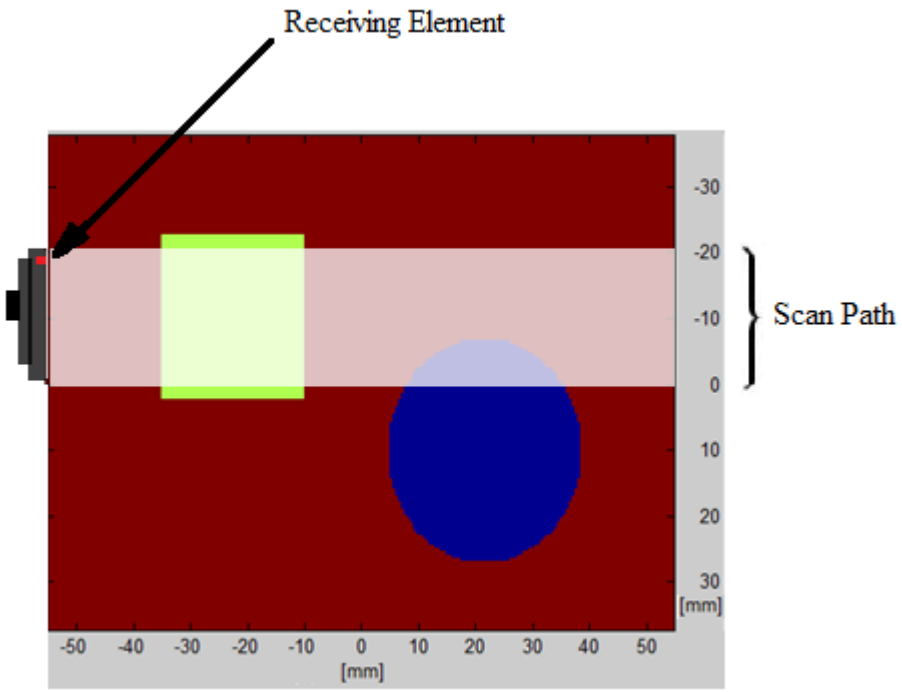

Figure 85: Phantom and transducer configuration. 16 channels of the transducer are excited synchronously. Scan path and the receiver element location are also shown.

The scan path and location of the receiver (second) element in the transducer are shown in Figure 85. Figure 86 shows the echoes obtained from the second channel in the array transducer. As the receiver channel is closer to the square inhomogeneity, the echoes from the front and rear surfaces of the square inhomogeneity must be dominant.

MUS application provides 1D theoretical calculations obtained along the horizontal line starting from the channel location. Thus, it shows the correct echo instants due to both surfaces. Echoes obtained from experimental data and simulations are clearly visible. k-Wave data shows similar behavior for the selected channel. The receiver is relatively insensitive to the boundary effects, finite beam width of the excitation and effects of other inhomogeneities inside the phantom. In the experimental studies, there are minor delays in the echoes originating from both surfaces when compared to the k-Wave and the MUS Application results. Since in both studies (simulations

and PHP applications) the geometry and acoustic properties are accurately defined, this behavior is expected. The echo amplitudes measured by the experimental system is apparently different that the calculation, and simulation results. In the experimental studies, there are noise in the measurements, imperfections in the inhomogeneity surfaces, deviations in acoustic properties, differences in the transducer configuration, and in location. The calculated and measured echo instants and relative intensities are shown in Table 10.

Table 10: The calculated and measured echo instants and relative intensities. Results of the PHP application, k-Wave simulation and experimental studies.

COMPARISON TABLE	SQUARE INHOMOGENEITY			
	Echo Duration (us)		Normalized Received Signal to Transmitted Signal Ratio	
	First Boundary	Second Boundary	First Boundary	Second Boundary
PHP BASED COMPUTER APPLICATION	24.23	56,23	1.00	0.67
k-WAVE BASED MATLAB SIMULATION	23.95	55.42	1.00	0.60
REAL ULTRASOUND SCAN FROM ACOUSTIC GEL OBJECT	25.05	57.08	1.00	0.79

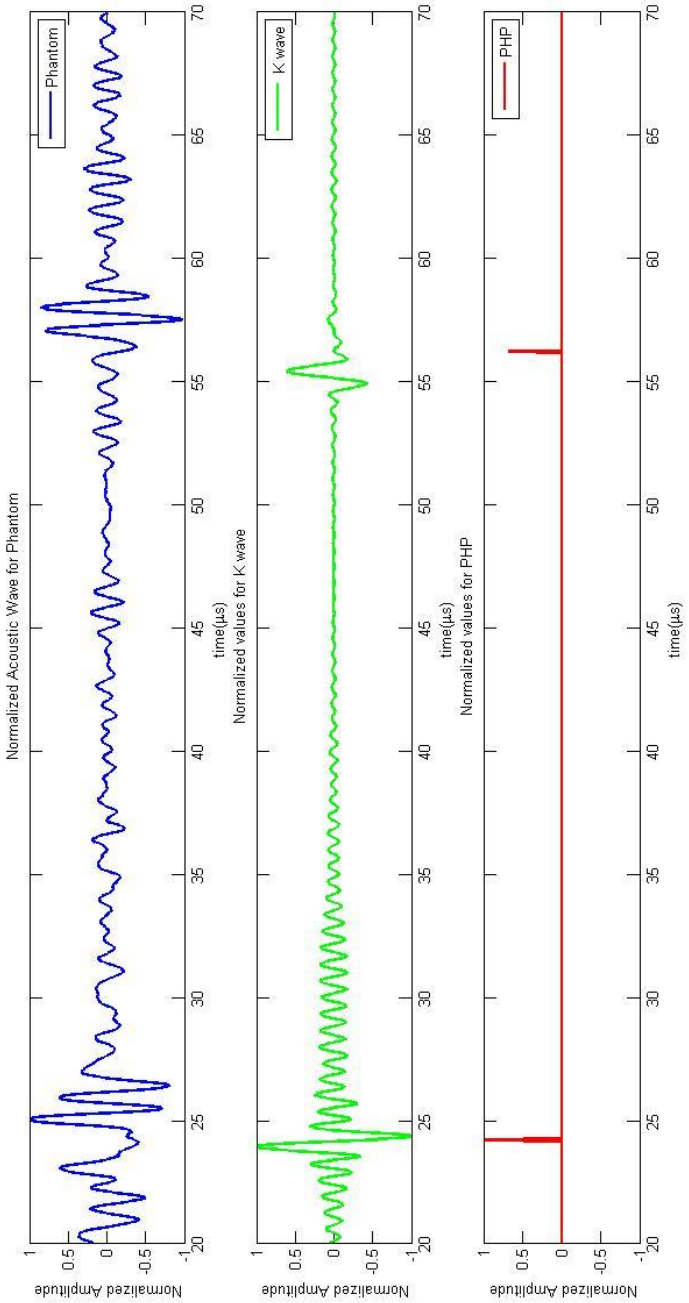

Figure 86: Pulse-echo signals taken from the Scan Path (Figure 85). Experimental data (top), k-Wave signal (middle), PHP application (bottom).

CHAPTER 6

CONCLUSION AND DISCUSSION

In this thesis study, the field of medical ultrasound was studied by 1) preparing assistive computer tools for the education of ultrasound, 2) simulating ultrasound waves in biological tissues based on k-Wave (an open source acoustic toolbox for MATLAB), 3) preparing ultrasound phantoms and conducting experimental studies using a commercial research ultrasound system. For this purpose, first a series of computer applications based on PHP programming language was prepared to describe the basic components and foundations of the ultrasound imaging system. Mathematical formulations and physical phenomenon of ultrasound system were introduced and user-friendly visual applications were obtained to ease the learning process. Next, ultrasound wave propagation was simulated using k-Wave toolbox of MATLAB. Finally, ultrasound phantoms were prepared and experimental studies were conducted using the research ultrasound system. Following are conclusions and discussion for each part this thesis study.

PHP Applications

To decide the programming language, e-learning trends, device ownership trends, operating system trends and programming language trends were searched. Because of its effectiveness, widespread usage, access easiness and device, operating system and browser independence, PHP server-side scripting language was chosen for computer-based applications.

During the thesis work, a series of computer based medical ultrasound applications were prepared and given into service for biomedical engineering students.

- Snell's Law
- Ultrasound intensity
- Attenuation
- Transducer design
- Near Field and Far Field calculations
- Doppler Effect and applications

Topics were studied and PHP based visual computer applications were developed and given into service.

Prepared applications were published on the internet as freely reachable educational documents. Generated software codes are accessible on the internet from the METU web servers at http://144.122.167.220:8080/us.php web address.

In addition to the partial ultrasound applications, the Medical Ultrasound System (MUS) application was also coded in PHP and implemented throughout the thesis studies. Results of the PHP based MUS application were compared with the

- Real ultrasound scans over generated phantoms and
- k-Wave toolbox for MATLAB.

k-Wave Simulations

Numerical simulations should produce the results with minimum error using low computer resources. To choose the more efficient discretization length and time step, a k-Wave simulation was prepared. The acoustic pressure wave for a point source (and a sensor) located in a homogenous medium is solved and solutions are compared with the analytical solutions. Numerical solutions are obtained for three different time steps. 25 ns time step were chosen because it produces phase errors less than 10 % and consumes less computer resources.

For space discretization, a grid size of half wavelength in homogeneous medium and 1/3 wavelength for the inhomogeneous medium was mentioned in [13]. In section 4.2.2, the solutions for grid sizes of 1/3 wavelength and 1/12 wavelength are

compared. The grid size of 1/3 wavelength condition was chosen because of its low error response (less than 7%). For the remaining of the simulations and three-way comparison of PHP application, ultrasound phantom scans and k-Wave simulations, the obtained discretization length and time step values were used as k-Wave parameters.

For the k-Wave simulations, a two-dimensional simulation matrix was generated according to the created phantom geometry as shown in Figure 78. In this geometry, acoustic parameters of the square, circle and background objects were chosen properly to match the phantom properties used for experimental studies. 16 acoustic point source were located in the same location where Imasonic phased array ultrasound channels stand. The k-Wave simulations and calculations obtained by PHP codes were examined. Duration of echoes arising from the object boundaries were calculated using both approaches.

Phantom Experiments

For the phantom experiments, the fixed MUS geometry was created as a 3D gel object as shown in the Figure 82. Three different gel with different acoustic properties were prepared for the background, square and circular objects. The components of each phantom and their measured acoustic properties were shown in Table 8 and 9 respectively. Ultrasound scans were obtained using the prepared acoustic phantom employing the Imasonic Open 179 ultrasound kit and 16-channel transducer. The acoustic experiment measurements were done in water tank to provide matching conditions. Related experiments were done and results were taken for the comparisons.

Ultrasound scans obtained from a specific phantom transducer configuration were compared with the data of PHP applications and k-Wave simulations. Echo durations and normalized signal values arising from the transition points measured and recorded for the experiments.

During the phantom experiments, some experimental differences and errors were observed, compared to the k-Wave simulations and PHP applications. This is due to

the imperfections in the real environment (phantom and transducer properties), and noise in the measurements, etc. In addition, there were some disruptions during the molding and cooling process of acoustic phantoms. This kind of impurities cause the pressure wave to scatter and produces undesired noise.

Another factor that affects the experimental studies was the contact between the transducer and phantom. The contact problems or stretching of phantom during transducer interaction produce a few mm of error and this error generates a few μs shift in echo positions.

In k-Wave simulation, the outer boundary of simulation domain is Perfectly Matched Layer (PML) but in real ultrasound scans over acoustic phantom experiments were done inside a water tank. These boundary conditions also produce differences in signal characteristics compared with the k-Wave results especially on the echo from the far edges.

In k-Wave simulation, the transducer was modeled with 16-point sources. For the real transducer, the beam width and behavior of transducer is different from the 16-point acoustic source. This difference causes difference in pressure distribution and echo signal characteristics between k-Wave and phantom experiment.

6.1 Future Work

In this thesis, ultrasound physics, mechanism and background was studied and previous works in the ultrasound simulation field was searched and described. A series of PHP based ultrasound applications is prepared. Although the developed codes are very useful for an ultrasound technician or education of biomedical engineering students, there are still some points that can be improved on the prepared work. In this part of the thesis, comments are given for the improvement of these applications.

- An application for 1D or 2D simulation of the ultrasound propagation should be added to the application list.
- The geometric shapes and types of the objects can be enhanced. Even real tissue size and shapes can be generated and used for the applications.
- Although it was an undesired effect for the measurement and observations, a suitable noise figure can be applied to get much more realistic visual outputs.
- Instead of phased array and linear scan, different transducer types and scanning formats can be improved such as convex or curved array, endo array, matrix array and rectangular, sector, trapezoidal, prism or donut shape scan.
- Applications for industrial usage can be developed. Acoustic properties of metals can be imported and applications can be used to locate cracks or internal breakdowns inside a machine part or determine metal fatigue.

Different k-Wave simulations can be made for more complicated transducer/body configurations. The solutions can also be used to test and develop inverse problem algorithms that explore material properties based on ultrasound data.

Phantom preparation procedure can be improved. Phantoms of different body tissues and malign/benign tumors can be prepared and used to develop inhomogeneous phantoms.

REFERENCES

[1] **Deved#ic**, Vladan, "*Semantic Web and Education*", P:9, USA: Information Science Reference, 2006

[2] http://www.smartinsights.com/mobile-marketing/mobile-marketing-analytics/mobile-marketing-statistics, "*Mobile Marketing Statistics compilation*", 26.01.2017, Dave Chaffey, Oct 2016

[3] http://www.smartinsights.com/marketplace-analysis/customer-analysis/digital-communications-use-statistics-2014, "*How important are digital communications in 2014?",* 26.01.2017, Dave Chaffey, Aug 2014

[4] https://www.orteccommunications.com/weblog/gartner-worldwide-tablet-shipments-will-finally-overtake-pcs-in-2015, Gartner: Worldwide tablet shipments will finally overtake PCs in 2015, 08.02.2017, Kelly Verdonk, Jul 2014

[5] https://www.freelancer.com/about/ , *"World's largest freelancing and crowdsourcing marketplace.", 26.02.2017,* Freelancer Technology Pty Limited, 2017

[6] Yacoub, Hatem Ben, "*Exclusive Report: PHP Freelancing, a 30% Growth in 2014",* Jan 2015

[7] http://www.medsim.com/, "*Reality in Ultrasound Simulation*: *Ultrasim Product*", p:1, 27.01.2017

[8] http://sonosim.com, "*The SonoSim Ultrasound Training Solution*", 27.01.2017, p:1, 2017

[9] https://www.nde-ed.org, "*NDT Resource Center*", 27.01.2017, Iowa State University, 2004

[10] http://www.ntnu.edu/isb/ultrasound/abersim, *"Abersim Smulation Software", 14.02.2017,* Norwegian University of Science and Technology, 2008

[11] http://www.egr.msu.edu/~fultras-web/index.php, *"Fast Object-Oriented C++ Ultrasound Simulator",* 14.02.2017, Michigan State University, 2017

[12] http://www.simsonic.fr, *"FDTD Simulation of Ultrasound Propagation",* 14.02.2017, Emmanuel Bossy, 2012

[13] http://www.k-wave.org/manual/k-wave_user_manual_1.1.pdf, 27.02.2017, "k-Wave A MATLAB toolbox for the time domain simulation of acoustic wave fields User Manual" p:5, 2017

[14] http://misclab.umeoce.maine.edu/boss/classes/SMS_491_2003/Week_10.htm, *"Physical solutions of everyday problems in aquatic sciences",* p:1, 27.01.2017, 2013

[15] Klein, Tassilo Johanes, "*Staatistical Image Processing of Medical Ultrasound Radio Frequency Data*", p: 11-17, Munich: Technical University, 2012

[16] Pedersen, Morten Hogholm, "*New Digital Techniques in Medical Ultrasound Scanning",* p: 24, Denmark: University of Copenhagen, 2003

[17] Raichel, Daniel R., "*The Scıence and Applıcatıons of Acoustıcs*",p: 410, USA: Springer Publishment, 2006

[18] Hendee, W.R., Ritenour, E.Russel, "*Medical Imaging Physics*",p: 304 – 310-319-314 4th Ed. USA: John Wiley & Sons, Inc., 2002

[19] Cannata, Jonathan M., Williams, Jay A., Zhou, Qifa, Ritter, Timothy A and Shung, K. Kirk, "*Development of a 35-MHz Piezo-Composite Ultrasound Array for Medical Imaging*", p:236, USA: USC University, Jan 2006

[20] Child, SZ, Hartman, CL, Schery, LA and EL Carstensen. "*Lung damage from exposure to pulsed ultrasound"*, p:817, 1990

[21] Henderson, J., Willson, K., Jago, J. R., and Whittingham, T. A., "*A survey of the acoustic outputs of diagnostic ultrasound equipment in current clinical use*", p:699 1995

[22] https://www.scienceabc.com/innovation/how-ultrasound-scanning-sonography-3d-sonogram-work-pregnancy-due-date.html, "*How Does an Ultrasound Machine Work?*", 27.01.2017, 2016

[23] Martini, Silvana, "*Sonocrystallization of Fats"*, p:11, USA:Springer Publishment, 2013

[24] Rheumatology Unit, "*Therapeutic Ultrasound in Soft Tissue Lesions*", p:1331, London: Oxford, Dec 2001

[25] Lutz, Harald T., Soldner, R., "*Basics of Ultrasound – World Health Organization",* p:3, Malta, 2011

[26] Mo, Steven, Coussios, Constantin C., Seymour, Len and Carlisle, Robert, "*Ultrasound-Enhanced Drug Delivery for Cancer*", p:9, Now 2012, WEB

[27] Supriyanto, Eko and Ramli, Norhafizah, "*Development of Performance and Safety Monitoring System for Low Cost Ultrasound Medical Devices for Prenatal Diagnosis*", p:14, Malaysia: 2008

[28] Hansson, Nils Mattias, "*Statistical Segmentation and Registration of Medical Ultrasound Data*", p:6, Sweden: MediaTryck Publishment, 2012

[29] Azhari, Haim, "*Basics of Biomedical Ultrasound for Engineers"*, p:18-313-156 – 161-272, USA: John Wiley & Sons, Inc., 2010

[30] Cox, Ben, "*Acoustics for Ultrasound Imaging*", p:17, Jan 2013

[31] Tole, Nimrod M., "*Basic Physics of Ultrasonographic Imaging: Chapter 3 Interaction of ultrasound with matter*", p:23, Kenia, 1995

[32] Wilhjelm, Jens E., Illum Andreas, Kristensson, Martin, Andersen, Ole Trier, "*Medical Diagnostic Ultrasound: Physical Principles and Imaging*", p:7, Oct 2013

[33] Graaff, Leon van der, "*Frequency and Angle Dependency of the Scattering of Ultrasound as A Contrast Mechanism for Imaging Blood in The Neonatal Brain*", p:9, Netherlands: Delft University of Technology, May 2015

[34] Jönsson, Marcus, "*Ultrasound Artefacts"*, p:11, Sweden: Lund University, April 2015

[35] Aljarboua, Ziyad, "*Ultrasound Effect on Biological Tissue*", p:3, May 2008

[36] Laugier, Pascal and Ha¨ıat, Guillaume, "*Introduction to the Physics of Ultrasound*", p:41, Nov 2010

[37] Hedrick, Wayne R., Wagner, Paul R, "*Study Guide and Laboratory Exercises for Technology for Diagnostic Sonography*", p:5, USA: Elsevier Publishment, 2013

[38] https://www.slicer.org/wiki/Slicer3:2010_GenericAnatomyColors, "*Generic Anatomy Colors*", p:1, 27.01.2017, 2012

[39] Shung, K. Kirk, Smith Michael, Tsiu, Benjamin M.W, "Principles of Medical Imaging", p:89, USA: Academic Press, 1992

[40] PNT Wells, "*Ultrasonic imaging of the human body, Reportson Progress in Physics"*, p:6, 1999, WEB

[41] Millodot, "Dictionary of Optometry and Visual Science, 7th edition". 2009 Butterworth-Heinemann

[42] Zemp, Roger James, "*Modelling Nonlinear Ultrasound Propagation in Tissue*", p: 8, Canada: University of Toronto, 2000

[43] Global International Research Thoughts, "*Study of Characteristics of Piezoelectric Materials for Sensor*", p:1, India, Sept 2015

[44] Mylvaganam, Janani, "*Characterization of medicalpiezoelectric ultrasound transducersusing pulse echo methods*", p: 13, Norway: Norwegian University, July 2007

[45] Mårtensson, Mattias, "*Evaluation of Errors and Limitations in Ultrasound Imaging Systems*", p:22, Stockholm, 2011

[46] Postema, Michiel, Kotopoulis, Spiros, Jenderka, Klaus-Vitold, "*Basic physical principles of medical ultrasound*", p:17, Germany & Norway.

[47] Yan, Chen, "*High-Frequency and Endoscopic Ultrasonic Transducers Based on PMN-PT and PIN-PMN-PT Single Crystals*", p:21, Hong Kong: Polytechnic University, 2013

[48] Bakken, Øyvind, "*Multiple Line Transmission in Medical Ultrasound Multiple Line Transmission in Medical Ultrasound*", p:22, Norway: University of Oslo, Oct 2009

[49] https://www.dcconferences.com.au/lcmc2013/pdf/2. Phlebology_handbook.pdf, 27.12.2016, "*Basic Physical Principles Of Ultrasound*", p:7, ICMC, 2013

[50] http://www.srmuniv.ac.in/sites/default/files/files/US1.pdf, 27.12.2016, *"Transducers",* 2017

[51] Hebden, Jeremy C. and Rennie, Janet M., *"Principles of Ultrasound*" p:1, United Kingdom: Cambridge University, Cambridge University Press, 2008

[52] Smith, Graham T., *"Machine Tool Metrology: An Industrial Handbook"*, p:362, England: Hempshire, Springer Publishment, 2016

[53] http://www.mrcophth.com/commonultrasoundcases/principlesofultrasound.html, 27.12.2016, "*The Principles of Medical Ultrasound*", 2014

[54] Khalid, Ghaidaa Abdulrahman, "*Al-Khwarizmi Engineering Journal*", Vol. 8, p:26-39, 2012

[55] D.R. Dance, S. Christofides, A.D.A. Maidment, I.D. McLean, K.H. Ng, "Diagnostic Radiology Physics: A Handbook for Teachers and Students", p: 311, Austria: Vienna, 2014

[56] Hagen-Ansert, Sandra L., "*Diagnostic Sonography*", p: 16, USA: Elsevier Publishment, 2012

[57] Bradley E. T., Jiri J. and Alistair P. R., Cox B. T.*"Modeling nonlinear ultrasound propagation in heterogeneous media with power law absorption using a k-space* pseudospectral method", p: 4328, Acoustical Society of America, 2012

[58] http://www.imasonic.com/Company/Identity.php, 23.02.2017, "Ultrasound for health and safety", 2017.

[59] Martin O. Culjat, David Goldenberg, Priyamvada Tewari and Rahul S. Singh, "A Review of Tissue Substitutes for Ultrasound Imaging"

[60] Top Can Barış, "*Harmonic Motion Microwave Doppler Imaging Method*", Turkey: Middle East Technical University, Sept 2013

[61] Chmarra, Hansen, Mårvik and Langø, *"Multimodal Phantom of Liver Tissue",* p:2

[62] S.A. Lopez-Haro, C.J. Trujillo, A. Vera, L. Leija, "*An Agarose Based Phantom Embedded in an in Vitro Liver Tissue to Simulate Tumors: First Experience"*, p:1

[63] Timothy J. Hall,Member, IEEE, Mehmet Bilgen, Michael F. Insana and Thomas A. Krouskop, "*Phantom Materials for Elastography*", p: 1356, IEEE, 1997

APPENDICES

FLOW DIAGRAMS OF GENERATED APPLICATIONS

A.1 Application-1 Flow Diagram

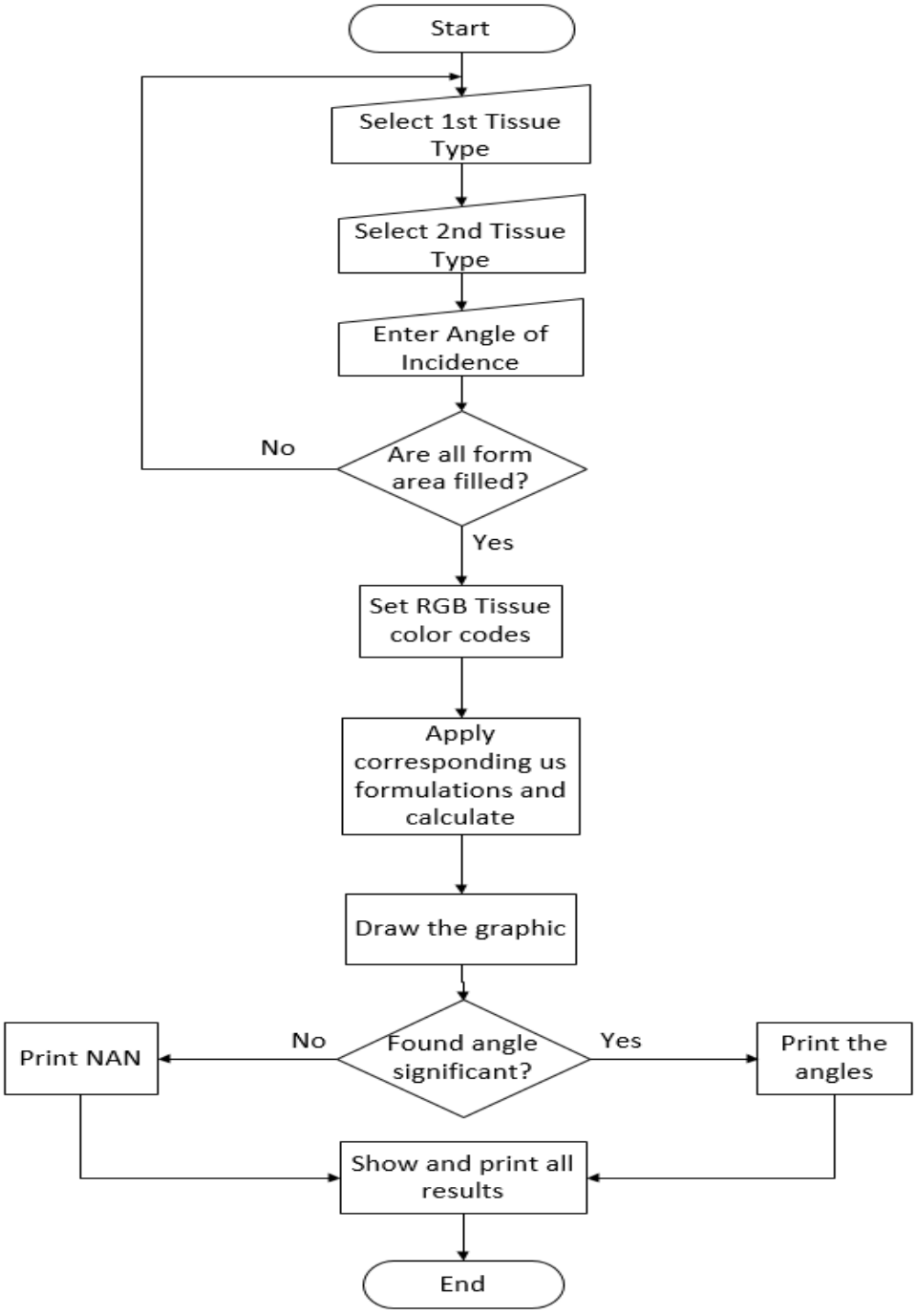

A.2 Application-2 Flow Diagram

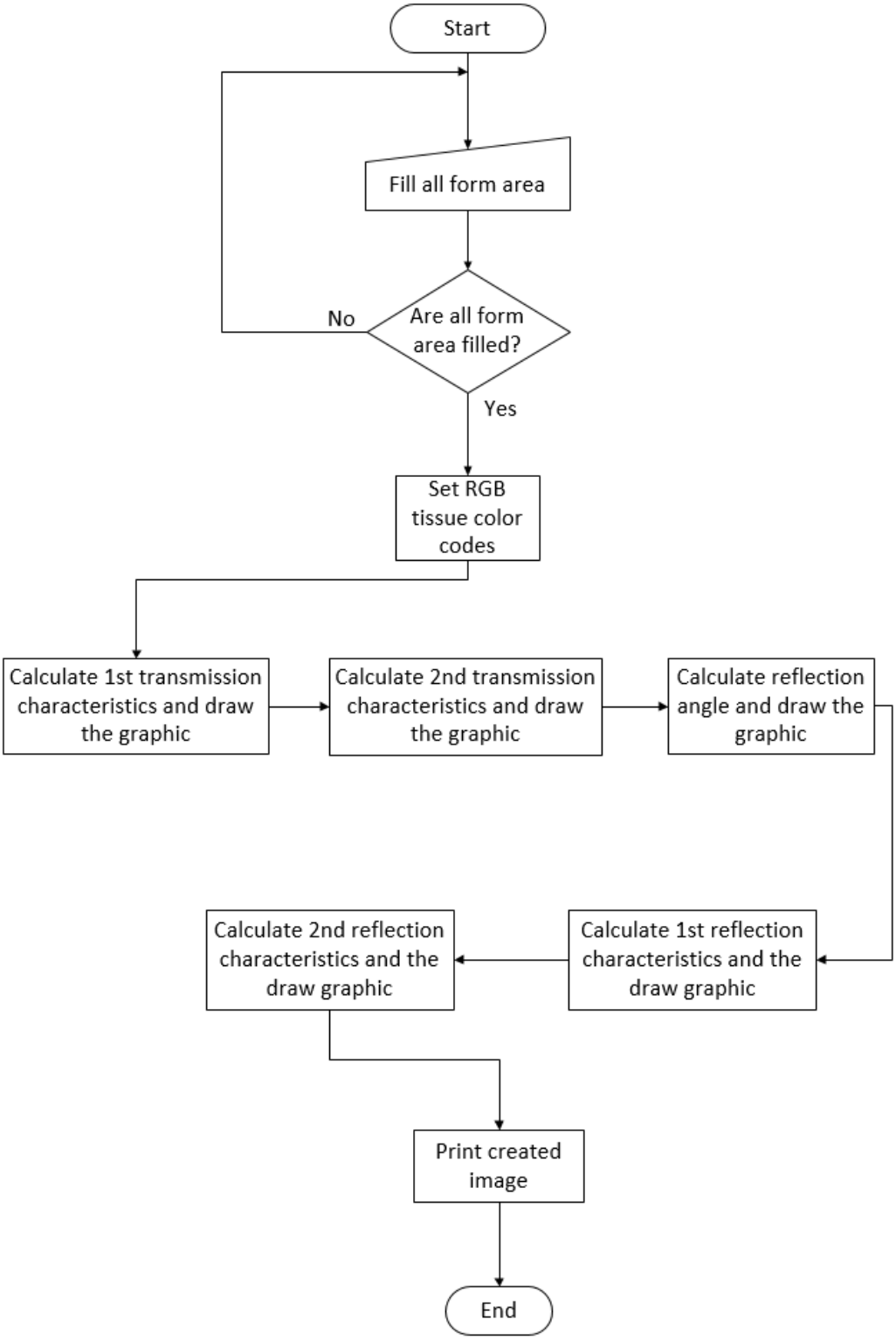

A.3 Application-3 Flow Diagram

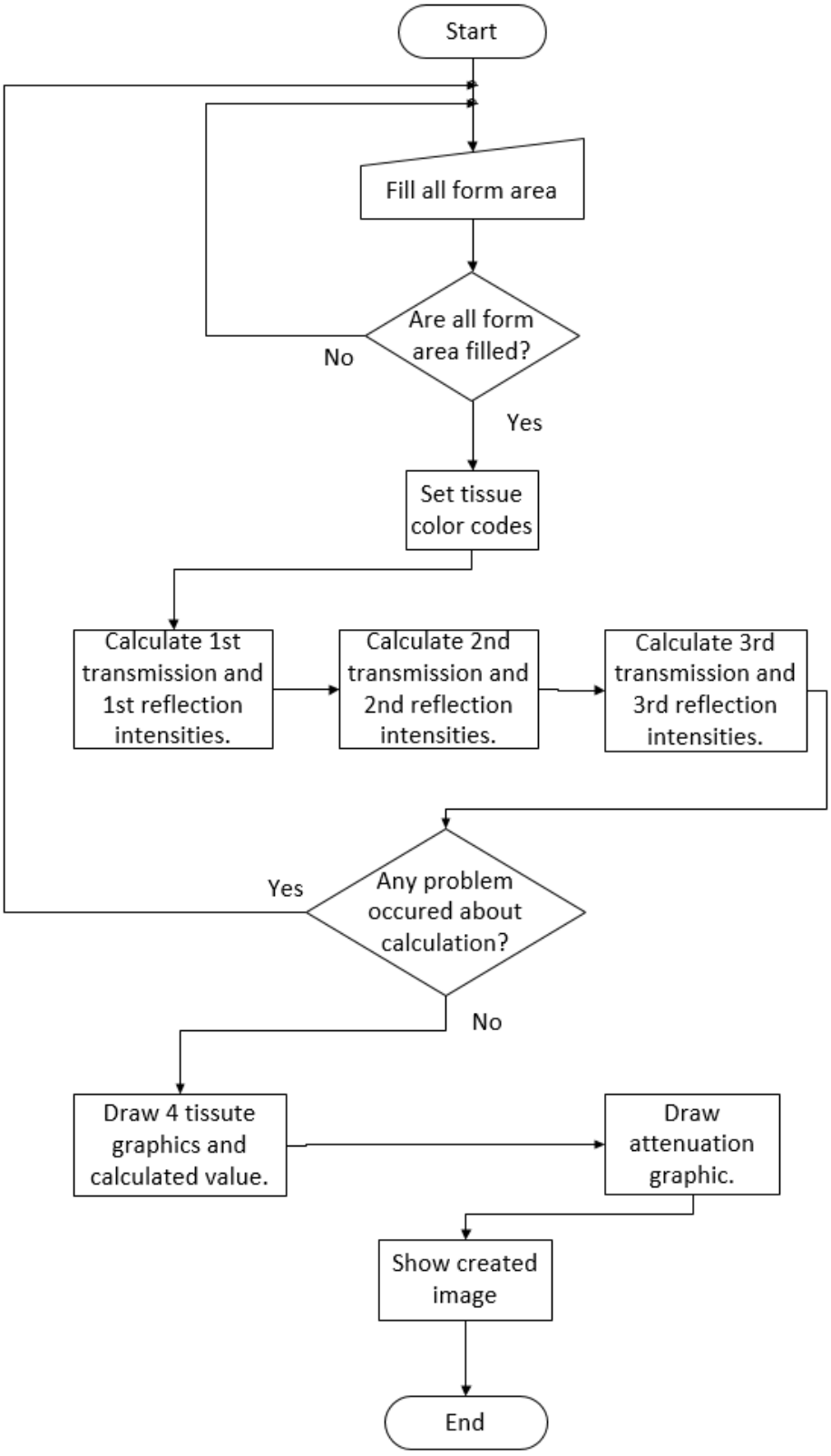

A.4 Application-4 Flow Diagram

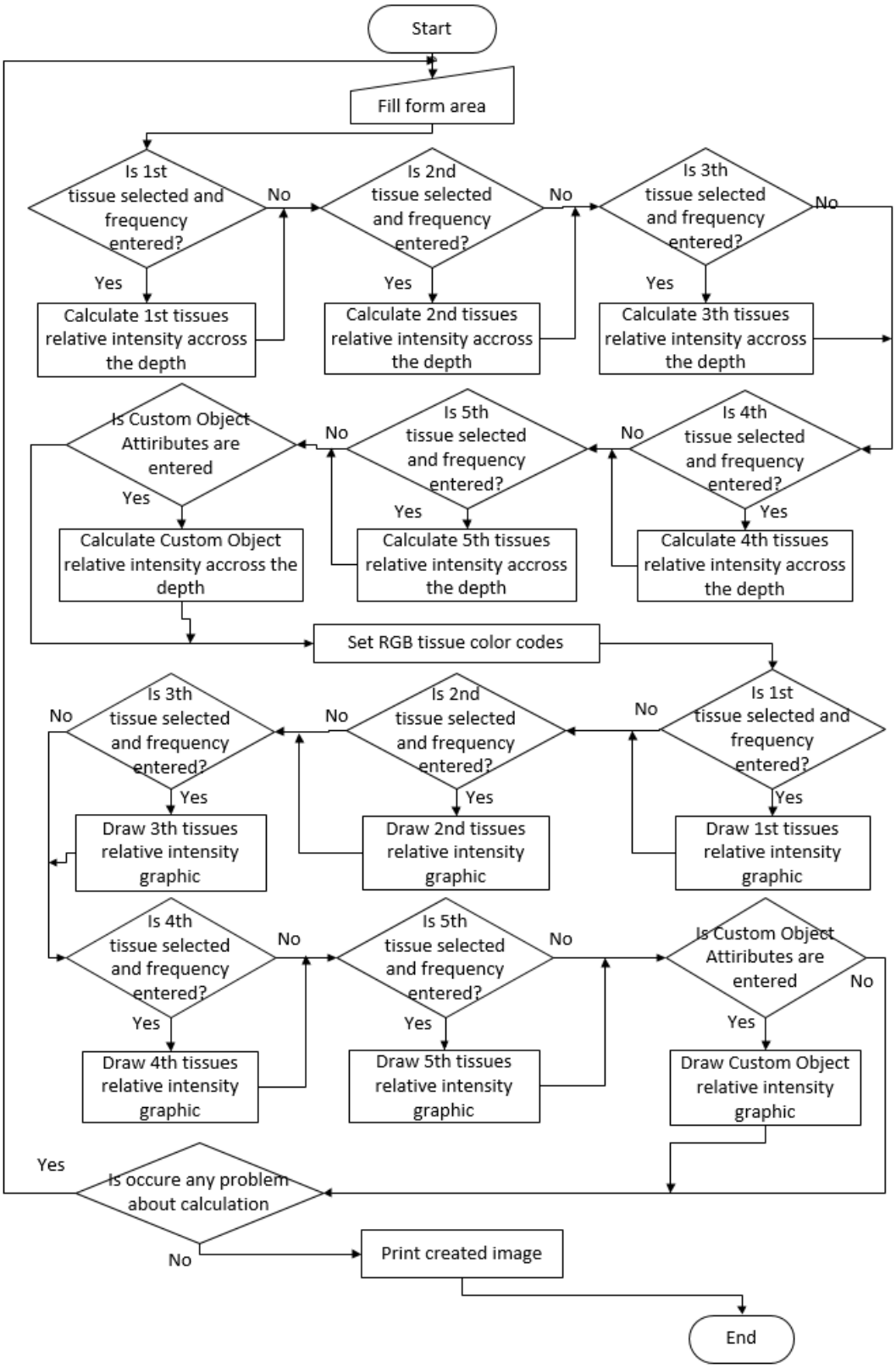

A.5 Application-5 Flow Diagram

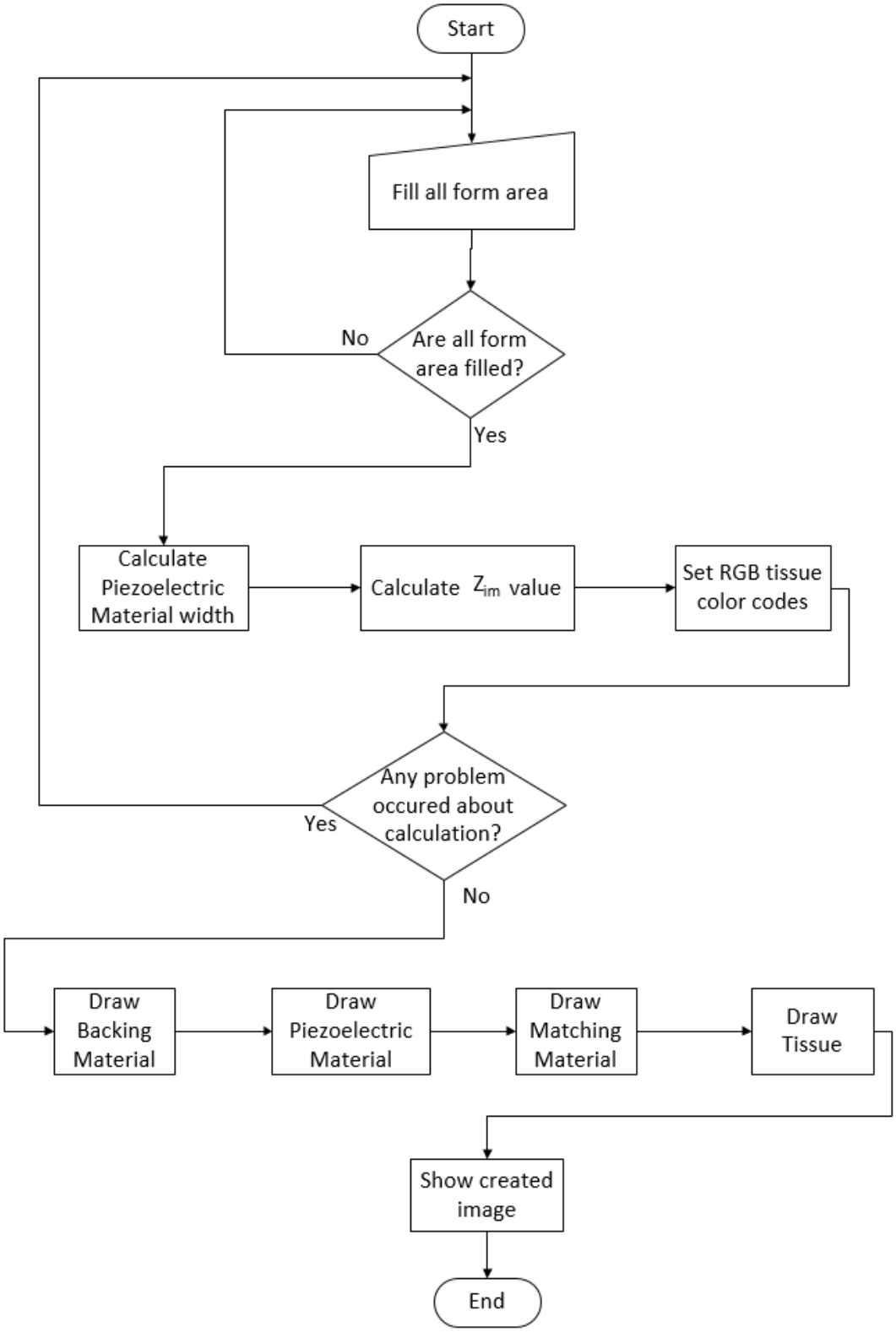

A.6 Application-6 Flow Diagram

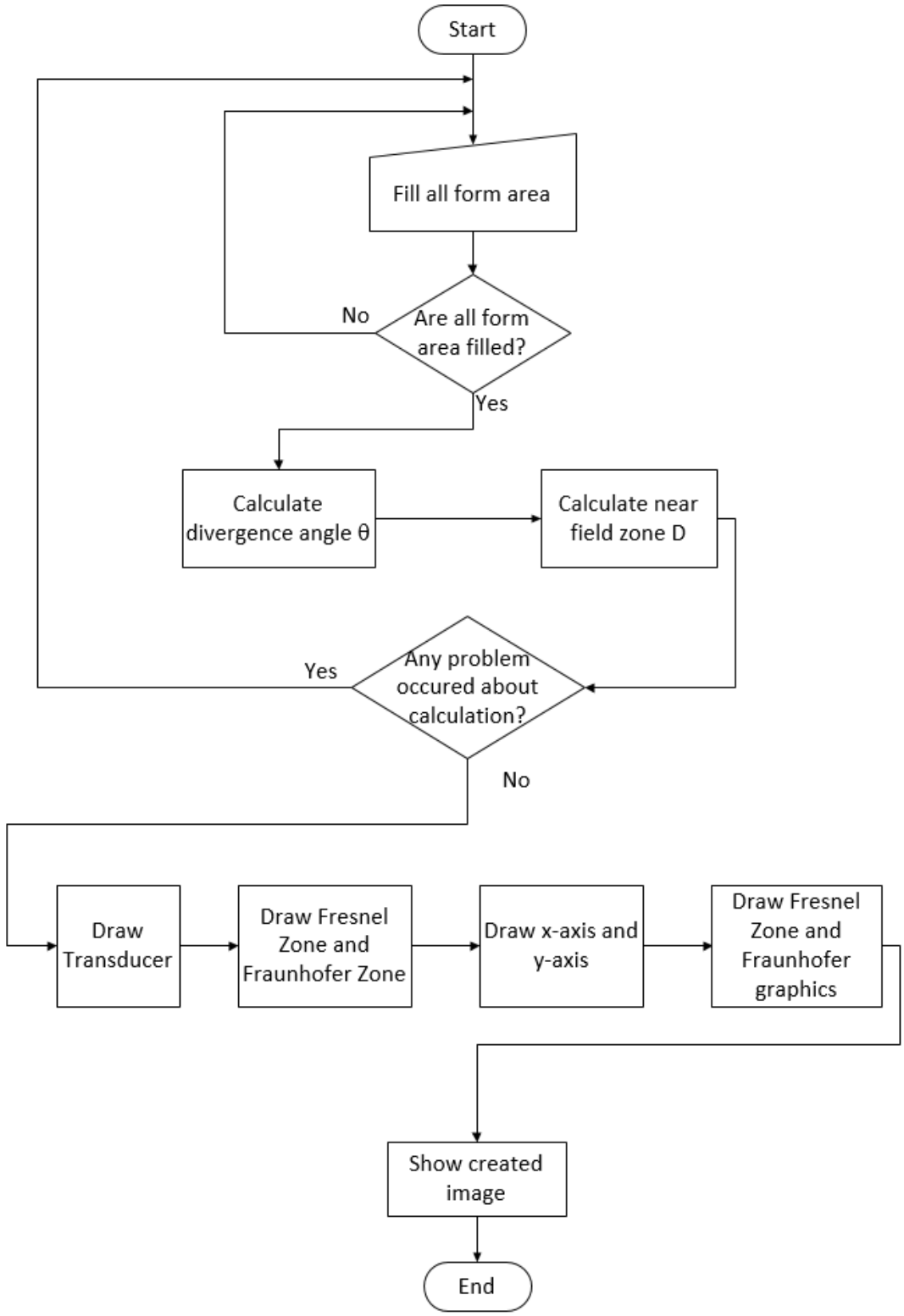

A.7 Application-7 Flow Diagram

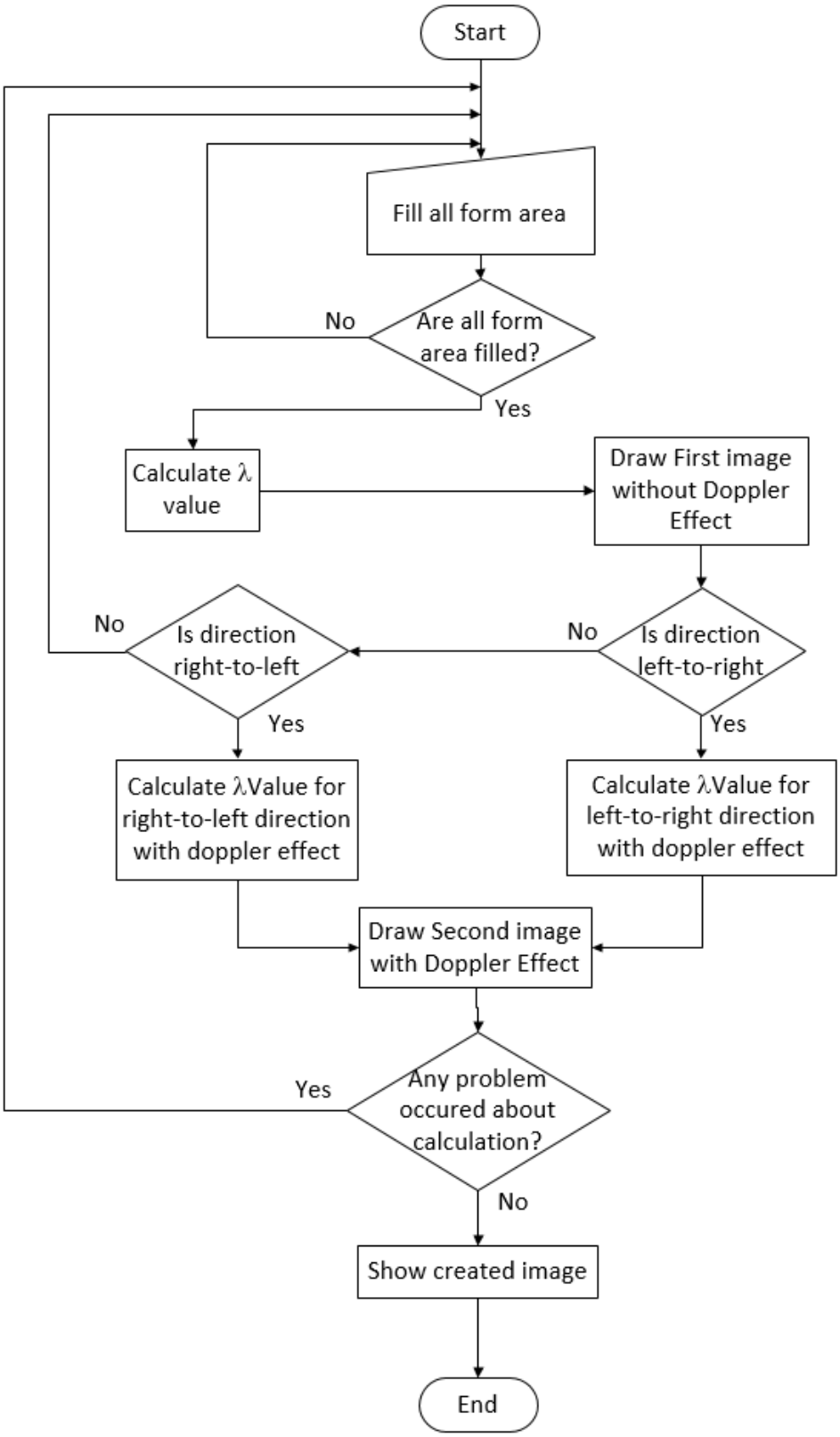

A.8 Application-8 Flow Diagram

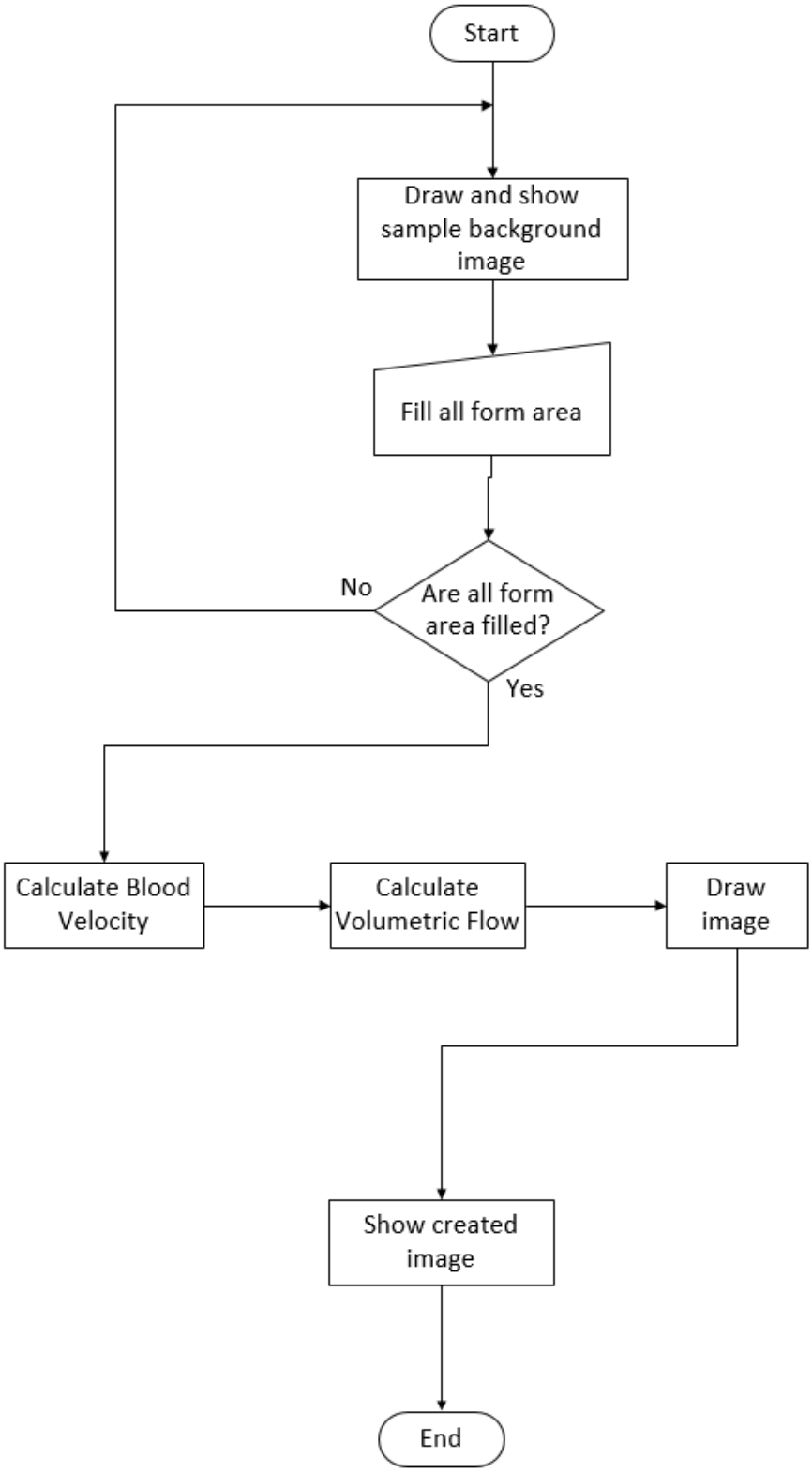

A.9 MUS Application Flow Diagram

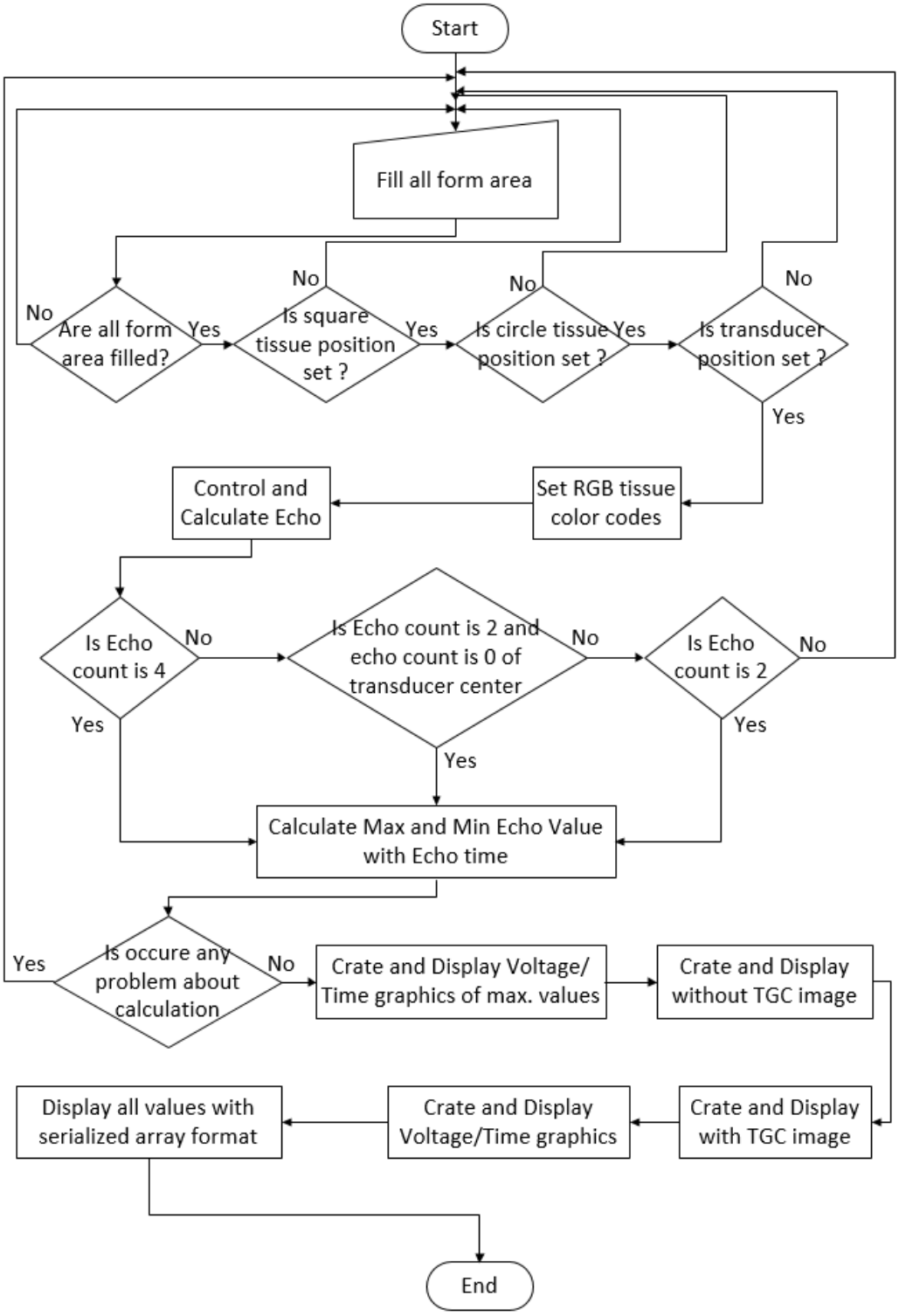

A.9 MUSr Application Flow Diagram